AUTOMATED PLASMA SPRAY (APS) PROCESS FEASIBILITY STUDY

FINAL REPORT

By

C.W. FETHEROFF

T. DERKACS

I.M. MATAY

TRW

**EQUIPMENT
MATERIALS TECHNOLOGY**

Prepared for

NATIONAL AERONAUTICS and SPACE ADMINISTRATION

NASA LEWIS RESEARCH CENTER

CLEVELAND, OHIO 44135

Contract NAS3-20112

1. Report No. NASA CR-165418	2. Government Accession No.	3. Recipient's Catalog No.
4. Title and Subtitle AUTOMATED PLASMA SPRAY (APS) PROCESS FEASIBILITY STUDY		5. Report Date March 1981
		6. Performing Organization Code
7. Author(s) C.W. Fetheroff, T. Derkacs and I.M. Matay		8. Performing Organization Report No. TRW ER-8019-F
		10. Work Unit No.
9. Performing Organization Name and Address TRW Materials Technology TRW Inc. 23555 Euclid Avenue Cleveland, Ohio 44117		11. Contract or Grant No. NAS3-20112
12. Sponsoring Agency Name and Address National Aeronautics and Space Administration Washington, D.C. 20546		13. Type of Report and Period Covered Final Contractor Report June 1976 to March 1981
		14. Sponsoring Agency Code

15. Supplementary Notes

Project Manager: John P. Merutka, Materials Division
NASA Lewis Research Center, Cleveland, Ohio 44135

16. Abstract

An automated plasma spray (APS) process has been developed to apply two layer (NiCrAlY and ZrO_2-12Y_2O_3) thermal-barrier coatings to aircraft and stationary gas turbine engine blade airfoils. The APS process hardware consists of four subsystems: a mechanical positioning subsystem incorporating two interlaced six-degree-of-freedom assemblies (one for coating deposition and one for coating thickness monitoring); a noncoherent optical metrology subsystem (for in-process gaging of the coating thickness buildup at specified points on the specimen); a microprocessor-based adaptive system controller (to achieve the desired overall thickness profile on the specimen); and commercial plasma spray equipment.

Over fifty JT9D first stage aircraft turbine blade specimens, ten W501B utility turbine blade specimens and dozens of cylindrical specimens were coated with the APS process in preliminary checkout and evaluation studies. The best of the preliminary turbine blade specimens achieved an overall coating thickness uniformity of $\pm$53 μm (2.1 mils), much better than is achievable manually. Factors limiting this performance were identified, and process modifications to minimize these limitations were defined. Comparative evaluations of coating thickness uniformity for manually sprayed and APS coated specimens were performed. One of the preliminary turbine blade evaluation specimens was subjected to a torch test and metallographic evaluation. Some cylindrical specimens coated with the APS process survived up to 2000 cycles in subsequent burner rig testing.

17. Key Words (Suggested by Author(s)) Plasma Spray Process Automation Thermal Barrier Coatings Dimensional Metrology Adaptive Control Turbine Blade/Vane Airfoils	18. Distribution Statement Unclassified - Unlimited		
19. Security Classif. (of this report) Unclassified	20. Security Classif. (of this page) Unclassified	21. No. of Pages 131	22. Price*

N81-31193-#

1.0 FOREWORD

This Final Technical Report covers work performed under Contract NAS3-20112, "Automated Plasma Spray Process Feasibility Study," during the period from June 1976 to March 1981.

The contract work was performed by the Materials Development Department of TRW Materials Technology, TRW Inc. The program was administered by NASA Lewis Research Center, Materials Division, with Mr. J. P. Merutka as Program Manager. The TRW Program Manager was Mr. I. M. Matay. The Principal Investigator was Mr. C. W. Fetheroff. Significant technical support on the program was provided by Mr. T. Derkacs, on dimensional metrology and process evaluations; by Mr. P. E. Neal, on computer technology and software; by Mr. J. Touhalisky, on electronic assembly and plasma spraying; by Mr. F. A. Sesek, on electromechanical assembly; and by Mr. H. A. Stieglitz, on design and fabrication of the Task I mechanical subsystem. Mechanical design and fabrication of the Task V mechanism and associated fixtures was under the direction of Mr. J. Woodcock of TRW Manufacturing Engineering Division.

The initial spray deposition process development effort was conducted under subcontract by Plasmadyne, Inc., a Geotel Company, at their Santa Ana, California facility. This activity was under the direction of Mr. A. Bernstein, General Manager, and was performed by Mr. J. R. Wiest, Principal Investigator.

TABLE OF CONTENTS

TABLE OF CONTENTS (Cont'd)

LIST OF FIGURES

LIST OF FIGURES (Cont'd)

vii

LIST OF FIGURES (Cont'd)

LIST OF TABLES

2.0 SUMMARY

An experimental effort was conducted to study the feasibility of developing an automated plasma spray (APS) process to uniformly and reproducibly apply two layer (NiCrAlY and $ZrO_2-12Y_2O_3$) thermal barrier coatings to gas turbine engine blade airfoils. The thicknesses of the metallic bond coat and oxide layers were approximately 0.10 mm (4 mils) and 0.25 to 0.38 mm (10 to 15 mils) respectively. The program target was to demonstrate feasibility of achieving a deposition uniformity of ± 38 μm (1.5 mils).

On this program an automated process was developed and demonstrated to be feasible for plasma spraying the two-layer thermal barrier coatings on both aircraft and utility gas turbine blade airfoils. The hardware fabricated and utilized for feasibility evaluations consisted of a five-degree-of-freedom specimen manipulator, a noncoherent optical instrument for monitoring coating deposition thickness buildup over the specimen surfaces, commercial plasma spray equipment and a microprocessor-based system controller. Both the plasma spray gun and the optical sensor each incorporated a single degree of freedom. The result was two interlaced six-degree-of-freedom subsystems, one for coating application and one for coating deposition thickness monitoring. The process demonstrations on this program were all conducted in normal ambient atmosphere, but the process system could readily be enveloped in an inert atmosphere. With some modifications it could also be utilized under low pressure ambient conditions.

During processing the optical sensor monitors coating deposition buildup at specific points on the airfoil surface and feeds this data to the microprocessor. The microprocessor closes the feedback loop by controlling the spray passes of the plasma gun so as to achieve the specified thickness at each point on the specimen surface. The process is thus applicable to deposition of controlled variable thickness coatings as well as uniform coatings.

All basic concepts involved in the APS process were successfully demonstrated. Critical problems solved included design of control and metrology subsystems capable of functioning in the adverse electromagnetic noise and dust environment inherent in the plasma spray process. The noncoherent optical sensor subsystem successfully demonstrated performance surpassing all design requirements. Repeatability runs on first stage JT9D aircraft engine turbine blade specimens consistently demonstrated standard deviations of ± 7.6 μm (0.3 mils) in measured values. Repeatability was also shown to be essentially independent of specimen surface finish, curvature and reflectance.

Based on the performance demonstrated on this program, technology transfer of the metrology subsystem concepts into production utilization was successfully implemented within TRW.

APS process system evaluations included spraying in excess of 50 JT9D first stage turbine blade specimens. This blade was selected as representative of the most difficult specimens to coat uniformly because of the small size and the small radii of curvature. In addition, however, ten larger W501B utility turbine blade airfoils were also coated to demonstrate applicability of the process to other specimens. Although not performed on this contract, the APS process system was also utilized to coat several dozen cylindrical specimens with thermal barrier coatings.

Process evaluations on the JT9D specimens showed that the best specimen achieved an overall thickness uniformity of ±53 µm (±2.1 mils), but was within the required tolerance range of ±38 µm (±1.5 mils) if the leading and trailing edge thickness measurements were ignored. The best coating uniformity measurements were achieved by periodically halting and restarting the automatic coating process, thus measuring coating thickness after allowing the blade to cool down to room temperature to eliminate erroneous measurements resulting from thermal warpage of the blade. Modifications to the process hardware to minimize this thermal problem in a production prototype system were defined. A number of areas have been identified where design improvements should also be made in the standard commercial plasma spray hardware items for a production prototype APS process system.

At the cooling passage exit holes on the trailing edge of the JT9D specimens, the deposited coating was well contoured to the edge. There was no need for masking the cooling holes and no plugging of the cooling holes occurred. This is a significant process capability for cost reduction, suggesting the reduction and/or elimination of currently expensive activities in hole masking, plugging, redrilling, etc.

One of the coated JT9D blades was submitted to a torch test at NASA for a preliminary evaluation of coating integrity. There was localized spalling at the hottest area on the leading edge after 23 hours of exposure. This was not unexpected since the coating parameters utilized were not to optimize the coating structure, but were simply to demonstrate deposition uniformity. Subsequent microscopic examinations, however, disclosed no cracks in the remaining coating in the area of the localized surface spalling.

A number of cylindrical specimens coated with thermal barrier coatings utilizing the APS process system were subjected to burner rig tests by NASA. Various combinations of process parameters were utilized in the coating of these specimens for NASA. The best of these specimens survived in excess of 2000 cycles in the subsequent burner rig tests.

3.0 INTRODUCTION

Gas turbines operating at higher temperatures show increased performance and improved fuel economy. Higher operating temperatures in such advanced gas turbines have been achieved through a combination of higher operating temperature materials and advanced cooling. Advanced cast alloys and directionally solidified alloys are reaching their limit of compositional improvements. Advanced cooling concepts are approaching their limitations due to complexity of component geometry, and limitations on engine performance gains due to the amount of compressor bleed air needed. For these reasons, an alternate approach involving the use of thermal barrier coatings to insulate the airfoil surfaces from the hot gases has been pursued by NASA Lewis Research Center and others.

The NASA developed thermal barrier coatings, which consist of a NiCrAlY type bond coat, approximately 0.10 mm (4 mils) thick, and an yttria stabilized zirconia overcoat, approximately 0.30 mm (12 mils) thick, have been used to lower air-cooled turbine blade temperatures by about 150°C (300°F) in ground base research engine tests. In addition, these coatings have survived over 500 engine cycles to full power. In burner rig tests, the coatings survived surface temperatures near 1370°C (2500°F) (Ref. No. 1).

These coatings were applied by manual plasma spray methods. As part of the continuing development effort, involving the determination of the applicability of thermal barrier coatings to various advanced aircraft gas turbines and utility gas turbines, a number of factors were considered. One factor was the ability to uniformly and reproducibly apply and document the thicknesses of the bond coating and thermal barrier coating on turbine blades. This is not possible using manual spray techniques.

The objective of this program, therefore, was to conduct an automated plasma spray (APS) process feasibility study. The concept of the APS process is based on an advanced processing approach, including the use of non-contact optical metrology and data processing systems that automatically control the plasma spray coating process to uniformly and reproducibly coat gas turbine blade airfoils. The APS process integrates a multi-degree-of-freedom specimen manipulator, a noncoherent optical instrument for coating thickness monitoring, conventional plasma spray equipment operating in an ambient environment and a microprocessor-based system controller. The APS process is intended to reduce the coating thickness non-uniformity, but more important, to eliminate the lack of reproducibility associated with the manual plasma spray (MPS) process.

The primary process evaluation efforts on this program were accomplished using JT9D aircraft engine first stage turbine blades. This specimen was selected as representative of the most difficult airfoils which would be encountered due to its small size and small radii of curvature. Extensive evaluations of both the basic

3

metrology subsystem performance capabilities and the spray deposition thickness uniformity were done on these specimens. During the final phase of the program activities, a number of larger W501B electric utility turbine blades were coated with the APS process system to demonstrate process applicability to other specimens. The APS process system was also utilized to apply thermal barrier coatings to cylindrical specimens subjected to burner rig testing by NASA. Although not part of this contract, the results of that effort are briefly summarized in this report.

The zirconia powder used during the earlier phases of this program contained 12% yttria. This was utilized at Plasmadyne on the preliminary test coupons and at TRW on the JT9D aircraft turbine blade specimens. Towards the end of this contract period, zirconia powder containing 8% yttria was supplied by NASA. This was used for the cylindrical specimens and the W501B utility blades. The NiCrAlY powder specification was not changed throughout the contract period. This specification was 17% chromium, 6% aluminum, 0.4% yttrium and the balance nickel. Particle size for both powders was -200 to +325 mesh.

This report contains dimensional measurement data obtained by the APS hardware in the English measurement system (mils). These were converted to the SI system (micrometers, μm) without rounding off.

4.0 PROCESS DEVELOPMENT

The concept of the Automatic Plasma Spray (APS) process is to apply an advanced processing approach, including the use of modern metrology and data processing systems, to control plasma spray coating deposition so as to uniformly and reproducibly coat gas turbine blades with a two-layer thermal barrier combination of NiCrAlY and yttria stabilized zirconia. This process will reduce non-uniformity, particularly the lack of reproducibility involved in the manual plasma spray (MPS) process.

The technical portion of this report is subdivided into five major subsections:

1)   Initial spray deposition process study

2)   APS process system development

3)   APS process system operation

4)   Preliminary APS system evaluations

5)   APS process application evaluations

The work efforts summarized in the first two subsections were conducted concurrently; the remainder of the work was conducted sequentially. The first three subsections, describing the basic process development work and operation, are contained in this section. The remaining two subsections, describing process system and process application evaluations, are contained in Section 5.

4.1   Initial Spray Deposition Process Study

The purpose of the initial spray deposition process development study was to select the specific plasma spray hardware to be incorporated into the APS system and to establish the process and control parameters associated with this hardware. The experimental portion of this study was performed by Plasmadyne, as a sub-contractor. This included selection of the specific process parameters to be used with the plasma spray hardware, preparation and spraying of specimens, and preparation of photomicrographs of selected coated specimens. Additional analysis of this data was done to develop control parameters unique to the APS process.

4.1.1 Introduction

Plasma spray is a process that produces coatings of a quality unachievable by other methods. There are three basic application areas that plasma spraying is extensively used for:

5

1) Environmental resistant coatings: application of specific material coatings to resist abrasion, oxidation, heat (thermal barriers), corrosion, erosion, fretting, friction, galling, etc.

2) Resurface coatings: rebuilding worn areas, salvaging mis-machined parts or improving the characteristics of a finished part. This often results in a part that will outwear the original by a factor of two, three or more.

3) Special characteristics: application of coatings to provide electromagnetic or electrostatic shielding, grip surfaces, thermal conduction, electrical conduction, electrical insulation, etc.

Plasma is often considered the fourth state of matter, after solid, liquid and gas. This extremely hot substance consists of free electrons, positive ions, atoms and molecules. Although it conducts electricity, it is electrically neutral. When a gas passes through an electric arc, the gas loses one of its electrons and becomes extremely hot plasma. Although temperatures can reach $16,650^{\circ}C$ ($30,000^{\circ}F$), most plasma spraying is performed at lower temperatures. As the plasma leaves the spray gun, powdered material is introduced into the stream in precisely controlled amounts. The material is caught up in the plasma stream, becomes molten, and is projected against the surface being coated.

When an individual particle impacts against the surface, thermal and mechanical energy is transferred to the substrate producing forces which favor interatomic bonding. Under these circumstances, plastic deformation of the particle and the local surface area occur. The greater the deformation of the particle upon impact, the greater the probability of interatomic bonding.

Despite the intense heat produced within the gun, the temperature drops rapidly across the intervening gun-to-work distance. This drop is a function of gas enthalpy, energy absorption of the powdered material, and work distance. The composition of the substrate, its mass, relative gun-to-substrate traverse speed, and coating material are factors determining substrate temperature. This temperature can be held to a few hundred degrees by maintaining recommended spray parameters. Auxiliary cooling will reduce substrate heating even further. In laboratory experiments, metals have been sprayed on mylar film without damage to the substrate.

Control of the substrate temperature also leads to a minimization of residual stresses in the coating after deposition. The stress distribution of the coating process results in a tensile stress at the surface which can cause cracking and spalling and a compressive stress at the interface which tends to weaken the bond between the coating and substrate and may cause coating breakaway.

Plasma sprayed materials can be sprayed onto virtually any properly prepared surface. Normally this preparation requires no more than grit blasting to slightly roughen the surface and remove any surface contamination. Since the energy of the surface also plays a significant role in the formation of interatomic bonds, this can explain the success of grit blasting. The work hardening of the grit blasted surface creates a higher energy level at the surface, and serves to promote the formation of interatomic bond.

A wide variety of metallic, ceramic and organic powders have been sprayed by the plasma process. The major criterion for spraying any material is that it has a distinct range of temperature over which it remains in the liquid phase. Material which sublimes cannot be sprayed, and those materials which have a very high viscosity as liquids are difficult to spray.

Once a particular powder chemistry is selected for a coating application several additional variables of the powder must be controlled:

1) Phases present - Materials of identical chemistry may have different crystalline phases present.

2) Particle shape, size and density - These characteristics of the powder have a controlling effect on the particle velocity.

It is important to closely control the particle size and size distribution of the powder. The particle size distribution range should be very narrow so that all the particles will require approximately the same thermal treatment for melting. In addition, a powder having a wide particle size distribution range will be subject to a great deal of segregation in the effluent prior to impact and this will result in a non-uniform coating layer.

The use of inert or semi-inert gases such as argon, argon/hydrogen, argon/helium or nitrogen gas mixtures permits the selection of materials which otherwise would oxidize if conventional flame spraying techniques were used. The use of hydrogen gas mixtures provides reducing conditions, increases the arc voltage and increases the heat transfer to the powdered particles.

For any specific arc gas, the effluent pressure, velocity and enthalpy are controlled by the combined effects of arc gas flow rate and input power to the torch. Within the envelope of stable operation these two variables are jointly regulated to accomodate different thermal properties of the various spray materials.

Other parameters which must be regulated during application of the plasma spray include gun-to-part standoff distance and rate of deposition. Too short of a spray distance generally causes overheating of the substrate. In addition, if the plasma torch is placed too close to the substrate, the powder has too short a dwell time and will not be completely molten upon impact with the substrate. Too large a spray distance is also undesirable since resolidification of the particle may occur prior to impact.

Based on the above considerations, the latest generation of Plasmatron (R) plasma spray equipment was selected for use in the APS process feasibility study. This equipment included a control console which could be interfaced with the APS process microprocessor by the simple addition of five interface relays. The plasma spray gun was supplied with two separate powder input ports to handle both constituents of the specified thermal barrier coatings. The powder supply hoppers use a volumetric control principle to accurately deliver the desired powder quantity without burdening the microprocessor with additional control functions. Powder delivery is determined by the rotational speed of the powder collection wheel inside the hopper canister.

Another feature of the equipment is the use of critical flow orifices instead of flowmeters to accurately control gas mass flows. A flowmeter is a mechanical device which depends on the mass and configuration of a float and tube to regulate flow past the float. The major drawback to this type of device is dependence on back pressure. Each flowmeter is calibrated at some given back pressure and the calibration is only valid at that back pressure. Since different plasma conditions require different chamber pressures, the flowmeter does not accurately indicate the true gas flow. The critical flow orifice, on the other hand, will deliver a constant mass flow of the arc gas start after start as long as the orifice downstream pressure stays below the critical level. The mass flow level can be accurately set with the orifice upstream pressure regulator without actually firing the gun.

4.1.2 Process Parameters

The process parameters investigated in the preliminary deposition process study were those normally associated with plasma spray equipment:

1) Gun type and operating power level

2) Powder injection angle

3) Powder feed rates

4) Powder gas flow rates

5) Plasma gas flow rates

6) Plasma gun to substrate distance

7) Plasma gun traverse speed

8) Powder deposit rate

(R) Registered trademark of Plasmadyne, Inc., Santa Ana, California

The scope of investigation was concerned only with maintaining a coating quality similar to that produced at NASA (Ref. 1), not optimization. Major emphasis was on establishing control parameters amenable to the APS process.

All samples were sprayed with the spray pattern normal to the surface. Other investigators had previously found no noticeable effect on the deposited coating with spray angles varying up to 0.8 radian (45 degrees) from the normal (Ref. 2). For the APS process, the major concern over the effect of substrate geometry on deposited coating morphology is the lens effect on concave surfaces of the target airfoils. The incident material around the periphery of the spray pattern may be reflected off the blade and back into the spray and then onto the substrate. This could result in cold particles entrapped in the deposited coating. For this reason, it was thought desirable to keep the spray pattern or beam as narrow as possible for the APS process to minimize this effect. It was likewise desirable to keep the gun relatively normal to the surface ± 0.35 radian (± 20 degrees), to maintain tighter control over the coating deposition thickness uniformity.

In establishing the process parameters, only the 40 kW subsonic and 40 kW mach I electrodes were evaluated. Several combinations of spray techniques (foreward and backward powder injection), power levels and anodes were evaluated both with and without auxiliary gas. From these investigations the 40 KW subsonic electrode with foreward powder injection was selected. The combinations of parameters shown in Tables I and II, for NiCrAlY and 12% Y_2O_3-ZrO_2 respectively, seemed to closely duplicate the microstructure presented in Reference 1. These were therefore selected for use in the APS feasibility demonstration.

4.1.3 Evaluations

Experimental evaluations during the deposition process study were of two types — those for establishing the process parameters and those for determining the deposition profiles and rates. For establishing the process parameters, 300-series stainless steel metallographic evaluation specimens 5 cm (2 inch) square by 0.23 cm (0.090 inch) thick were coated with each of the coating materials (NiCrAlY and 12% Y_2O_3-ZrO_2) as well as with the two-layer composite. For the deposition profile and rate measurements, carbon steel specimens 15 cm (6 inch) square by 0.32 cm (0.125 inch) thick were used. Each of these specimens contained a two-pass buildup and a four-pass buildup of plasma-sprayed coating over separate traverse lines.

The evaluation specimens were all sprayed by hand. To obtain the accuracy required for the profile determination specimens, the plasma gun was fixtured on a pneumatic drive device. The surface speed of the drive was 40.6 cm/s (16 in/s), and the specimen to be coated was fixtured at a 6.35 cm (2.5 inch) standoff distance. CO_2 cover gas was used while coating all specimens, and the substrate temperatures were kept below $204^{\circ}C$ ($400^{\circ}F$). All specimens were prepared for spraying by grit blasting with 80 mesh aluminum oxide at 6.3 to 7.0 kgm/cm^2 (90 to 100 psig).

TABLE I

Plasma Spray Parameters For NiCrAlY

OPERATING MODE   Subsonic

GUN TYPE   SG-100

      Anode: 2083-135

      Cathode: 1083A-129

      Gas Injector: 1083A-113

OPERATING PARAMETERS

      Power: 21 kW

      Voltage: 30 volts ± 3 volts

      Current: 700 amps ± 25 amps

      Arc Gas: Argon

      Flow Rate: 0.77 l/s (98 scfh)

      Auxiliary Gas: None

      Powder Gas: Argon

      Flow Rate: 0.09 l/s (12 scfh)

      Powder Feed Rate: 0.70 g/s (42 g/min)

      Standoff Distance: 6.35 cm ± 0.89 cm (2.5 in ± 0.35 in)

      Surface Speed: 40.6 cm/s ± 5 cm/s (16 in/s ± 2 in/s)

      Normal: ± 0.35 rad (± 20°)

      Cover Gas: CO_2

TABLE II

Plasma Spray Parameters For 12% Y_2O_3 - ZrO_2

OPERATING MODE   Subsonic

GUN TYPE   SG-100

    Anode: 2083-135

    Cathode: 1083A-129

    Gas Injector: 1083A-113

OPERATING PARAMETERS

    Power: 32 kW

    Voltage: 37 volts $\pm$ 3 volts

    Current: 800 amps $\pm$ 25 amps

    Arc Gas: Argon

    Flow Rate: 0.77 l/s (98 scfh)

    Auxiliary Gas: Helium

    Flow Rate: 0.20 l/s (25 scfh)

    Powder Gas: Argon

    Flow Rate: 0.09 l/s (12 scfh)

    Powder Feed Rate: 0.63 g/s (37.6 g/min)

    Deposit Rate: 0.23 g/s (13.8 g/min)

    Stand-Off Distance: 6.35 cm $\pm$ 0.89 cm (2.5 $\pm$ 0.35 in)

    Surface Speed: 40.6 cm/s $\pm$ 5 cm/s (16 in/s $\pm$ 2 in/s)

    Normal: $\pm$ 0.35 rad ($\pm$ 20°)

    Cover Gas: CO_2

Figure 1 shows the microstructure of the two-layer composite coating deposited by Plasmadyne on one of the 5 cm (2 inch) square specimens using the process parameters selected for use in the APS process feasibility demonstration. Figure 2 shows the microstructure of a typical coating applied by NASA at that time. A comparison of these two photomicrographs indicates that the two coatings were very similar in structure and density. The as-sprayed surface finish of the Plasmadyne-coated samples was 10 μm RMS. By light sanding, using 400 grit silicon carbide paper, the surface finish went below 3 μm RMS.

Eight composite 50X photomicrographs were prepared from each of the 15 cm (6 inch) square specimens used to determine spray deposition profiles. Data was subsequently taken from the photomicrographs and subjected to a computer statistical analysis. The purpose of this analysis was to determine the optimum traverse or scan line spacing for each of the coatings to achieve maximum overall coating thickness uniformity. The effective coating thickness per pass using the optimum scan line spacing was also desired. The curve shown in Figure 3 was generated by the computer using a polynomial regression program to fit a second order curve through the data obtained for the 12% Y_2O_3-ZrO_2 coating. No significant difference was found between the two pass and four-pass data. Therefore, the curve shown is applicable to any single traverse of the plasma spray gun.

The curve shown in Figure 3 was then used by the computer to determine the optimum spacing between scan lines for overall coating thickness uniformity. This spacing was determined to be approximately 5 mm (195 mils) for the 12% Y_2O_3-ZrO_2 coating. Figure 4 shows profiles generated by the computer assuming six passes of the plasma gun along each scan line. The lower (solid) curves are the deposition profiles which would result along each scan line in the absence of the others. The resultant overall coating thickness profile from summing all the scan line depositions is shown by the crosses at the top of the figure. The overall coating thickness from six passes per scan line is almost 127 μm (5 mils) with peak-to-valley variations of approximately 7.5 μm (0.3 mils). The effective overall coating thickness per scan line pass is thus approximately 21 μm (0.82 mil). In actual coating applications a slight "feathering" (slight off-setting of the scan line from nominal between passes of a multiple pass application) would further minimize the surface ripples in the overall coating thickness.

The same type analysis was performed on the data for the NiCrAlY alloy coating. There was a significant difference between the data for the two-pass coating buildup and that for the four-pass buildup. Plasmadyne stated that it was not unusual for the first pass to result in a thicker coating buildup than subsequent passes, although the exact reason was not identified. The computer analysis therefore resulted in different deposition profiles for the first pass and subsequent passes for the NiCrAlY. These two curves are shown in Figures 5 and 6 respectively.
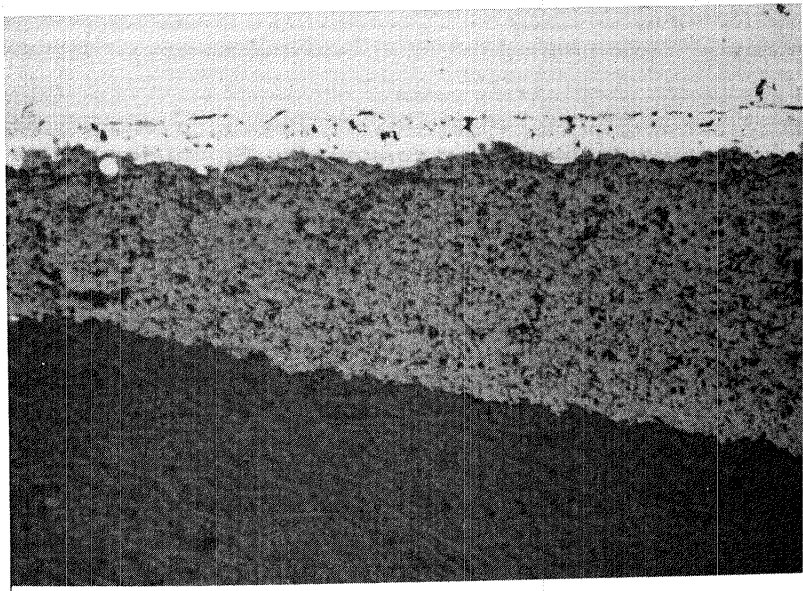
Figure 1. Microstructure of Two-layer (NiCrAlY/12% Y_2O_3 - ZrO_2) Plasma-sprayed Specimen Prepared by Plasmadyne Using Parameters Selected for APS Process. (100X)
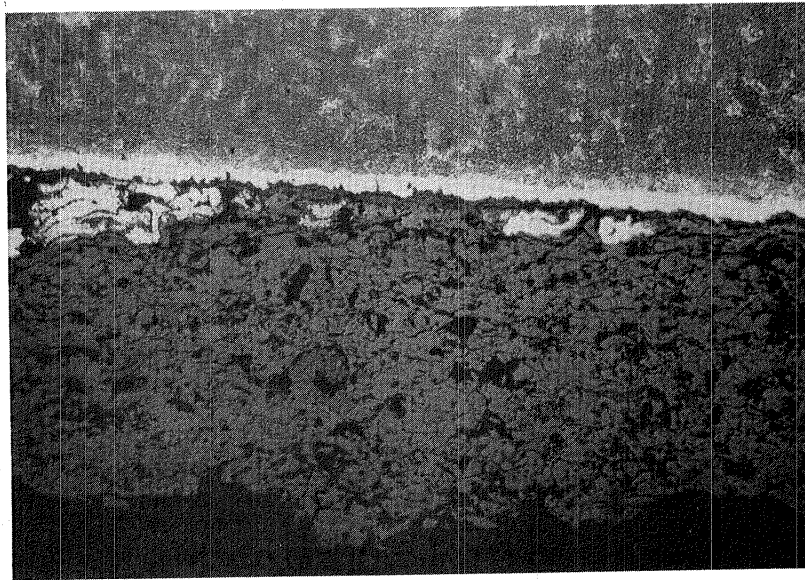
Figure 2. Microstructure of Typical Specimen Prepared by NASA in 1976 (Reference No. 1). (100X)
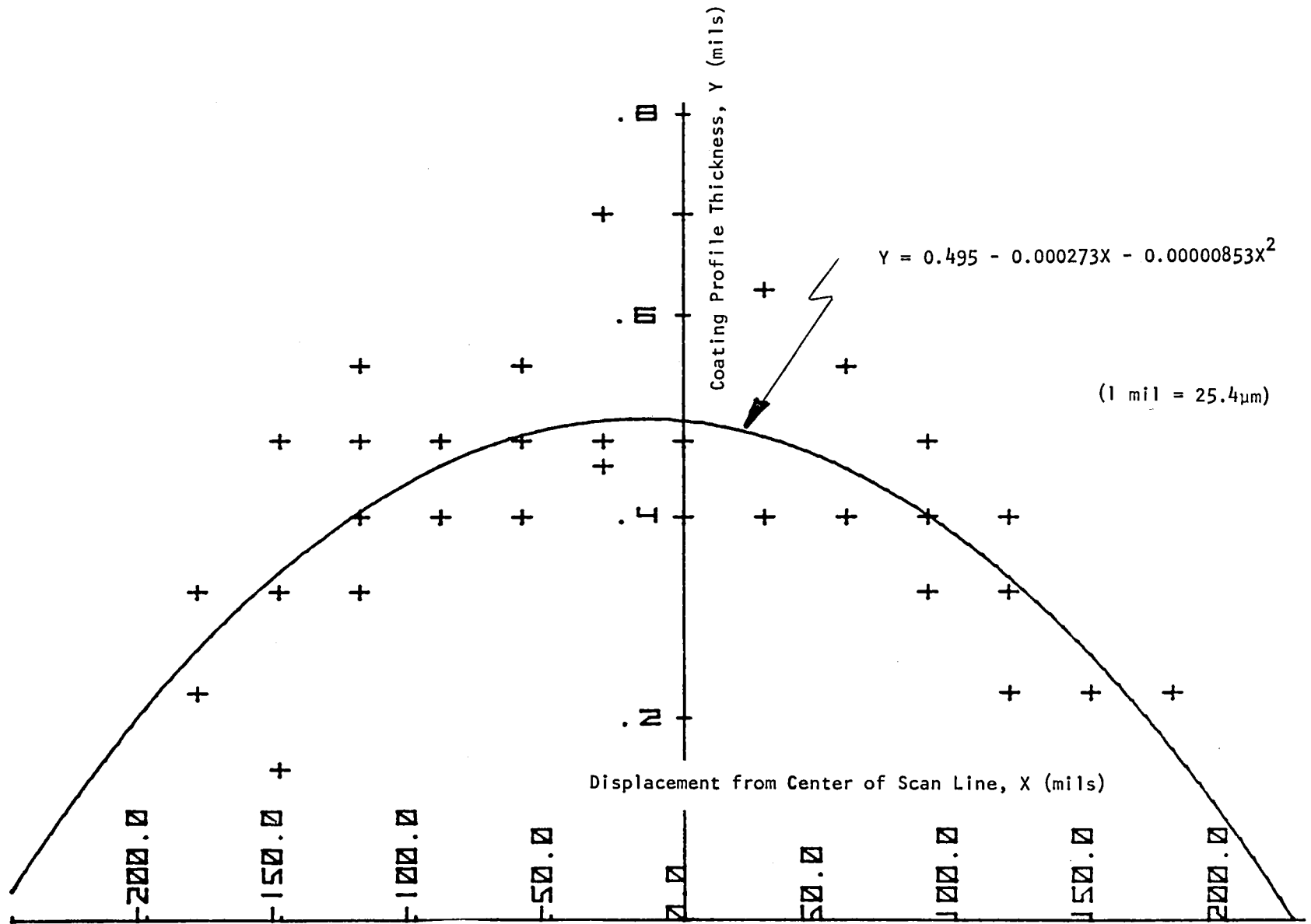
Figure 3. Spray Deposition Profile for a Single Scan Line Pass Using 12% Y_2O_3 - ZrO_2.

The figure shows a plot with Y-axis labeled "Coating Profile Thickness, Y (mils)" and X-axis labeled "Displacement from Center of Scan Line, X (mils)". The fitted curve equation is:

$$Y = 0.495 - 0.000273X - 0.00000853X^2$$

(1 mil = 25.4μm)
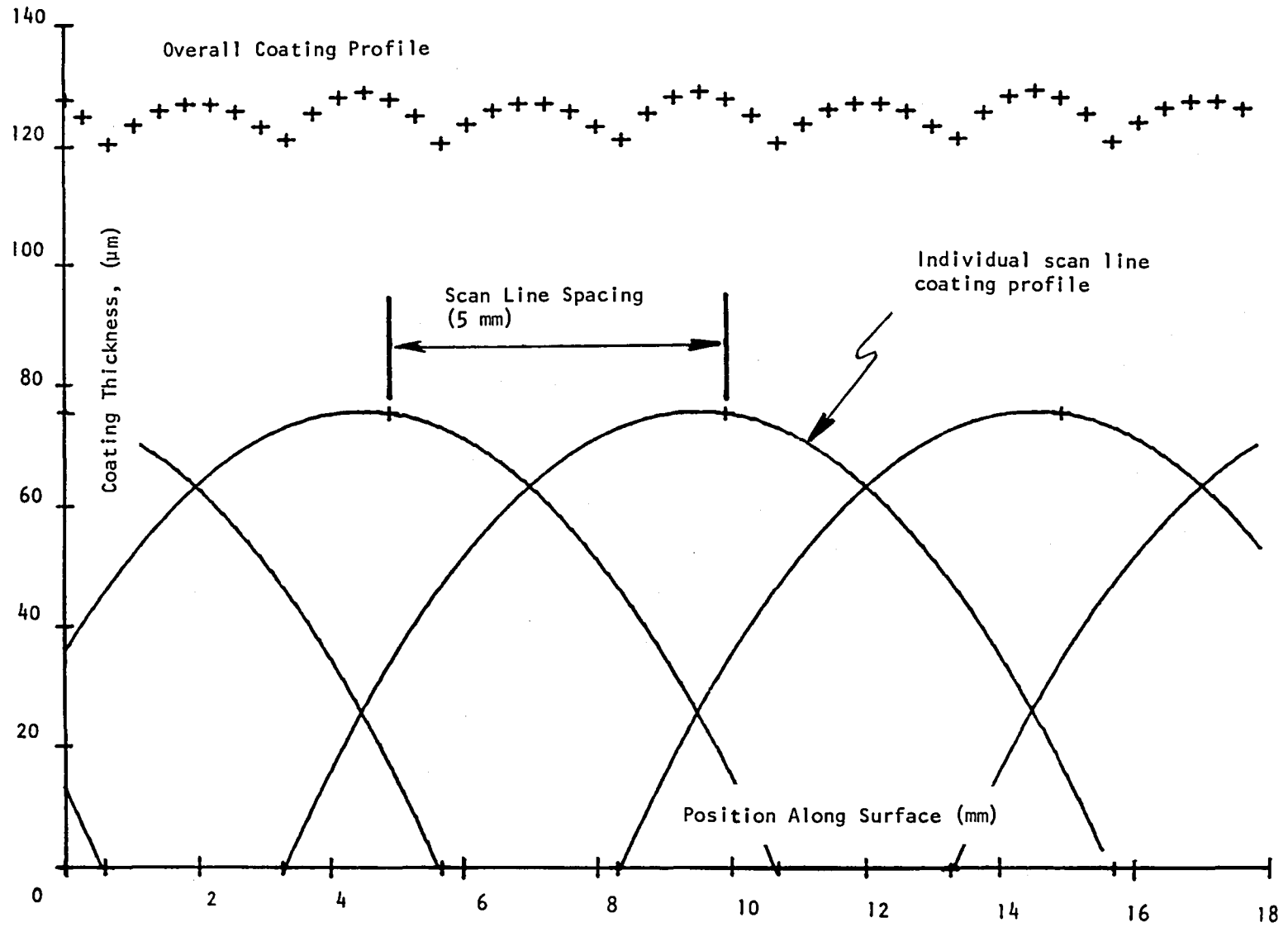
Figure 4. Coating Deposition Thickness Profiles (Yttria Stabilized Zirconia, 6 Passes per Scan Line).

15
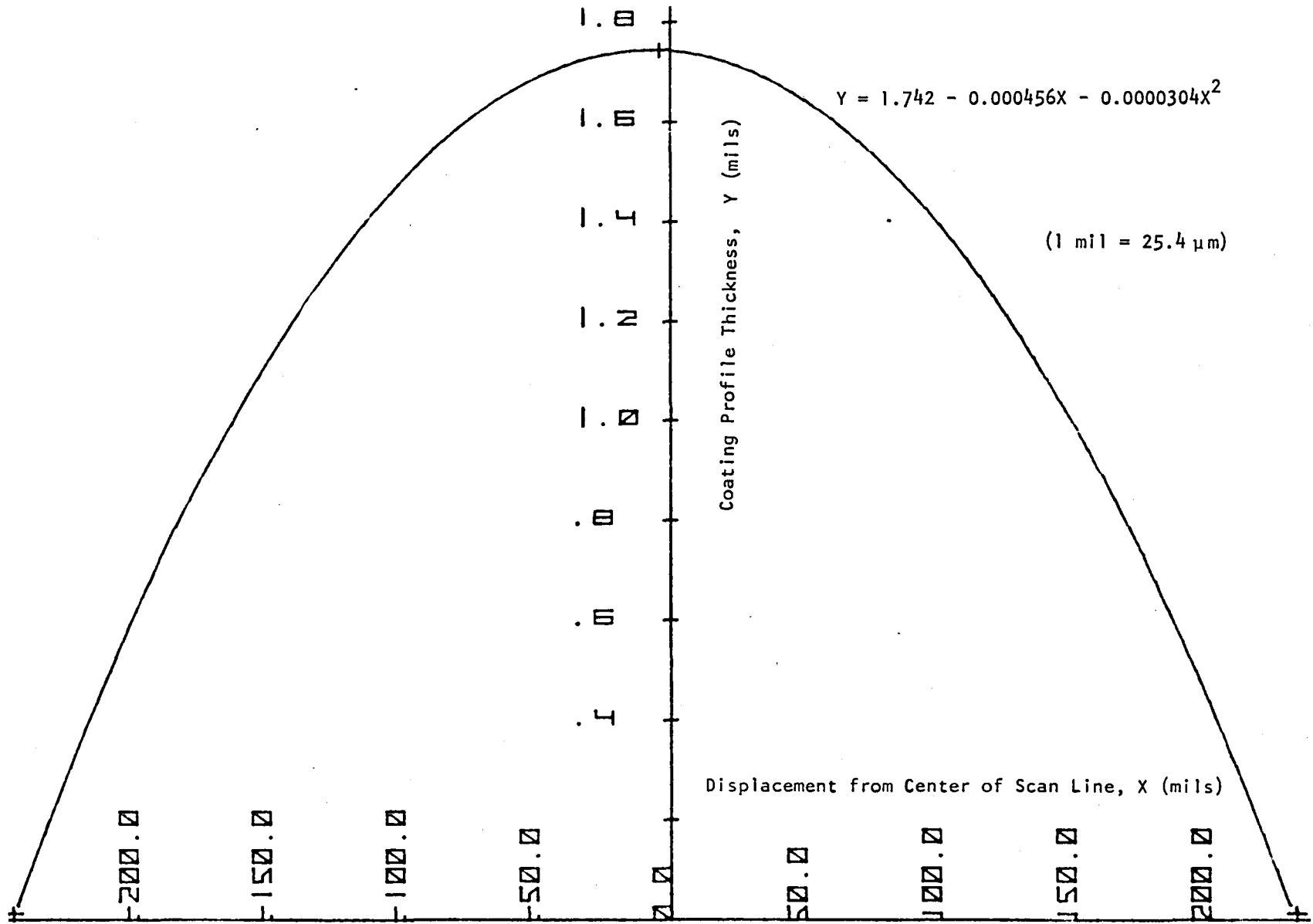
Figure 5. Coating Deposition Thickness Profile for Single Scan Line
First Pass Using NiCrAlY.

$$Y = 0.410 - 0.000107X - 0.00000717X^2$$

(1 mil = 25.4μm)

Coating Profile Thickness, Y (mils)

.4

.3

.2

.1

Displacement from center of Scan Line, X (mils)

200.0   150.0   100.0   50.0   0   50.0   100.0   150.0   200.0
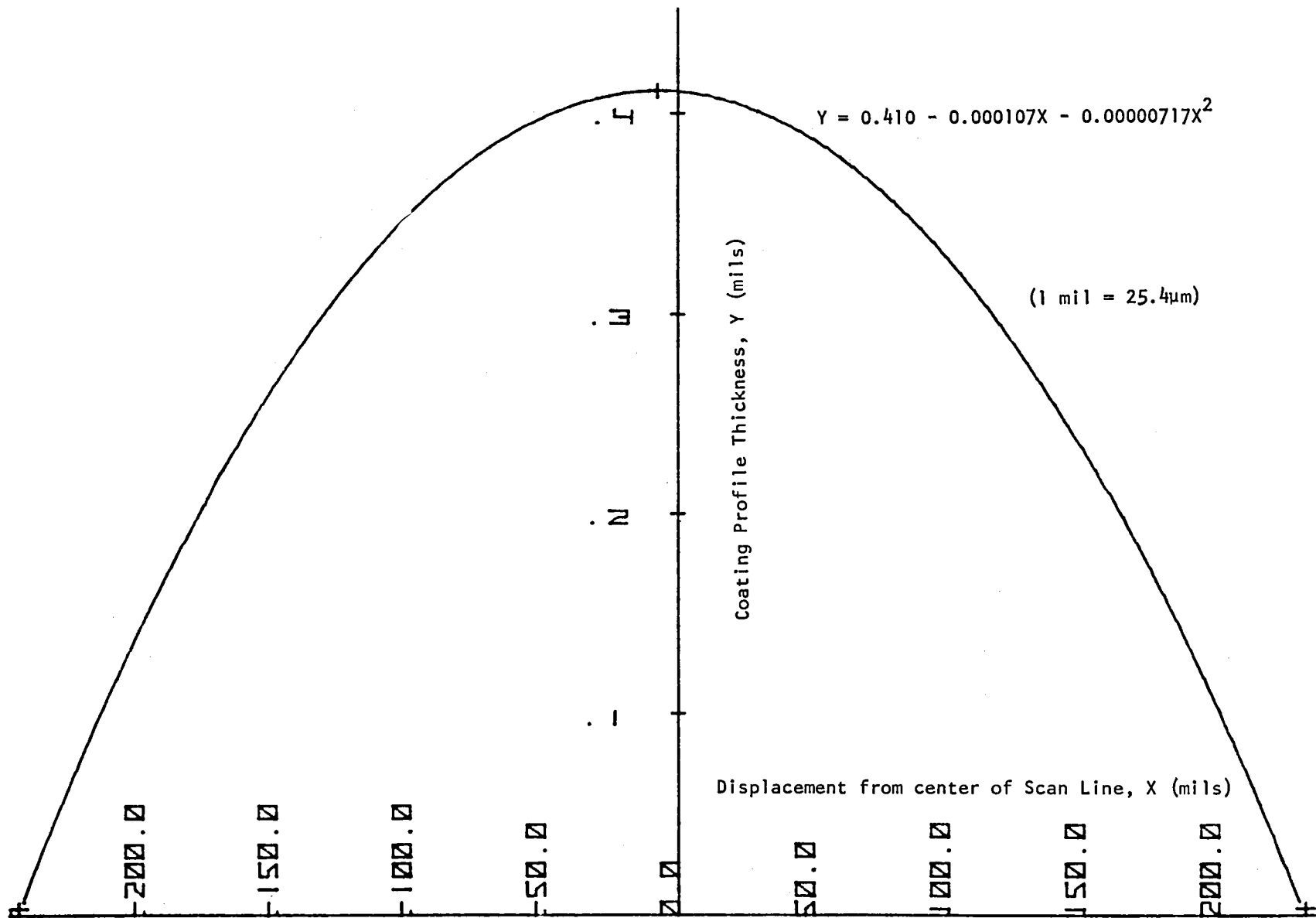
Figure 6.   Coating Deposition Thickness Profile for Passes Other than
First for Single Scan Line Using NiCrAlY.

The computer determined the optimum scan line spacing for the NiCrAlY. However, in this case, both of the curves shown in Figures 5 and 6 had to be used. The optimum scan line spacing was found to be approximately 5mm (195 mils). Figure 7 shows profiles generated by the computer assuming four passes of the plasma gun along each scan line. The lower solid curves are again the deposition profiles which would result along each scan line in the absence of the others. The crosses again designate the summation of all the individual scan line depositions. For the NiCrAlY four passes on each scan line results in a total coating thickness of approximately 127 μm (5 mils) with peak-to-valley variations of approximately 5.5 μm (0.2 mil). The effective overall coating thickness was approximately 75 μm (3 mils) for the first scan on all the scan lines and 16 μm (0.64 mil) for each subsequent pass.

Based on the initial spray deposition process development study results, the specific plasma spray hardware configuration and the associated process and control parameters to be used for the initial APS process feasibility investigations were selected.

4.1.4 APS Process Parameters

The APS process was operated under normal ambient atmosphere conditions. No vacuum or other sealed chamber was used. An inert cover gas (CO_2) was directed at the specimen being coated while the process was operational.

Coating deposition was accomplished using one plasma spray gun having two powder injection ports, each being independently fed by its own powder hopper. One powder hopper supplied the NiCrAlY material; the other supplied the yttria-stabilized zirconium oxide material. Essentially the same plasma spray hardware parameters were specified for both materials. The differences were the torch power, use of an auxiliary gas with the zirconium oxide material, and use of different powder feed rates on the two hoppers. Most of the plasma spray operating parameters could therefore be manually preset; very few control interfaces were required with the APS process control hardware. In a production system, of course, it may be desirable to control additional parameters automatically. For this feasibility demonstration only five interface relays needed to be added to the plasma spray control console. The five signal interfaces were:

1)   Start (or Run)

2)   Hopper #1 Activate

3)   Hopper #2 Activate

4)   Power Level (#1 or #2)

5)   Stop (or Purge)
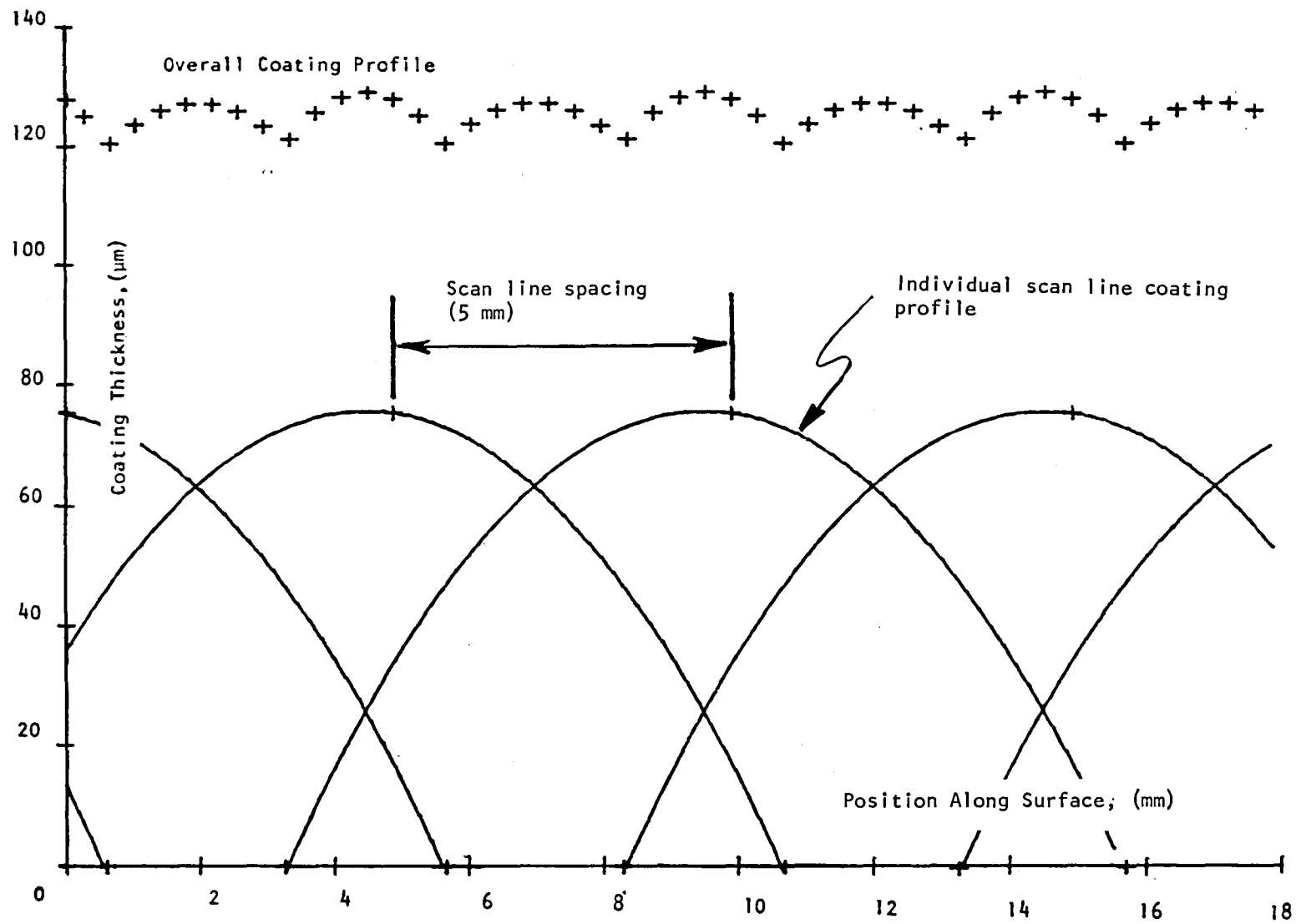
Figure 7. Coating Deposition Thickness Profiles (NICrAlY, 4 Passes).

Various control parameters were also provided for use in initial process software preparation. The nominal scan line spacing and the number of passes required to build up a desired coating thickness are typical of these. Since the coating buildup per pass is relatively thin (16 μm for the NiCrAlY and 21 for the zirconia) it is possible to control coating buildup on the various specimen surfaces to the desired $\pm$38.1 μm ($\pm$1.5 mils). The possibility of using the same scan line spacing for both materials also reduced the burden on process firmware tables, since separate coordinate tables were not required.

The study did indicate that a slight amount of "feathering" may be required during coating deposition to maximize coating thickness uniformity over the specimen. However, it was felt that normal slight variations in the process parameters and in positioning system tolerances may provide adequate natural "feathering." The effects of surface curvature on the turbine blade specimens would also contribute in providing some blending of the theoretical profiles generated by the computer.

Finally, it should be emphasized again that this initial deposition process study was not intended to optimize the system parameters. It was intended to select parameters to be utilized in demonstrating feasibility of automatically controlling plasma spray deposition with tight control of thickness uniformity on turbine airfoils.

4.2 APS Process System Development

This phase of the APS process development effort was concerned with development of the various hardware and software subsystems with the exception of the specific plasma spray equipment (commercial items) selected during the initial deposition process study. The hardware subsystems included the various mechanical positioning subsystems and fixturing, the metrology subsystem for in-process monitoring of coating thickness buildup on the specimens, and the microprocessor-based process control subsystem. The software included both the software subroutines used by the microprocessor to control the overall APS process and the firmware tables which defined specific process and specimen characteristics. This phase of the program was conducted in parallel with the initial deposition process study and incorporated results of that study as they became available.

4.2.1 Technical Approach

The conventional approach in attempting to deposit uniform thickness plasma-sprayed coatings has been to utilize large standoff distances between the gun and specimen. The spray pattern diverges as it leaves the gun and tends to become more uniform as it fans out over larger and larger areas. If a large enough standoff distance is used, and the specimen being sprayed is not too large, an entire side of the specimen can be coated at one sweep. Vacuum chambers are often used to allow even greater standoff distances.

The standoff distance cannot be increased, however, without a trade-off in coating quality. Frequently the optimum standoff distance will not yield adequate uniformity in coating thicknesses. The conventional approach, therefore, is not

amenable to close control of the localized uniformity variations over a specimen surface. This is particularly true for specimens having complex geometries and small radii of curvature.

The approach selected was diametrically opposite to the conventional approach. The APS process utilized relatively small gun-to-part standoff distances and normal ambient atmospheres. This produced a minimum instantaneous deposition spot size which could be controlled to more uniformly coat curved geometries. An in-process optical gage was utilized to monitor the localized coating thickness buildup over the specimen. Feedback from this gage to the process controller allowed the process to adapt to process variations and vary the deposition patterns until the desired coating thickness and uniformity were achieved over the entire specimen.

A simplified functional block diagram of the APS process, defining the major subsystems of the approach, is shown in Figure 8. The system consists of four major subsystems - a mechanical positioning and scanning subsystem, a metrology subsystem for deposited coating thickness monitoring, the plasma spray hardware, and the overall process control subsystem. The plasma spray equipment consists of essentially standard commercial items with the exception of the interface modifications to allow APS process control. The other three subsystems, developed for the APS process, will be discussed in the following paragraphs.

A microprocessor was selected as the basis for the system controller. This provided an intelligence unique among the various alternatives considered - i.e., hard-wired logic, relay controllers, numerical control, etc. The microprocessor is capable of making decisions based on the desired thicknesses and the data from the in-process optical gage. It can then automatically initiate iterations of the coating deposition cycle over selected portions of the specimen surface to produce the desired thicknesses. By utilizing firmware lookup tables (i.e., erasable programmable read-only memory (EPROM) tables of geometric coordinates and process specifications) unique to each type of specimen, a single set of process control software routines could accommodate almost all types of parts to be coated. Changes in the process were readily incorporated by relatively easy software changes rather than hardware changes.

In APS process application to coating turbine parts, the microprocessor-based system proceeded as follows:

1) The part was loaded in the fixture and the plasma gun prepared for operation.

2) When the run button was activated, the microprocessor indexed the part to the gaging station and recorded the bare part reference values at specified locations.

3) The part was indexed through specified scan orientations while the plasma spray gun was automatically activated at the proper time intervals.

21
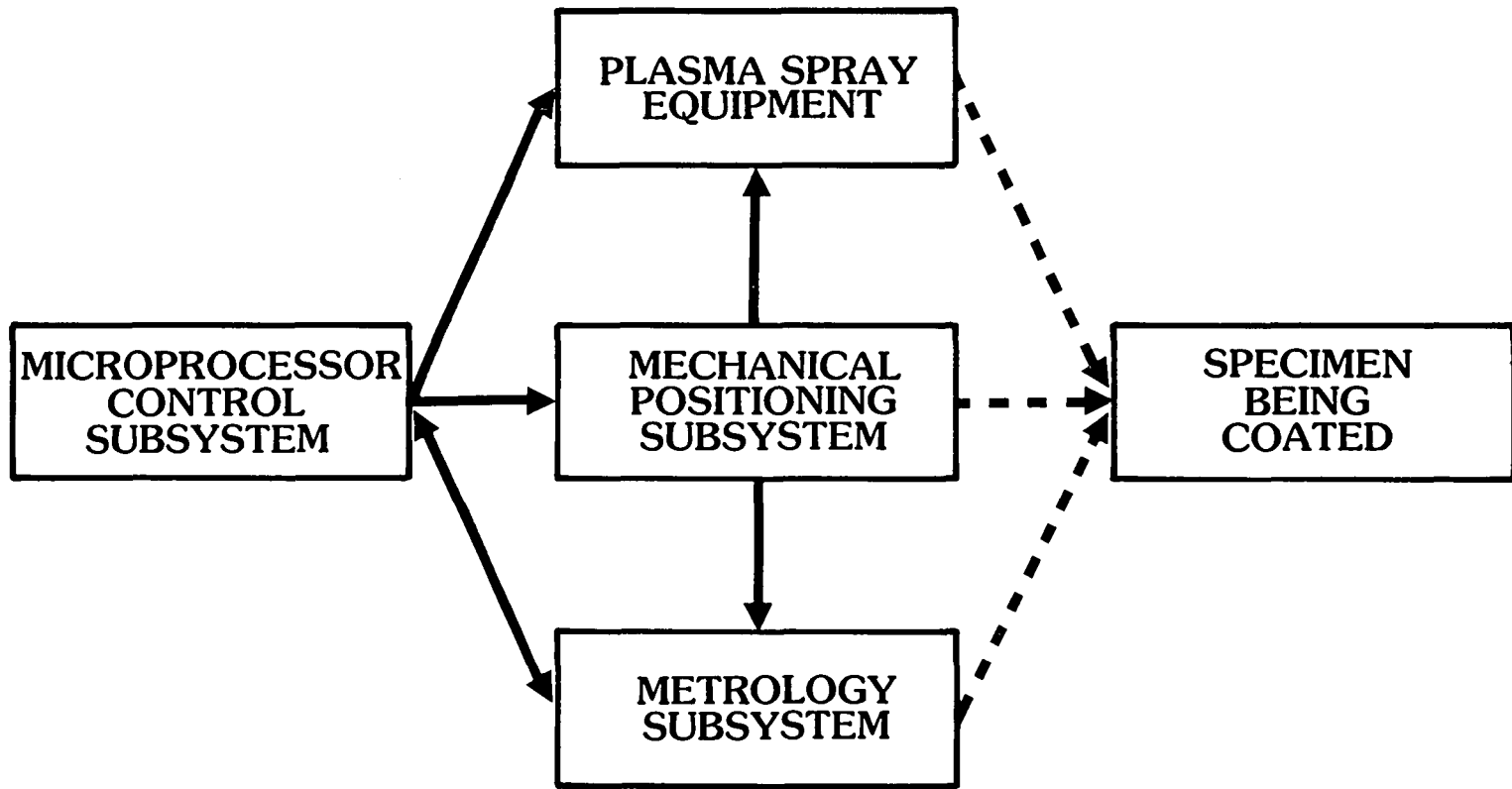
Figure 8.   APS System Functional Block Diagram.

4)   After completion of a percentage of spray scans slightly under the required number, the part was indexed to the gage position and the thickness values were measured at the specified locations.

5)   The microprocessor calculated the remaining scans required on each line to achieve the required coating thickness and uniformity.

6)   Step 3 was repeated for the required scan iterations.

7)   The part was indexed through a final gage cycle to verify the coating thickness and uniformity.

8)   If all portions of the part were not up to the required thickness, Steps 5 through 7 were repeated until all were; the microprocessor then output the actual measured coating thickness at each gage point on a digital printout.

9)   The part was indexed to the load position for removal and replacement with a new part.

The APS process subsystems developed to accomplish this procedure are described in the following paragraphs. The detailed data are in Appendices 3, 4, 5 and 6.

4.2.2 Mechanical Subsystem

The mechanical subsystem provides the required component positioning and scanning functions as commanded by the system controller. These functions may be further subdivided into three subassemblies: the specimen manipulator, the plasma spray gun manipulator and the optical detector positioner. Each of these subassemblies is described separately.

4.2.2.1   Specimen Manipulator

The primary application for the APS process on this contract was coating turbine airfoil geometries. Therefore the blade profile characteristics to be accommodated had a strong influence on the concept selected for specimen orientation. A major portion of turbine airfoil profiles can be closely generated by families of straight line segments lying within the blade surface. It therefore appeared reasonable to apply the plasma spray while scanning along these straight line segments. By sequentially positioning the various line segments, or scan lines, in front of the plasma spray gun so as to precisely control the spray deposition overlap between adjacent lines, very uniform surface coating thickness could be produced. Precise control of spray gun traverse speed provided coating uniformity along the scan lines. Since the coating thickness applied per scan line traverse was on the order of 13 to 25 μm (0.5 to 1.0 mil), the total coating thickness was built up of repetitive gun traverses over each scan line. Minor local surface thickness variations on the airfoil surface could therefore be minimized by slightly staggering the scan line locations between repetitive scans so as to "feather" the deposition profiles. All the motions required were implemented by relatively simple algorithms in the microprocessor logic controller.

To implement this APS process concept for the feasibility demonstration, a five axis specimen manipulator was designed and fabricated. The five axes of motion which the manipulator could impart to the blade specimen are indicated in Figure 9. The two translational axes, X and Y, controlled blade motion transverse to the locations of the plasma spray gun and optical detector and blade standoff distance from the gun or detector respectively. The three rotational axes, A, B and C, provided blade rotations around the X and Y axes and around a longitudinal axis of the blade, respectively. With these five degrees of freedom, any selected scan line on the surface of the blade airfoil could be positioned in a vertical orientation at a selected standoff distance from the spray gun. Only a single degree of freedom, an up/down scanning motion (ZZ), was therefore required on the plasma spray gun to spray the selected scan line. Likewise, only a single degree of freedom was required for the optical detector to allow it to be focused on any selected gage point on the airfoil surface. This was provided by the vertical translation axis Z.

The APS system concept illustrated in Figure 9 is thus seen to provide essentially two six-degree-of-freedom subsystems with only seven axes of motion. The five specimen manipulator axes plus the ZZ axis provide six degrees of freedom for plasma spray deposition on the specimen. The Z axis plus the five specimen manipulator axes provide six degrees of freedom for positioning the optical detector probe relative to the specimen surface during coating thickness metrology. This concept implementation required the minimum number of control interfaces to provide the required six degrees of freedom between the blade specimens and both the spray gun and the optical detector. In the most basic operational mode, the motions required of the X, Y, A, B and C axes were all index motions between coating deposition traverses of the plasma spray gun. These index motions positioned the selected scan line in front of the gun. Coordinates for the scan line were selected from firmware EPROM by the microprocessor. The firmware data also established the limits of the gun traverse and the desired coating thickness to be applied. The gun traverse cycles along the ZZ axis were normally the only component motion during the actual coating deposition.

A photograph showing the first model of the specimen manipulator implementation for the APS process feasibility demonstration is shown in Figure 10. This implementation was used for the process evaluations on the JT9D aircraft turbine blades. The system controller, the optical detector positioner and the plasma gun manipulator are also shown in this figure. The positioning subassemblies were mounted on a heavy duty machine base to provide the stiffness and ruggedness required for the high resolution measuring and positioning involved. The blade specimen (shown towards the right center of the assembly) is suspended upside down below the specimen manipulator translating cradle to minimize dust protection requirements during spray application. Actually, little additional dust protection was incorporated into the feasibility demonstration models. The leadscrews and gears were exposed. Covers would, of course, be required on a production model.

Figure 11 is a photograph of the second implementation of the mechanism for the APS process feasibility demonstration. This model was used for the larger electric utility turbine blades as well as the cylindrical burner rig test specimens coated for NASA. In concept this mechanism was identical to the first model. However, the second model was considerably larger, more rugged and more durable than the first model.
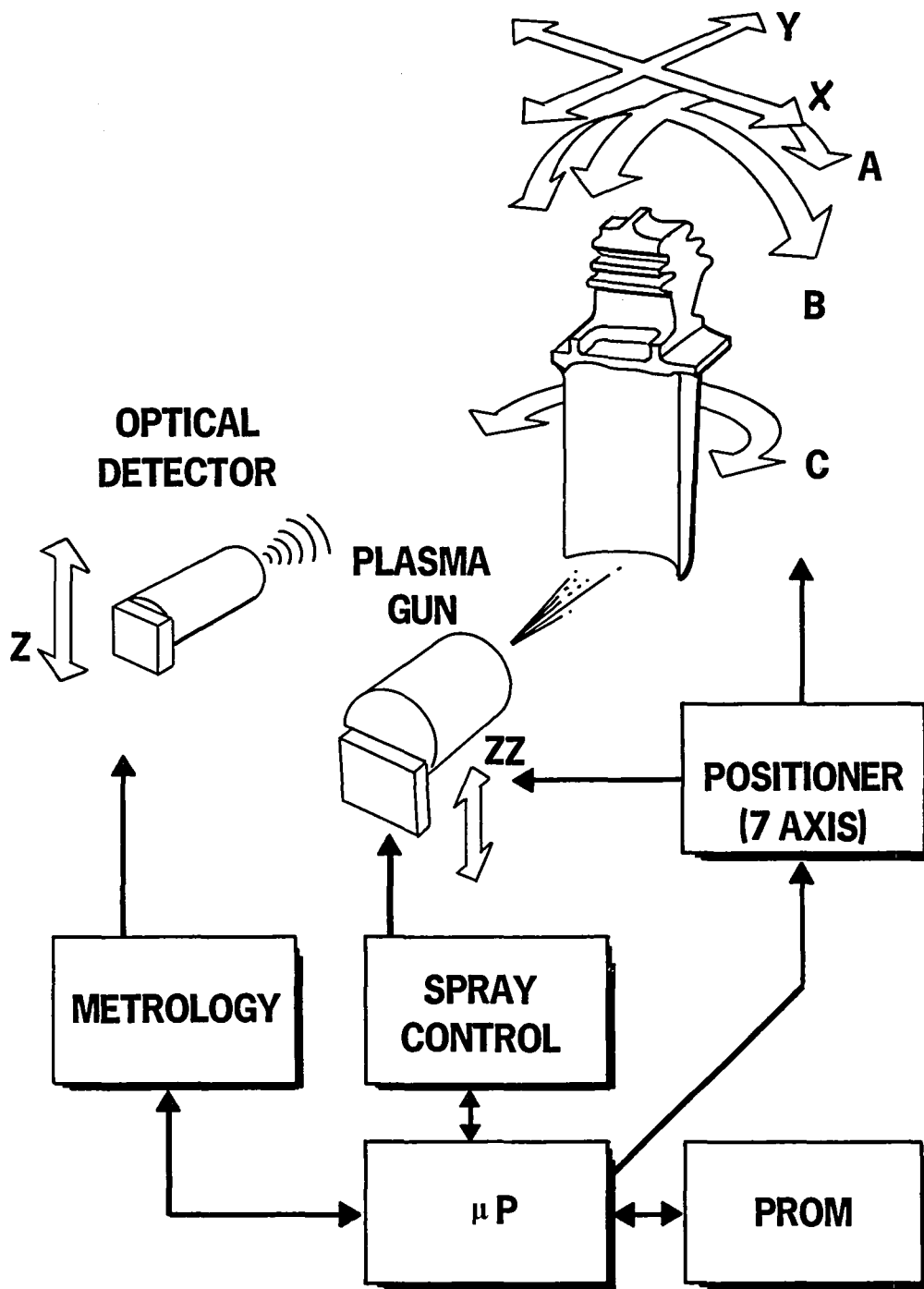
Figure 9.   APS System Concept Defining the Seven Axes of Motion.
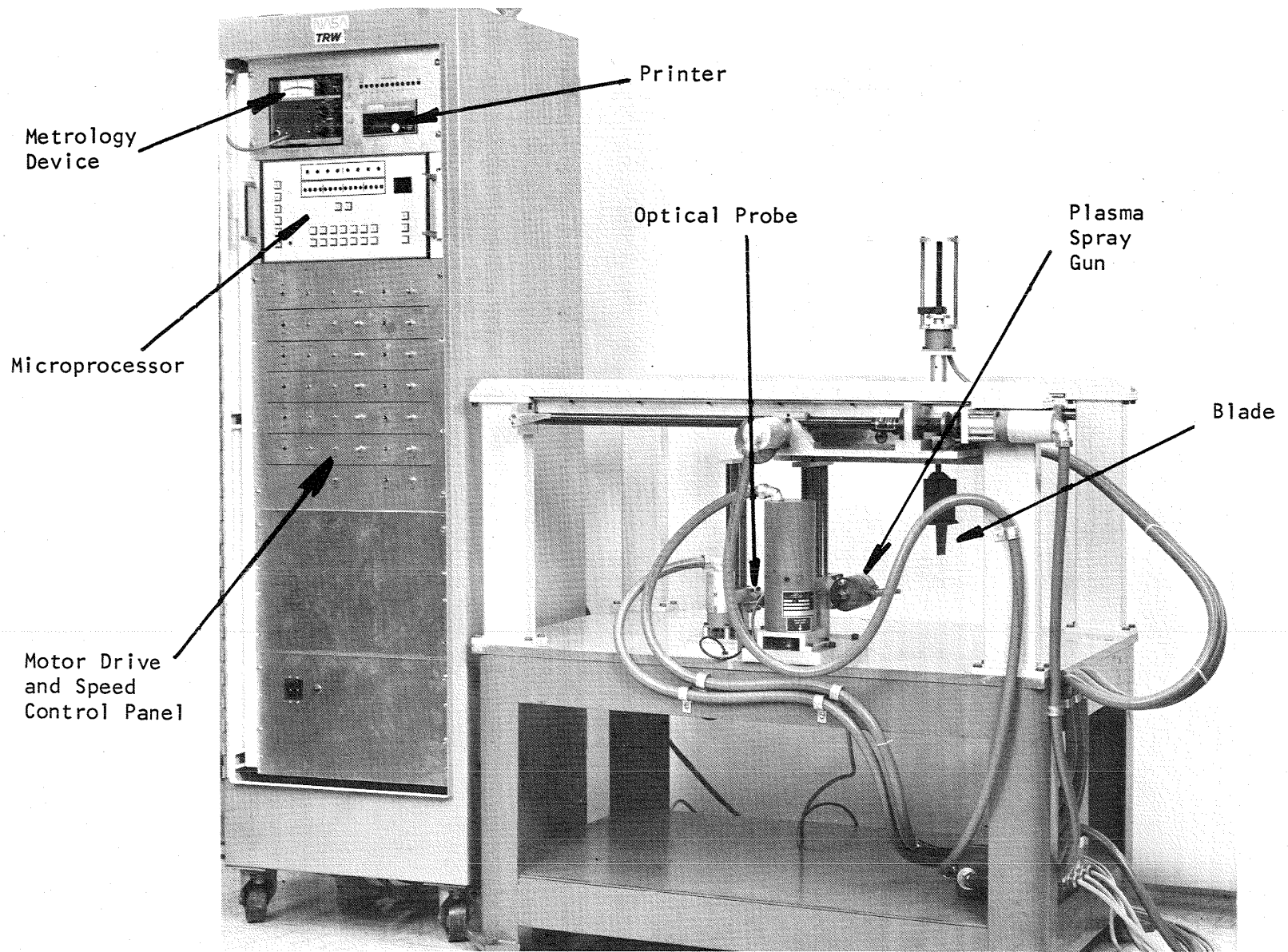
Figure 10. APS System Controller and Mechanism Model No. 1 as
Implemented for APS Process Feasibility Demonstration.
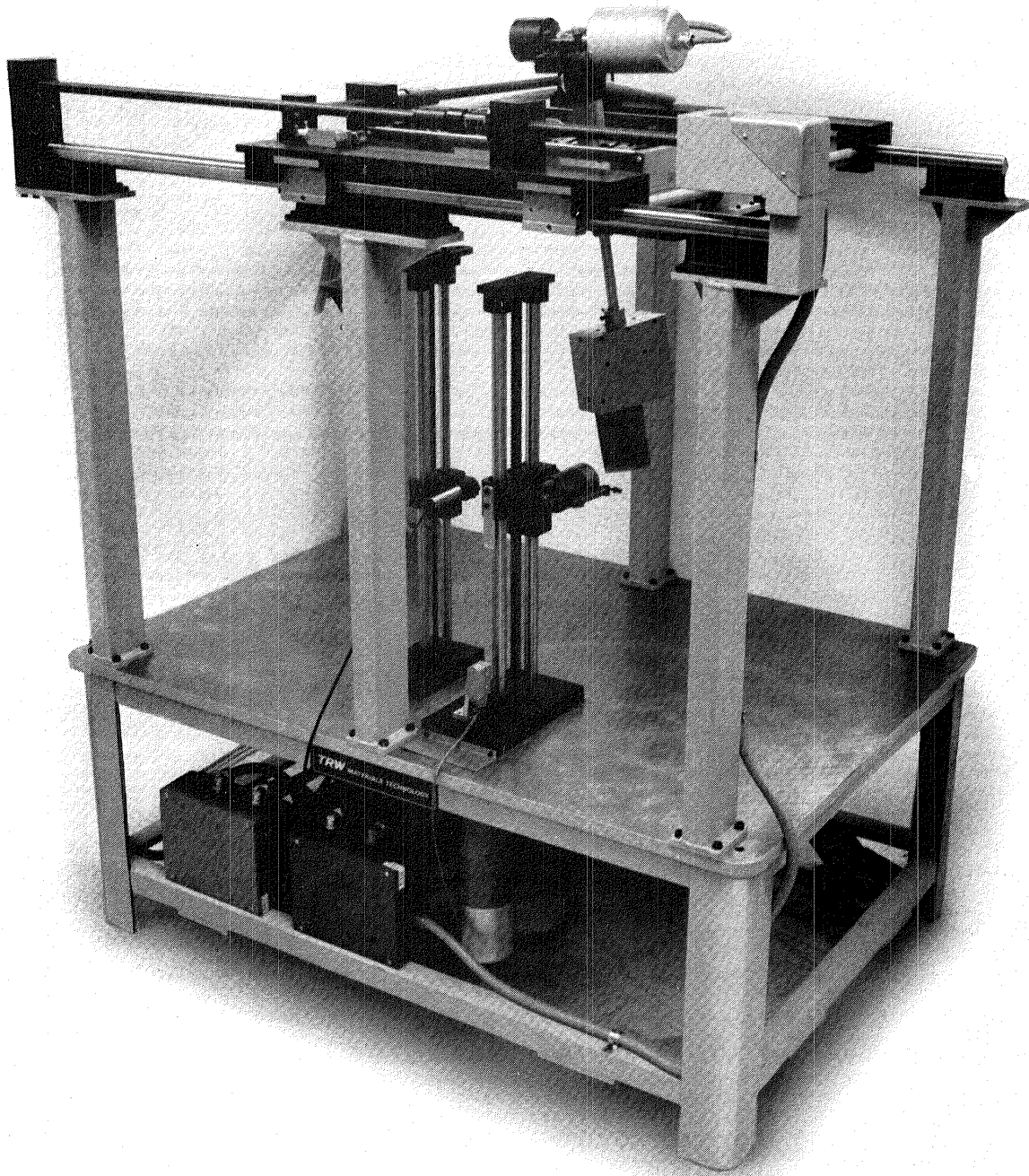
Figure 11.   APS Mechanism Model No. 2 for APS
Process Feasibility Demonstration.

Mechanical Design Concept

The X and Y translational axes of the specimen manipulator were provided by preloaded ball-screw/ball-nut subassemblies. The A and B rotational axes were also driven by ball-screw/ball-nut subassemblies due to incorporation of a unique dual gimbal assembly supporting the blade holding fixture. The lower gimbal assembly was fixed in the cradle bottom plate. The upper gimbel assembly was translated in a fixed horizontal plane relative to the lower assembly by the two ball-screw assemblies thru a dual slide assembly. This resulted in the compound angle rotations required by the A and B axes. The C axis on the Model No. 1 mechanism was a straight 180/1 rotational stepdown through a commercial speed reducer from the stepping motor to the blade holding fixture. On the second mechanism a much higher resolution stepping motor (2000 steps per motor revolution) was utilized along with an 18/1 rotational stepdown through a worm gear. This provided a much more rugged assembly capable of withstanding full motor stall torque in case of inadvertent collision between the specimen holding fixture and any other component. A photograph of the three rotational drive subassemblies on the second APS mechanism is shown in Figure 12.

All five axes on the specimen manipulator were driven by digital stepping motors. The step size resolutions provided by the respective motors through the leadscrew and/or gear assemblies were 25.4 μm (0.001 inch) for the X axis, 5.08 μm (0.0002 inch) for the Y axis, and 0.175 milliradians (0.01 degree) for the three rotational axes on the Model No. 1 mechanism. These resolutions were required to provide the desired ±38.1 μm (±1.5 mil) coating thickness tolerance on airfoils up to 25.4 cm (10 inches) square assuming a repeatability of ±1 step for each axis. On the Model No. 2 mechanism, due to its larger size and longer radii of rotation, the step size resolutions provided by the A and B axes were increased to 0.07 milliradians (0.004 degree).

Although very small resolutions were provided on the specimen manipulator axes, absolute accuracies of this magnitude were not critical. This was due to the technique of comparing differences in repetitive measurements to measure coating buildup. Repeatability of the positioning systems was a critical factor in the achievable measurement accuracy however. This meant that all backlash in the positioning loops had to be minimized. For these reasons it was possible to use rolled, rather than ground, ball screws on the specimen manipulator; but opposing, preloaded, ball nut pairs were utilized to minimize backlash. In addition, software compensation for the backlash was provided for the A, B and Y axes where the probability of problems was greatest.

Electrical Design Concept

To avoid potential EMI (electromagnetic interference) problems in the plasma spray facility, no shaft encoders were incorporated into the specimen manipulator. Only the relatively high level motor drive electrical signals were in close proximity to the plasma arc. These were heavily shielded. Solid state integrated circuit counters for each axis were located back in the microprocessor chassis. These counters kept track of the absolute position of each axis. Since these counters had no memory when
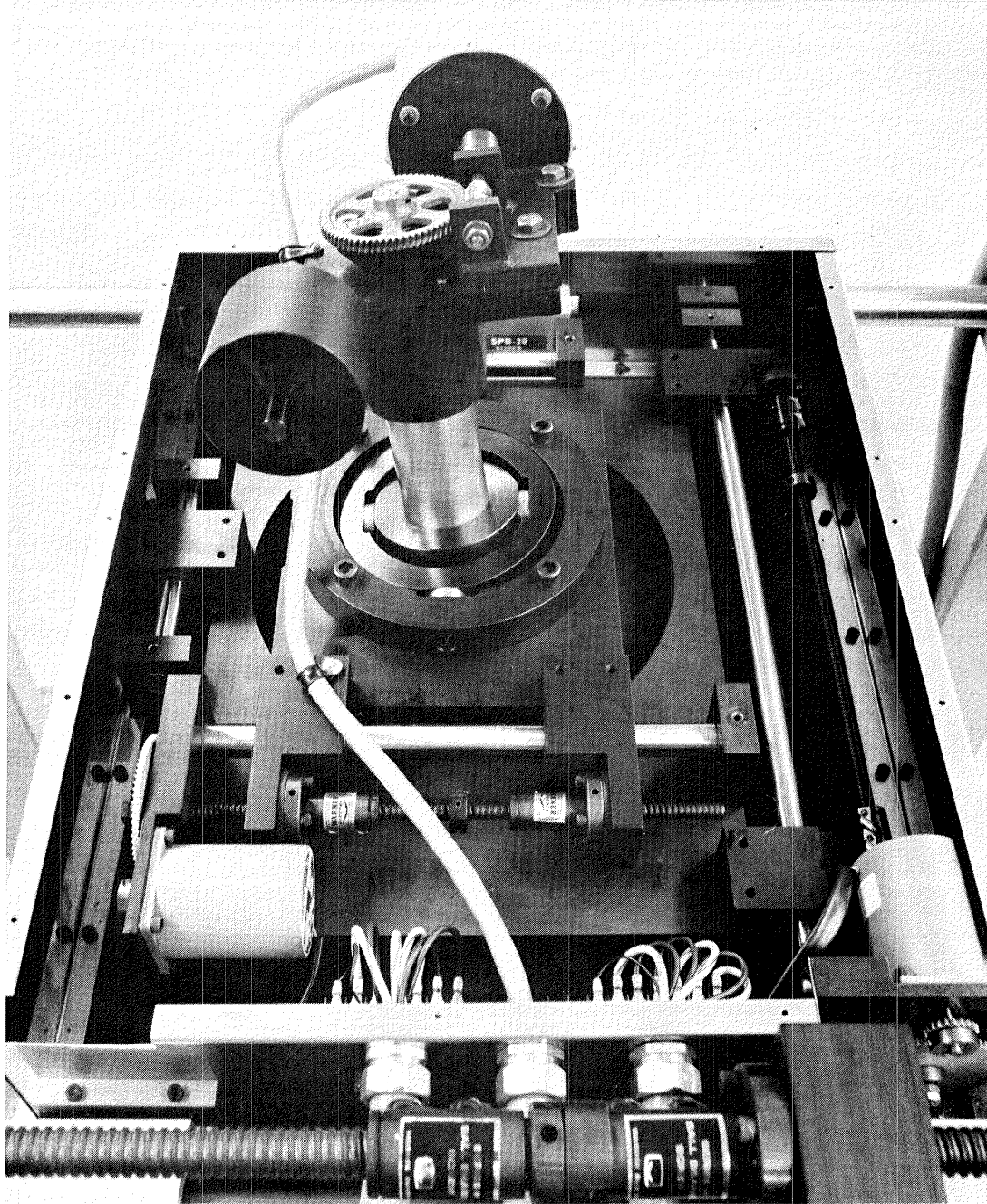
Figure 12.   Photograph of Dual Gimbal Subassemblies on
APS Mechanism Model No. 2.

power was removed from the system, it was necessary to equip each axis with a "zero reference" hard stop. After any system power up, each motor was automatically driven to its zero reference stop and the respective counter was cleared. The hard stop was provided at one extreme of ball screw travel for each axis. An auxiliary ball screw with a translating stop subassembly was mounted on the rear end of the C-axis motor on the Model No. 1 mechanism to provide a zero reference stop for this motor. This subassembly is visible above the top of the specimen manipulator in Figure 10. On the Model No. 2 mechanism this translating stop subassembly was replaced with a multi-revolution rotating stop subassembly. Limit switches were also added to this mechanism to remove motor power after driving against the zero reference stops.

<center>Specimen Holding Fixtures</center>

The holding fixture for supporting the specimen being sprayed was mounted on the end of the C-axis shaft. One of the earlier models of this fixture for JT9D first stage turbine blades is visible in Figures 10 and 13. The specimen was slid into the clamp and locked by a single set screw. A cover dropped down over the clamp, the blade root and the edges of the blade platform. This protected these areas from deposition of the sprayed coating without the need for masking. A later model of this fixture utilized a smaller, simplified, cylindrical design.

Figures 11 and 14 show the holding fixture used with the Model No. 2 mechanism for coating of the W501B first stage utility turbine blades. This fixture was similar conceptually to that for the JT9D blades except that it was much larger. One side of this fixture slid out to allow insertion and removal of the specimen being coated.

One additional item to be noted in Figure 14 is the graphite barrier shield assembly shown just above and in front of the plasma gun. This shield intercepted the plasma beam while the gun was reversing its scan motion at the top of the stroke. This minimized the heat injected into the fixture considerably. Both the barrier shield assembly and the specimen holding fixture had provision for cooling gas flow. These features were incorporated primarily to improve accuracy of the specimen gaging and are discussed in Section 5.1. Recent studies on improving the durability of thermal barrier coatings have indicated it may be desirable to cool the specimen during the coating process to improve the thermal stress characteristics of the coating (Ref. 4).

4.2.2.2   Plasma Gun Manipulator

Various views of the plasma gun manipulators used on the two APS mechanisms are visible in Figures 10, 11, 13 and 14. As discussed in the previous section, only a single degree of freedom was required for this subassembly, the ZZ-axis (Figure 9).

The spray gun motion was guided by two parallel vertical ball rod/ball bushing subassemblies. It was driven by a ball screw. The drive motor, unlike those on the specimen manipulator axes, was not a typical digital stepping motor. A stepping motor could not be found with a high enough torque/speed characteristic to handle the

<center>30</center>

Blade Holding
Fixture

Blade

Optical Probe

Plasma Spray Gun

Plasma Spray Gun
(ZZ Axis)
Drive Motor
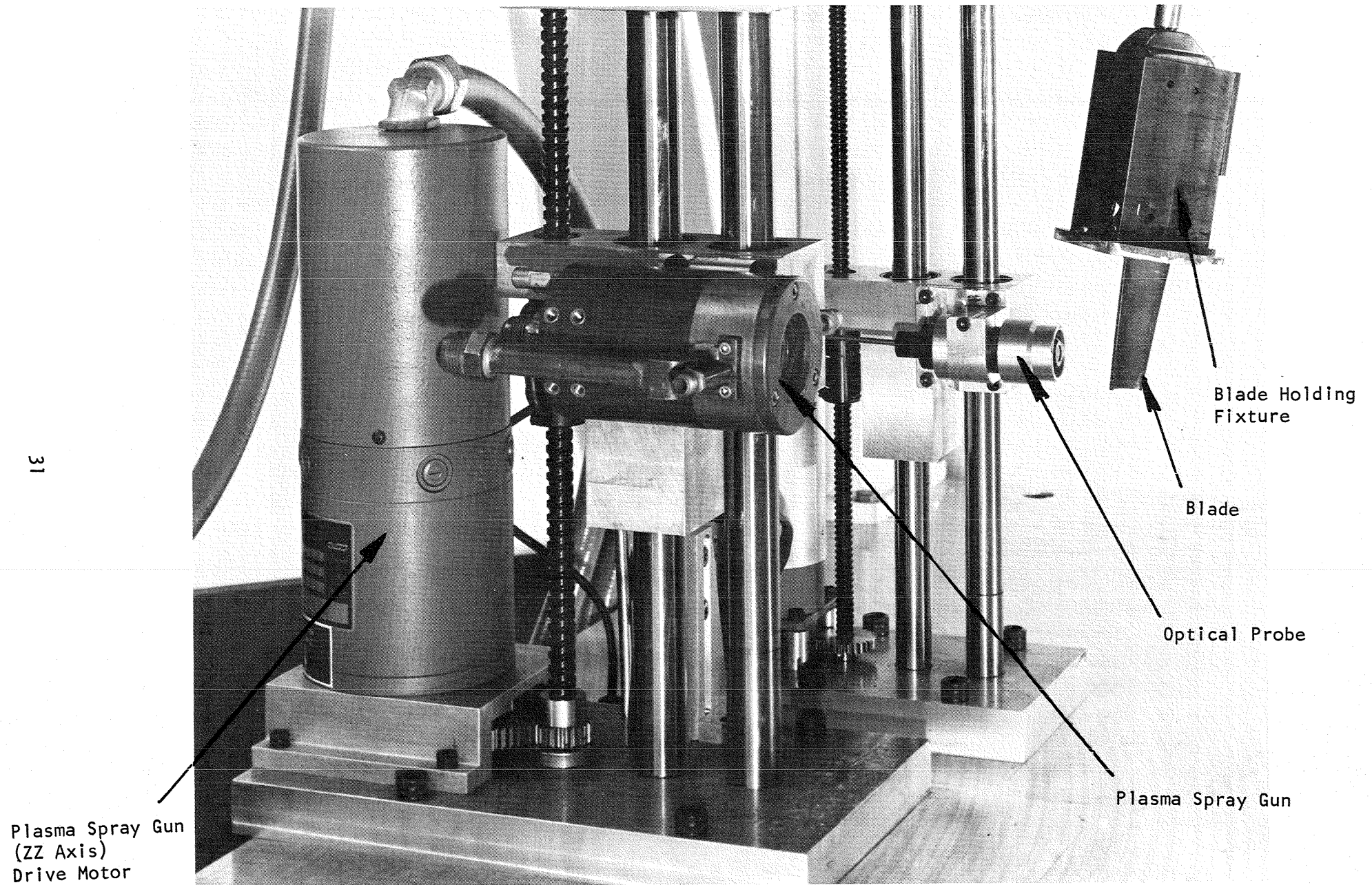
Figure 13.   Closeup of Blade and Optical Probe on Mechanism Model No. 1
During Gage Point Measurement Routine. Spray Gun also
Shown in Left Foreground.
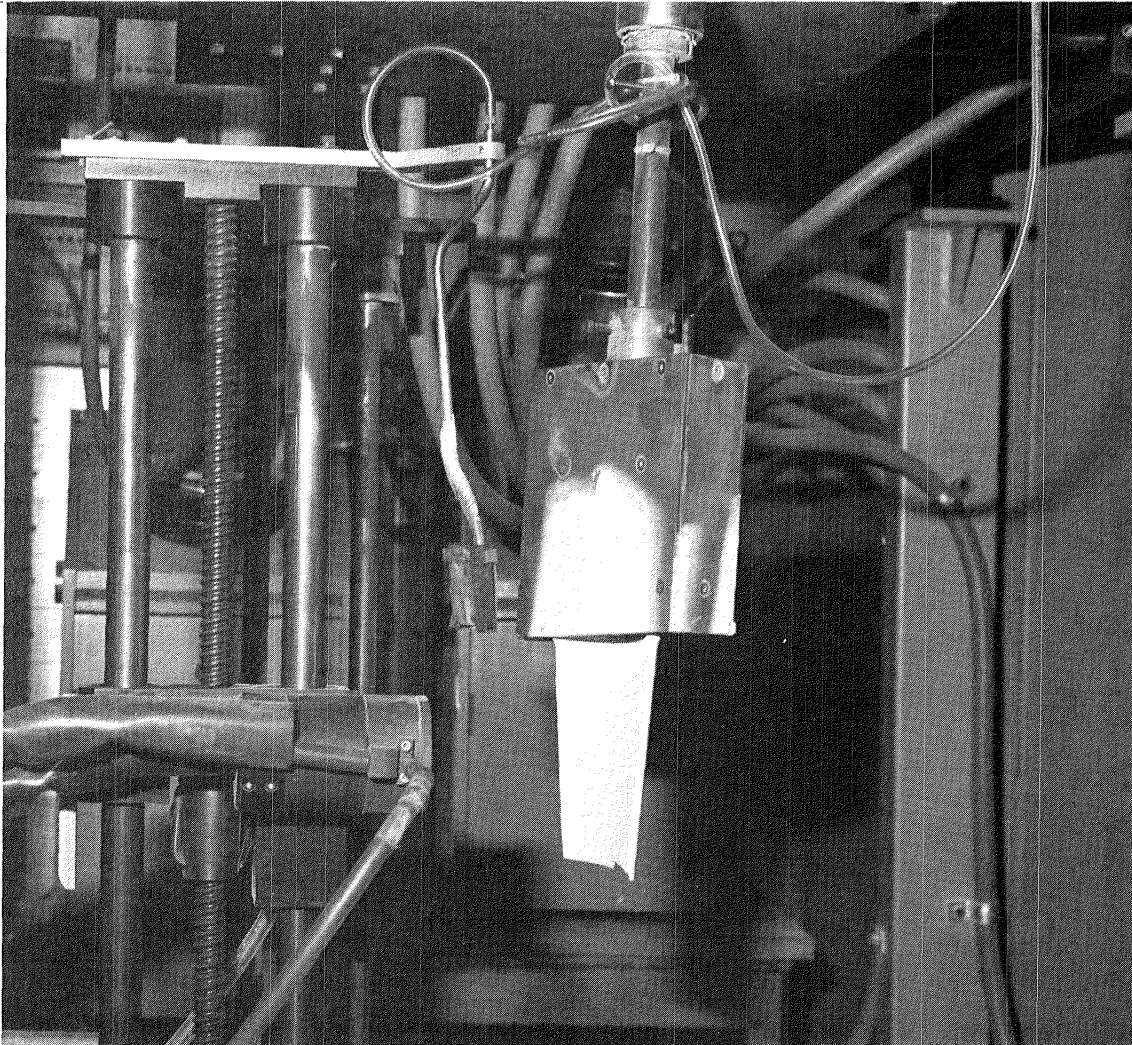
Figure 14.   Closeup of Plasma Spray Gun and Utility Blade Specimen
             on Mechanism Model No. 2.

requirements of this axis. Instead, the drive motor was a dc servomotor/resolver subassembly with a digital interface driver. To the control microprocessor it appeared almost identical to a digital stepping motor. In operation, the specimen manipulator provided a cyclic up/down scanning motion to the plasma spray gun. To achieve uniform coating deposition along a scan line the motor speed was digitally controlled by a remote clock pulse generator in the process control console. For the 40.6 cm/s (16 in/s) traverse speed specified by the initial deposition process study (Tables I and II), the clock rate was 2667 Hz.

The motor used on the plasma gun manipulator was of considerably heavier duty than would normally be required for the specified speed and torque load. The reason was the extremely short stroke length utilized for small specimens such as the JT9D turbine blade. For this specimen the manipulator provided between 3 and 4 scan line traverses per second while depositing the coating. A major portion of the motor duty cycle consisted of decelerating, reversing and accelerating the spray gun assembly at each end of the gun traverse. This had to be done very rapidly to provide uniform speed and hence coating deposition on the specimen. The limiting characteristic of the motor was therefore the thermal duty cycle rating rather than the torque/speed characteristic. While the duty cycle requirement could be lessened by employing fewer part traverses per second, this would result in considerably lower powder utilization efficiency. It would also create thermal problems in the blade clamping fixture subassembly by increasing plasma beam dwell on this subassembly during gun reversal.

Because of the high speed scanning requirement for the plasma gun manipulator and the lessened requirement for precise stationary positioning, the step size resolution for the ZZ axis was only 0.15 mm (6 mils). This was considerably coarser than all the other axes.

4.2.2.3   Optical Detector Positioner

The optical detector positioner for coating thickness measurement was very similar to that for the spray gun manipulator. It is also visible in Figures 10, 11 and 13. Again the motion was guided by two parallel vertical ball rod/ball bushing subassemblies and driven by a ball screw. However, a conventional stepping motor was used to drive the ball screw. A finer ball screw subassembly was also employed, since precise positioning was required instead of high speed scanning. Step size resolution along the Z axis was 25.4 μm (0.001 inch).

During the gaging operation, the selected gage point on the specimen surface was positioned in front the optical detector probe by simultaneously indexing the Z axis and the five specimen manipulator axes to the gage point coordinates selected from the EPROM firmware lookup table by the microprocessor. The Y-axis on the specimen manipulator then initiated a sequential stepping, or scanning, motion until the "valley point" in the optical detector response curve was located. The Y-axis coordinate position at this valley point was then stored in RAM (random access memory) by the microprocessor for use in coating thickness determination. (A detailed description of the metrology subsystem operation is discussed in the next section.) This procedure was repeated at each gage point specified for the particular specimen being coated.

33

The fiber optic probe utilized with the optical detector agreed with the general APS hardware design philosophy. It exposed no low signal level electronic circuitry to the high EMI ambient in the near vicinity of the plasma arc. Again the only electrical signals to the optical detector positioning subassembly were the relatively high level drive currents to the stepping motor.

4.2.3 Metrology Subsystem

The metrology subsystem consisted of the optical probe, the Y-axis of the specimen manipulator in the mechanical subsystem, and selected portions of the microprocessor.

The optical probe used in the feasibility evaluations was a commercially available instrument, the KD-100 Fotonic Sensor, manufactured by MTI Instruments, Latham, N.Y. It operated on a well-known principle illustrated in Figure 15. At one end a light source was used to illuminate half of the elements in a bundle of optical fibers, while a photo detector interrogated the other half of the fibers for returning light. At the other end the fibers were mixed together to form the measurement probe. The relative amount of light received at the detector as a function of distance of the probe from a reflecting surface is shown in Figure 16. The received intensity, which is zero at contact, increases linearly with separation as more and more of the cone of light from each transmitting fiber is reflected onto a receiving fiber. When the receiving fibers are completely illuminated, the intensity reaches a peak and then falls off as the square of the distance. This type of probe provides two regions of measurement. The rising side of the curve provides a region of high sensitivity but short range, while the falling side of the curve provides considerably reduced sensitivity, but is fairly linear over a much wider range. In either case the probe must be in relatively close proximity to the target.

A modification to this basic design is to add a lens system to the end of the probe to focus the end of the probe on the target. This allows a standoff distance which is a function of the optics and also allows the light spot to be made larger or smaller than the probe at the focal point of the optical extender. Figure 17 shows the intensity versus distance from the end of the lens system to the target. The portion of the curve from the focal point to the right is nearly the same as for the probe alone. A mirror image of this curve extends from the focal point in toward the target. Therefore there are two high sensitivity regions and two lower sensitivity regions. This makes it possible to make measurements with a significant standoff distance between the target and the probe.

Using the intensity versus displacement curve for measurement has a number of limitations, either with or without the optical extender. First, the intensity is a function of a number of factors other than the distance from the target. Among these factors are surface emmissivity, color, texture and curvature. This means that accurate measurements can only be made on a uniform surface. Second, the measurements are affected by the long term drift of the electronic readout. Third, the range over which measurements can be made is still limited by the probe design.
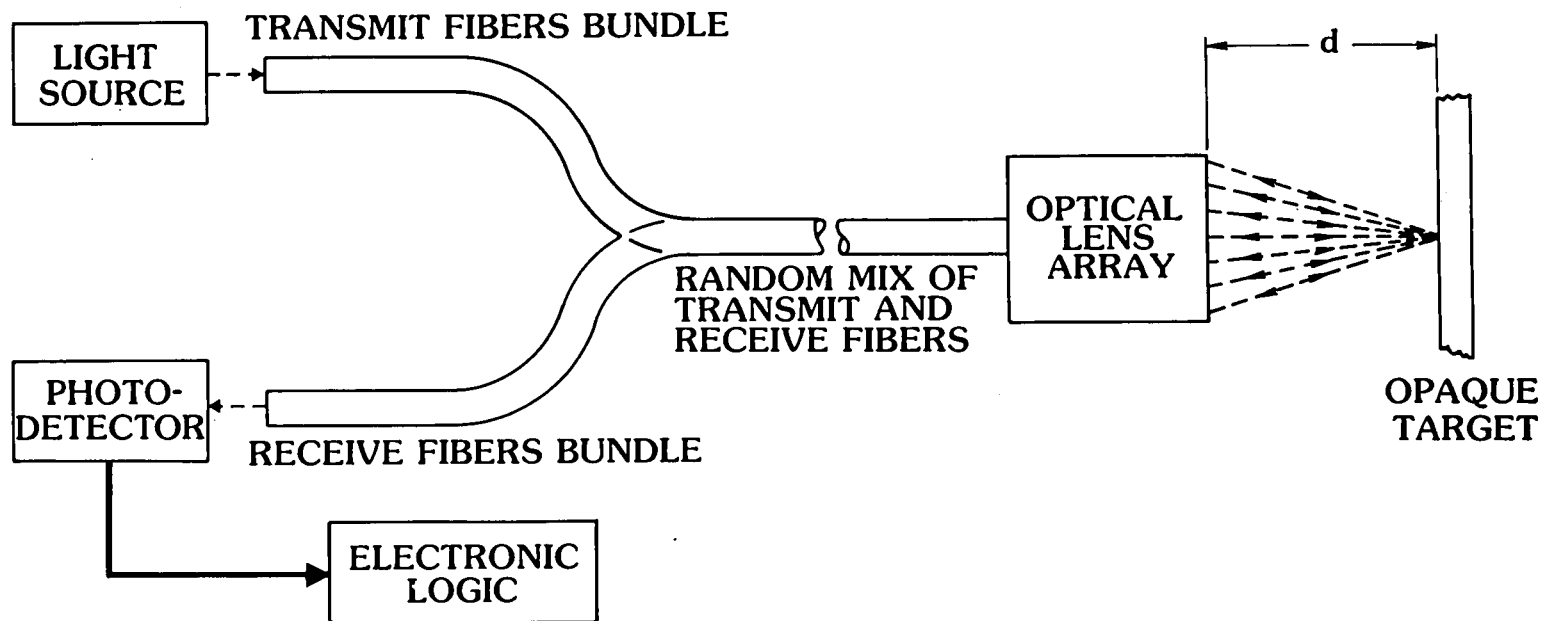
Figure 15.   Concept Diagram of Noncoherent Optical Probe.
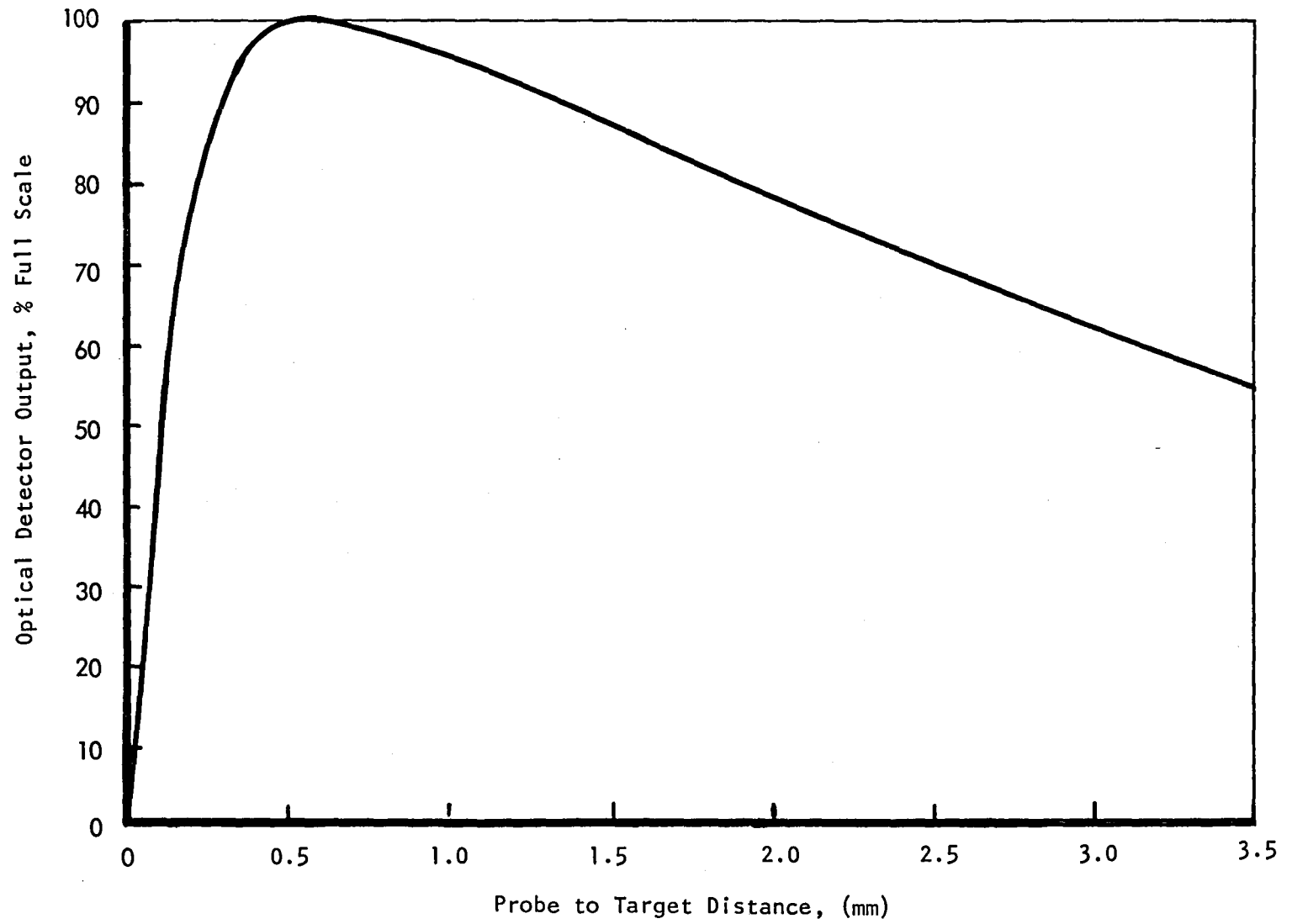
Figure 16.   Typical Optical Detector Response With Bare Fiber Optic Probe.
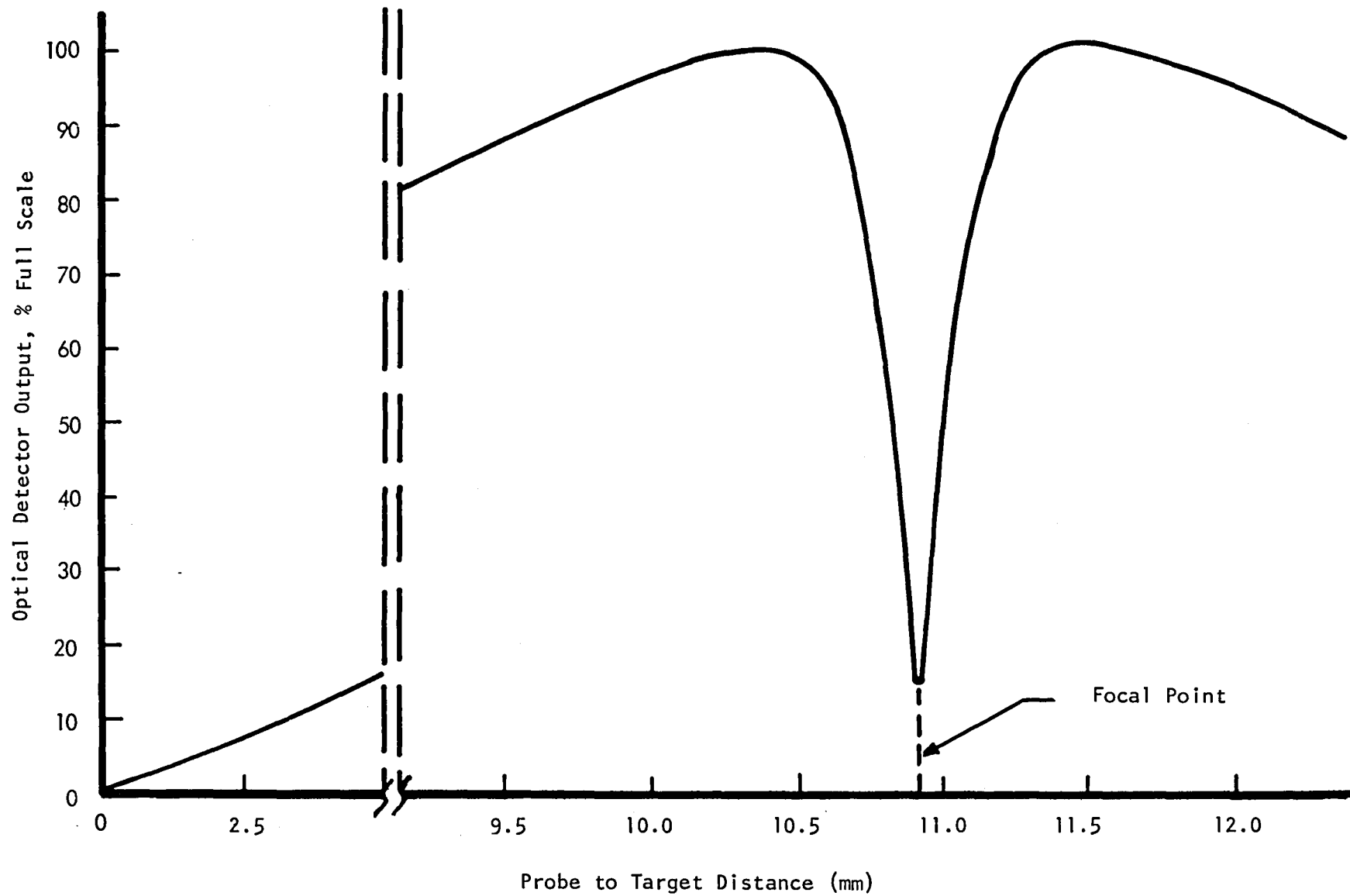
Figure 17.   Typical Optical Detector Response With Fiber Optic Probe
and Optical Extender.

These shortcomings can be overcome, however, by taking advantage of the characteristic curve created by the optical extender. At the focal point of the lens system, the intensity curve shows a sharp local minimum. The location of this minimum is independent of factors such as the color, texture and curvature of the target. It is a function only of the optical extender and the location of the probe with respect to the lens system. Using these principles, the optical probe and extender were mounted on a precision axis of movement with position indication. Thereby the probe was able to be moved with respect to the target until the local minimum, or valley, was detected. This technique is not affected by the target characteristics; its range depends only on the mechanical positioning device, and its accuracy depends on the precision of the positioning axis and the accuracy with which the valley can be located.

For the APS process this measurement scheme was implemented for the particular case of a random bundle of 76 μ m (0.003 inch) diameter optical fibers with an optical extender providing a 1 cm (0.4 inch) standoff distance. This probe, which had an active diameter of 0.22 cm (0.086 inch), had a sensitivity of 0.2 μ m/mV (7.8 μin/mV) over a range of about 76 μ m (0.003 inch) on the rising curve and a sensitivity of 0.6 μm/mV (23.2 μ in/mV) over a range of about 0.18 cm (0.070 inch) on the falling curve. The noise level at a response frequency of 30 kHz was about $\pm$35 mV which limited the high speed measurement accuracy. However, with appropriate filtering the noise could be reduced to less than $\pm$1 mV.

The output of this probe with the optical extender is shown in Figure 18 over a limited range near the valley. The location of the valley was at 1.10 cm (0.433 inch) distance between the target and the end of the optical extender. With a maximum output of 9V the output at the valley was 0.5V. The width of the valley over which the voltage change was less than 1mV was about 10 μ m (0.0004 inch). The target in this case was a bright, but fairly rough ZrO_2 plasma-sprayed surface. For changes in the brightness, curvature or surface texture of the target, the difference between the peak and valley voltages increased or decreased. This had a small effect on the accuracy with which the valley could be detected. Under the various conditions, the location of the valley did not change.

For the purpose of making measurements, the end of the fiber optic bundle and optical extender were mounted on the Z-axis, which positioned the probe vertically along the length of the airfoil. The A, B, C and X-axes of the specimen manipulator were used to position the gage point to be measured in front of the probe with the surface normal to the probe. The Y-axis was then used to change the probe to airfoil distance in 5.0 μ m (0.0002 inch) increments. The filtered analog voltage output from the probe was fed into an analog-to-digital (A/D) converter which could be sampled by the microprocessor (μP) control system. The μP also controlled the Y-axis stepping motor to change probe-to-target distance, and determined where the valley was. For safety purposes the target was brought in close to the probe and then valley detection was accomplished while backing away from the probe. The valley detection program was set up so that if the valley was not detected on the first pass, one or more parameters were incremented and another attempt was made. This allowed measurements to be made at maximum sensitivity on targets which varied considerably in reflectivity.
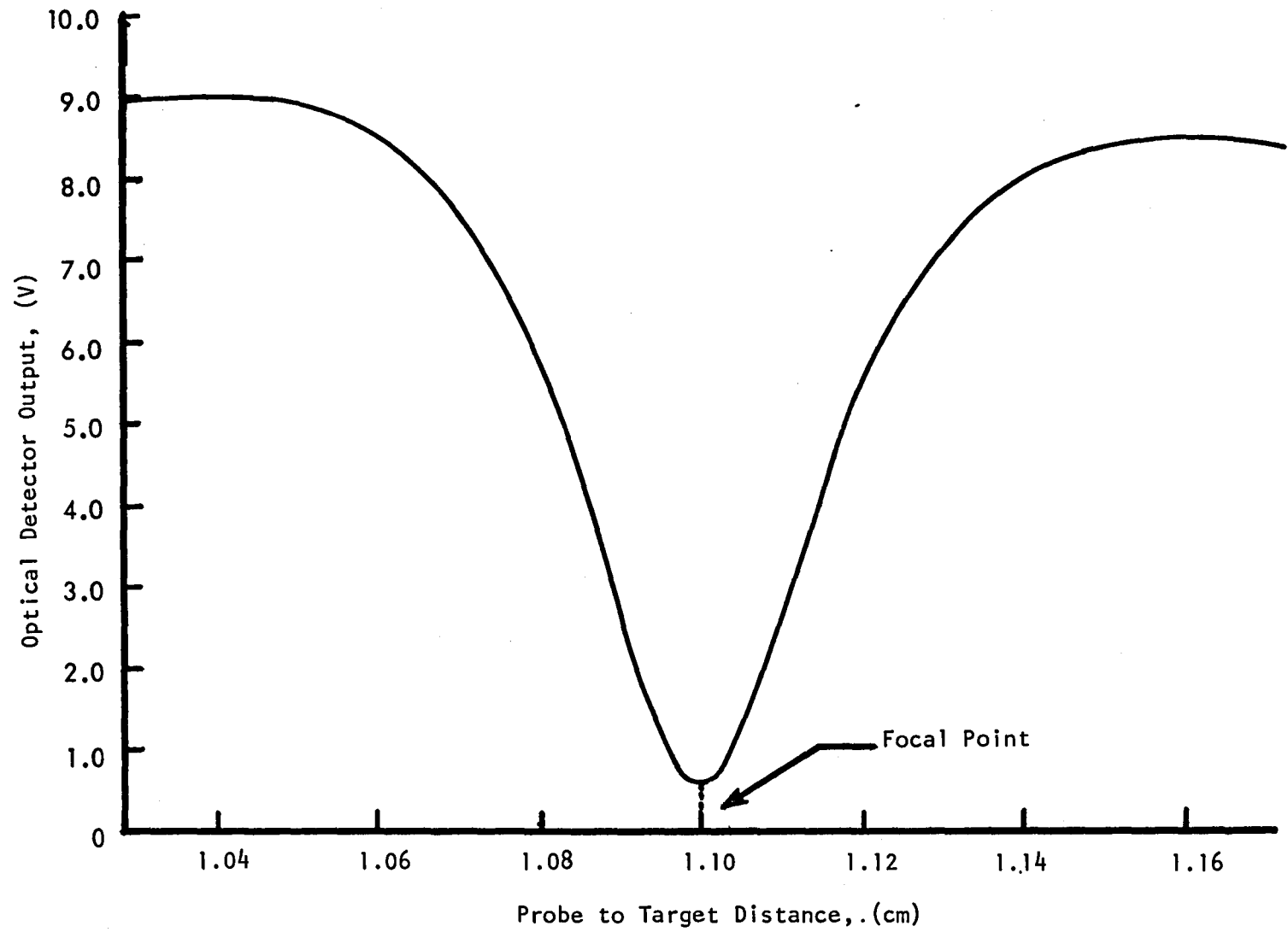
Figure 18.   Optical Detector Output Response in the Valley Region.

The procedure by which the valley was detected by the μP is illustrated in Figure 19. A set of eleven memory locations, number 0 to 10, was set up to constitute a first-in-first-out (FIFO) memory. On the first step the voltage was read and entered into the first FIFO location. On each successive step of the motor a new voltage reading was entered into the first FIFO location and all previous measurements were moved back one location in memory. A reading which reached the last memory location was lost on the next step. The FIFO, therefore, always contained the last eleven voltage readings and their corresponding probe coordinates in steps. When the first reading exceeded the last by a specified voltage, the valley was assumed to be detected and the coordinates of the sixth memory location were taken as the valley position. The program was also set up to detect the negative slope preceding the valley and the positive slope following the valley by looking for appropriate differences between the first and last FIFO readings. Parameters that could be varied automatically searching for the valley were the voltage differences that defined the slopes and the valley, and the position at which the valley detect routine started. Another feature of the program was that the number of measurements taken at each step could be any multiple of 2 from 1 to 128. The value entered into the FIFO was then the average of the readings. This feature could be used to minimize the effect of noise spikes. In the final system software configuration, the FIFO length could also be varied up to 32 memory locations to further minimize noise sensitivity.

For measurement of coating thickness, the Y-coordinate at the valley for each measurement point on the bare blade was stored in a memory location designated Table 0. After coating the specimen, each point was measured again and the new Y-coordinates were stored in a second memory location designated Table 1. The coating thickness in hexadecimal steps of the Y-axis was determined by subtracting the values in Table 0 from the corresponding values in Table 1. The μP converted this data into decimal values in mils and output it on the printer as a list of measurement point numbers and corresponding coating thicknesses.

4.2.4 Control Subsystem

The APS system controller was the subsystem that tied all the other subsystems together into one integrated system. Since the control subsystem was microprocessor-based, its development included both hardware and software efforts. These efforts are summarized in the following sections.

4.2.4.1 General Discussion

The general configuration of the APS process control subsystem is shown in the simplified block diagram in Figure 20. The subsystem was configured around the bus concept; i.e., all system components interfaced into the microprocessor bus or motherboard. Each appeared to the microprocessor as one or more memory address locations. Using standard memory addressing commands, the microprocessor could thus have two-way communication with any system device just as it would read from or write into memory.
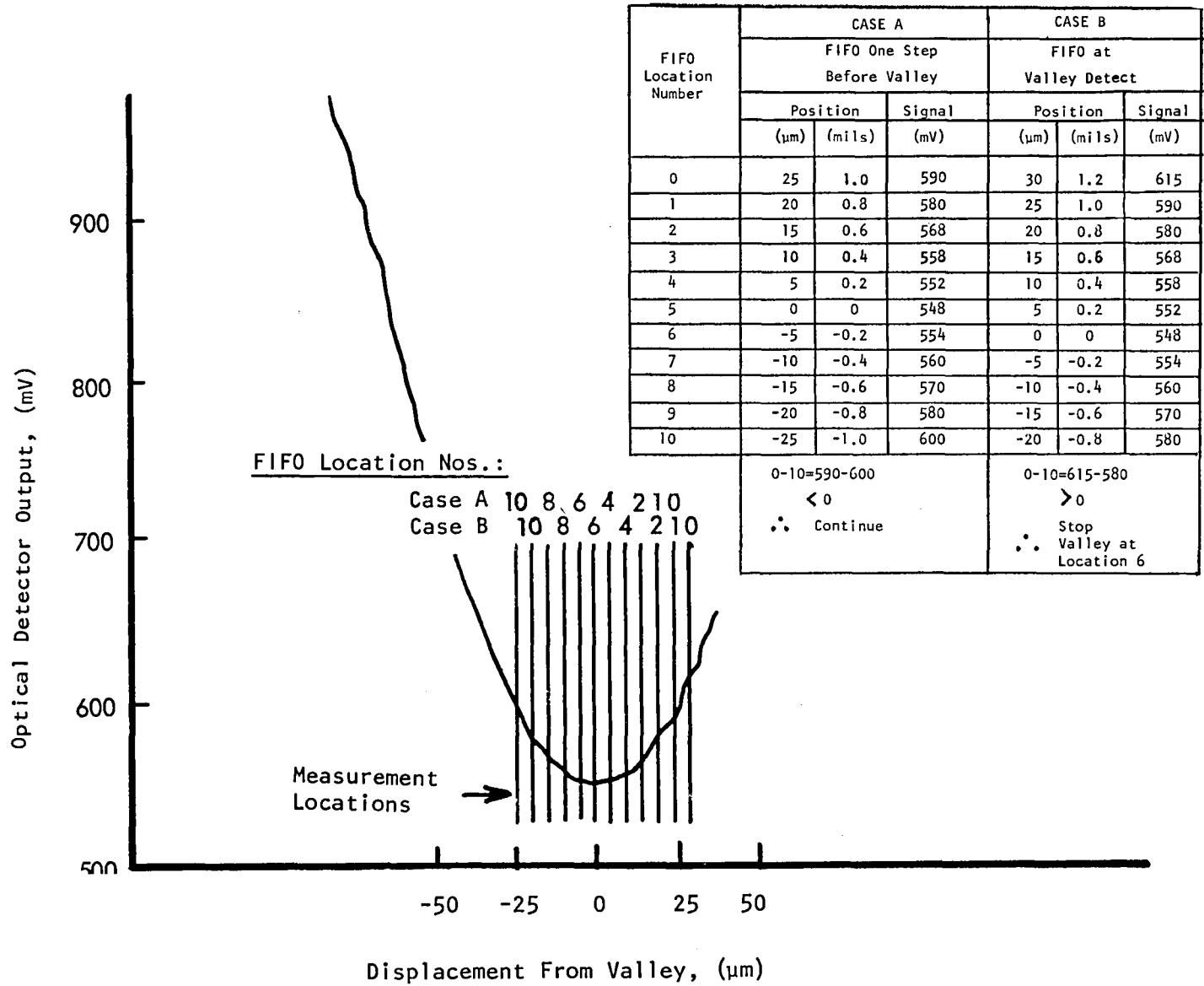
Figure 19.   Example of FIFO Valley Detect Concept.

The table shown in the figure:

FIFO Location Number	CASE A FIFO One Step Before Valley			CASE B FIFO at Valley Detect		
	Position		Signal	Position		Signal
	(μm)	(mils)	(mV)	(μm)	(mils)	(mV)
0	25	1.0	590	30	1.2	615
1	20	0.8	580	25	1.0	590
2	15	0.6	568	20	0.8	580
3	10	0.4	558	15	0.6	568
4	5	0.2	552	10	0.4	558
5	0	0	548	5	0.2	552
6	-5	-0.2	554	0	0	548
7	-10	-0.4	560	-5	-0.2	554
8	-15	-0.6	570	-10	-0.4	560
9	-20	-0.8	580	-15	-0.6	570
10	-25	-1.0	600	-20	-0.8	580

Case A: 0-10=590-600, < 0, ∴ Continue

Case B: 0-10=615-580, > 0, ∴ Stop Valley at Location 6

FIFO Location Nos.:

Case A   10 8 6 4 2 1 0
Case B   10 8 6 4 2 1 0

Measurement Locations

Optical Detector Output, (mV)

Displacement From Valley, (μm)

41

Figure 20.   Block Diagram of APS Process Control Subsystem.

Using the bus concept the system was readily expandable. The only limitation on the number of system devices was the maximum number of addressable memory locations - 64k. Thus, it was easy half way through system development, to add a digital printer to furnish hard copy inspection readouts of the actual coating thicknesses deposited on each specimen. It was also possible to plug a remote terminal into the bus during system checkout or modification to exercise keyboard control of any system device or the entire system. In a production model it would be a straightforward task to interface additional plasma spray console parameters into the bus. Some of the spray parameters manually preset on the APS process implementations for the feasibility evaluations performed on this program could thus be automatically preset or adjusted by the microprocessor as desired.

The devices interfaced into the microprocessor bus in the feasibility models of the APS process controller are indicated in Figure 20. These included microprocessor memory for program control software, firmware and scratchpad. Control interfaces for seven motor-driven axes on the specimen manipulator, the optical detector positioner and the plasma gun manipulator were provided. A signal conditioning interface fabricated around an A/D converter allowed the microprocessor to read the output of the optical detector on command. Five triac output interfaces allowed the microprocessor to exercise control over the plasma spray console as previously described in Section 4.1. Finally, the microprocessor front panel also interfaced into the bus. This panel contained a number of control pushbuttons, a switch register and several LED (light emitting diode) status and data displays. The digital printer could also be grouped as one of the display outputs, though it was physically located on a separate panel.

Utilization of the printer could conceivably eliminate an entire operation in the production process. It could provide a record of the actual applied coating thicknesses as a byproduct of the deposition control process. This would eliminate the need for a subsequent gaging inspection station. Each of these interfaces is described in more detail in the following section on hardware development.

4.2.4.2   Hardware Development

A more detailed functional block diagram of the APS system controller is shown in Figure 21. This figure summarizes the hardware configuration of the various interfaces.

A Motorola M6800 microprocessor was the heart of the APS system controller. At the time TRW was designing pc (printed circuit) boards to utilize this chip, a set of populated boards became available. The MM02 CPU (central processor unit) board was subsequently selected for use on this project. Auxiliary pc boards provided up to 16k of EPROM and 8k of dynamic RAM. The M6800 bus actually consisted of three buses, a 16-bit address bus, an 8-bit bidirectional data bus and a control bus. These buses and a number of additional power supply, supervisory control and clock lines were all contained on a large pc motherboard located in the microprocessor chassis. The CPU board, the memory boards and all system device interface boards plugged into this motherboard.

43
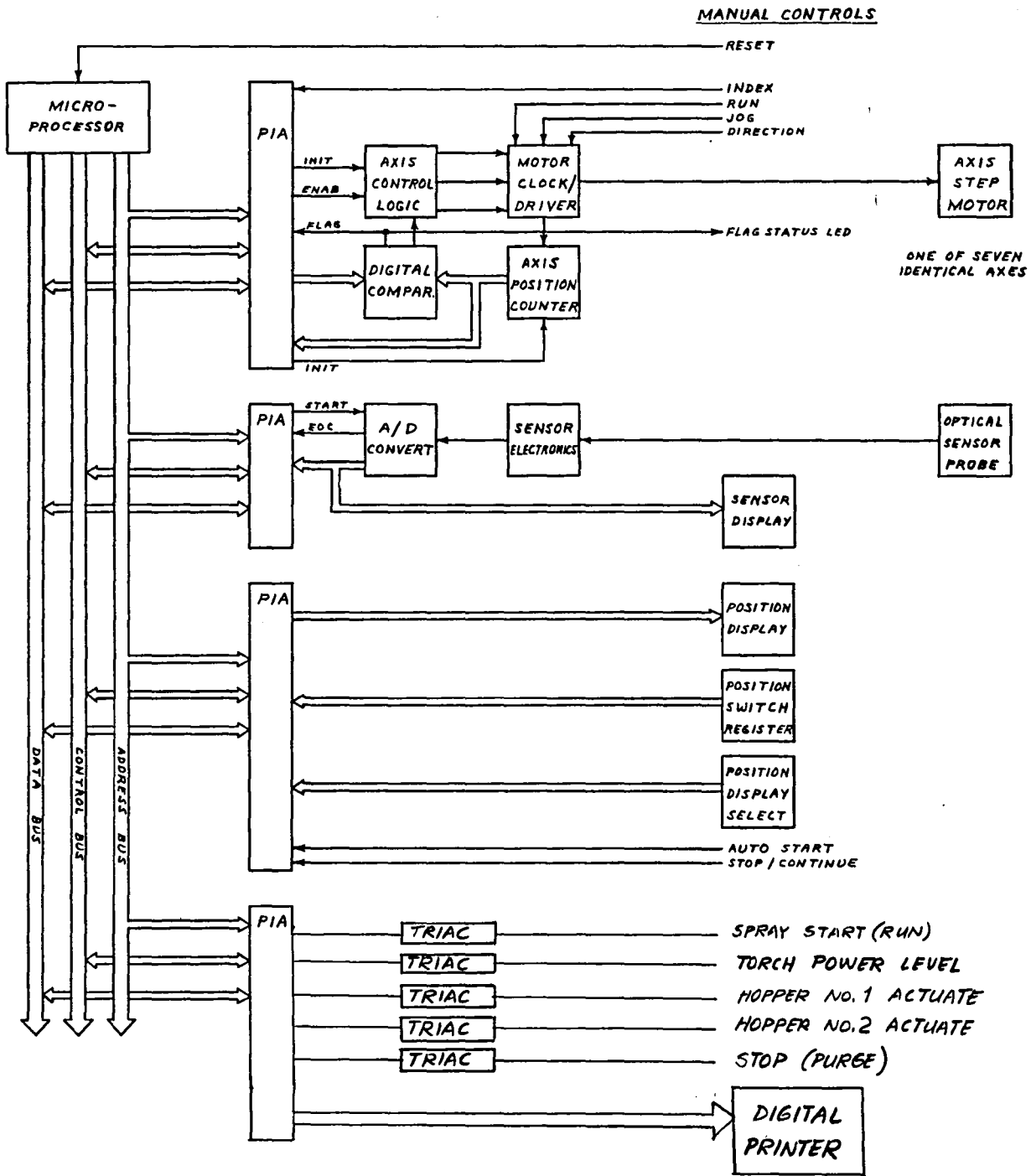
Figure 21.   Functional Block Diagram of APS System Controller.

Each device interface contained a PIA (peripheral interface adaptor) chip to provide bus interface. Instead of the normal M6820 chip, an Intel 8255 PIA chip was used in the APS. This chip provided four extra I/O ports (24 instead of 20) which greatly simplified design of the motor interfaces.

Figure 21 indicates the functional block diagram of a typical stepping motor interface. The motor clock/driver board was a commercial board obtained from the stepping motor vendor. It contained adjustable clock pulse generators for high and low motor speeds, pulse rate ramping to accelerate and decelerate the motor without pole slippage, motor driver circuits and TTL (transistor-transistor logic) compatible remote control inputs. The interface board also contained a 16-bit integrated circuit axis position counter which counted the drive pulses fed to the motor to record instantaneous motor position. The counter counted up for motor steps away from the zero reference stop and down for motor steps toward the stop. During system startup initialization, the counter was cleared when the motor was driven against the reference stop. The counter output was fed to the PIA to allow it to be read by the microprocessor. It was also fed to one input of a 16-bit digital comparator. The other input of the digital comparator was a reference position register in the PIA.

In operation the microprocessor could set any desired position reference in the motor PIA register. The comparator indicated to the axis control logic circuits the motor direction required to move to the designated reference position. The motor would move in that direction upon receipt of a "motor enable" signal from the microprocessor. When the motor reached the designated position, indicated by equality of the two digital inputs to the comparator, the comparator signalled the control logic circuits to cease motor motion. It also flagged the microprocessor that the motor had reached the commanded position. The digital comparator was of unique design, in that it supplied an "almost equal" output to the control logic as well as an "equal" output. This allowed the logic to drive the motor at high speed until almost at the designated target position, then ramp down to a lower approach speed so as to stop without overshoot or pole slippage when comparator inputs equality was reached. During system startup initialization, the control logic circuits drove the motor in the negative direction into the zero reference stop to permit counter synchronization.

The combination of hardware and software logic utilized to control the axis drive motors combined some of the good features of each mode of control. The hardware logic circuits could be "tuned" to individually optimize the high and low speed performance of each axis without unnecessarily overcomplicating the software. The microprocessor could thus operate in a supervisory handshake mode by designating a target to each motor and then proceeding to other tasks until flagged by the axis hardware that the targets had been reached. Thus, all motors could simultaneously proceed at their individual optimum speeds. Not only did this provide better CPU utilization, but it allowed the system to proceed at optimum speed regardless of specimen size or geometry. The same system software could thus be utilized with very different specimen geometries by providing firmware lookup tables of target coordinates unique to each specimen. The system automatically proceeded at maximum speed in each case without software modification.

The six interfaces for the stepping motor axes were identical. The seventh motor axis, for the plasma gun manipulator servomotor, was very similar. The motor driver for this axis did not contain an internal clock pulse generator so an external clock circuit was fabricated. Also, only a standard digital comparator was required for this axis. It was not necessary to switch over to a lower speed clock upon approaching the target with the servomotor. The internal control loops within the motor translator accomplished the motor ramp to zero speed, without overshoot, automatically. Two motor interface circuits were fabricated on each interface board for insertion into the microprocessor motherboard. A total of 3-1/2 boards was therefore required to accomodate the seven motor interfaces. The motor driver boards were mounted directly on the motor power supplies, eliminating the need for separate card racks for these circuits.

The interface for the optical sensor contained a 12-bit A/D converter in addition to the PIA chip. The microprocessor could signal the A/D converter to initiate a sample of the detector output by sending a "start conversion" pulse. The conversion took approximately 25 microseconds, after which the interface signalled the microprocessor that the digitized data was ready to read. The rapid conversion time allowed the microprocessor to take multiple samples of the detector output after each step of the Y-axis motor during gaging operations to average out the possible detrimental effects of noise spikes, interference, etc. The last digitized data output was also displayed on a front panel LED register for use in system checkout. It was also necessary to provide high frequency ripple filtering on the analog input to the A/D converter to utilize the full 2.44 millivolt/bit sensitivity of the A/D converter. The optical detector interface circuits also occupied one half of an interface board in the microprocessor chassis. These circuits were located on the same board as the plasma gun manipulator servomotor interface logic circuits.

The interface circuits for the digital printer and the plasma spray console also shared a common interface board. The interface for the printer was essentially just the 8255 PIA chip and associated address select logic. The interface for the plasma spray console consisted of bistable latches with associated address select logic. The latches were set by the microprocessor to actuate the respective spray console functions. Heavy duty solid-state ac switches (TRIAC's), located at the bottom of the APS control console, were actuated by the interface latches through optical decouplers. The TRIAC's, in turn, actuated the remote interface relays in the plasma spray console. LED status lights were mounted on the rear inside of the APS control console to monitor the status of the control output signals to the plasma spray console.

The final interface board handled the various microprocessor front panel controls and displays. This board contained three 8255 PIA chips, associated address select logic, bistable latches and lamp drivers. The front panel displays consisted of two LED status registers, one 8-bit and one 16-bit, which could be utilized to display contents of memory locations and registers such as the contents of the position counters. Status lights were also located in the front panel pushbuttons. A four hexadecimal digit thumbwheel switch register could be used to manually insert data to selected registers. These displays, the register, and most of the pushbuttons were strictly for use in system evaluation and/or setup when a remote terminal was not

available. These pushbuttons could also be utilized to manually index the various axis motors to designated coordinates, but the remote alphanumeric terminal was much more convenient to use. The only front panel controls normally used were the "Run" pushbutton and occasionally the microprocessor "Reset" pushbutton. The microprocessor front panel is visible in Figure 10.

Considerable attention was given to designing the hardware to provide insensitivity to the high EMI environment within the plasma spray facility. As mentioned previously, this was one of the major reasons for utilizing the remote position counters instead of axis encoders. All cabling outside the APS control console was shielded. The outputs to the plasma spray console were also optically decoupled to minimize EMI conducted back into the APS control console. These precautions paid off when the system was ultimately installed in the facility.

Manual controls for the seven axis drive motors were also provided on the front of the APS control console. (See Figure 10.) These controls bypassed the microprocessor and interfaced directly into the motor drivers. With these controls each motor could be jogged (single-stepped) or run at high or low speed in either direction. The high and low speed adjustments were also located on this panel. These controls were often used in system setup and/or maintenance.

More detailed information on the design and fabrication of the various control hardware circuits can be found in the schematic diagrams appended to this report.

4.2.4.3   Software Development

Development of the APS process software was in modular subroutine packages. These subroutines were linked together and/or called by the executive software program as required to formulate the system software program. This approach provided maximum flexibility for system update, modification and/or debug. It also subdivided the software development effort into more easily defined, easily handled subtasks. In all, there were well over 200 software subroutines utilized in the APS process software used in the feasibility evaluations.

General Executive Program Description

Figure 22 is a simplified flow chart of the APS process software executive program. This flow chart defines the procedures which the APS process followed in the automatic mode of operation to spray bond and barrier coatings separately or in sequence.

Depression of the reset pushbutton or powerup caused the microprocessor to initiate the "startup" routine. This routine initialized the microprocessor stack pointer, initialized the modes of all the PIA interface registers, and performed a number of general housekeeping chores to ready the microprocessor subassembly for operation. It also drove all seven axis motors against the zero reference stops and cleared the respective position counters to synchronize them with the motors. At the
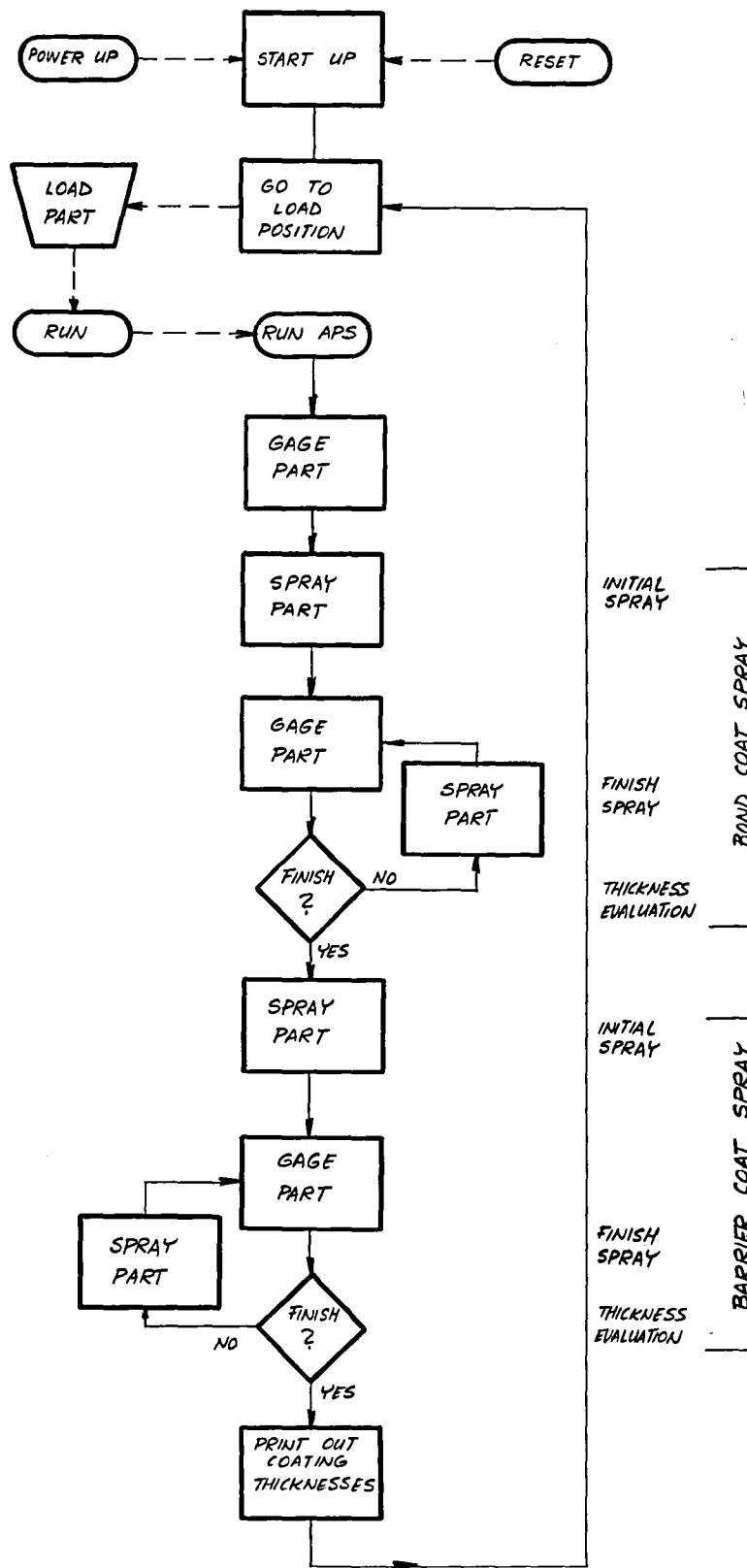
Figure 22.   Simplified Flow Chart of APS Process Software
             Executive Program.

conclusion of the startup routine all system axes were automatically indexed to the "load" position. At this point the system stopped until directed by the operator to proceed. Several options were available to the operator at this point. He could utilize any of the front panel function pushbuttons to evaluate system status, or transfer system control to a remote video terminal for further evaluation. For continuation of automatic operation, he would load a specimen to be coated by the plasma spray subsystem and depress the "run" pushbutton. Depression of the "run" pushbutton caused the system to resume automatic operation. System operation was then controlled by the "run APS" routine in software. This routine is functionally described by the remainder of the flow chart in Figure 22.

The "gage part" subroutine was the first one to be exercised to gage the bare specimen. The specimen manipulator and optical detector positioner motors were all sequentially indexed to the gage point coordinates as defined in an EPROM firmware lookup table. At each point the valley point coordinate was determined and stored in a RAM scratchpad table (Table 0) using the procedure described earlier. At the conclusion of this subroutine, Table 0) contained the bare blade coordinates at all the specified gage points.

The initial "spray" subroutine applied the bond coat constituent to the specimen. The thickness applied, specified by EPROM firmware, was typically slightly less than the final thickness desired to assure that no points were coated too heavy. Deposition was accomplished by sequentially indexing the specimen manipulator axes to the scan line coordinates specified for the specimen in an EPROM firmware lookup table. After each scan line was positioned vertically before the plasma spray gun at the required standoff distance, the gun was cycled up and down the required number of passes to deposit the nominal coating thickness specified. The microprocessor automatically signalled the plasma spray console to initiate and terminate the gun power and powder flow at the proper instants.

The "gage part" subroutine was used to gage the thickness of the coating actually applied at each gage point. This was accomplished in the same manner as the initial bare specimen measurements were taken. In this case, however, the gage point valley location coordinates were stored in a different RAM table (Table 1).

In the thickness evaluation subroutine, the software directed the microprocessor to make a decision which way to proceed. By taking the difference between the respective coordinate values stored in Tables 1 and 0, the microprocessor determined the actual coating thickness applied on each scan line during the initial spray application of the bond coat constituent. Comparing these values to the desired thickness specified in EPROM, the microprocessor determined which lines, if any, required additional coating passes to bring the thickness up to the minimum acceptable value. The number of passes required on each line to achieve this minimum acceptable value was also calculated.

If all lines were not coated with at least the minimum required coating thickness, the respray subroutine for the bond coat constituent was utilized. This subroutine was actually the same subroutine used for initial spray application, except only the coordinates of the selected scan lines and the respective numbers of spray application passes calculated per line were utilized. At the conclusion of this subroutine the microprocessor looped back to the "gage part" subroutine for the bond coat constituent. This subroutine was executed the same as previously, updating the coordinate values stored in Table 1 where additional coating was deposited. This loop, alternately spraying and gaging the bond constituent was traversed as many times as necessary to bring all gage points up to the minimum acceptable coating thickness. Typically, however, no more than one respray was required. One exception to this was in areas of extremely high curvature such as the leading edge of a JT9D first stage turbine blade. This will be discussed further in Section 5.

After determining that all gage points had at least the minimum acceptable thickness of the bond coat constituent, the microprocessor initiated the subroutine to deposit the initial application of the barrier coat constituent. This subroutine was actually the same subroutine used for application of the bond coat constituent, except a different desired coating thickness was specified by EPROM firmware. A different gun power level and the second powder hopper were also designated by the microprocessor. Again, as for the barrier constituent, the software directed the microprocessor to deposit slightly less than the desired coating thickness on each line to assure that no lines were coated too heavy.

The software loop formed by the next three subroutines shown on Figure 22 for the barrier coat constituent was identical to the loop just discussed for the bond coat constituent. The coated part was gaged, the calculated coating thickness was compared to the desired thickness, and the respray or finish pass subroutine was utilized as required. When all gage points were determined to have at least the minimum acceptable total coating thickness, the microprocessor emerged from the loop.

The final subroutine indicated on Figure 22 is the "Print coating thickness" subroutine for the actual deposited coating thicknesses at each gage point as determined by the optical detector. These values were tabulated to tenths of a mil (1 mil = 25.4 μm) by gage point number on the digital printer. The thicknesses of the bond constituent coating could be tabulated as well as the total applied coating deposition.

While the printout was being generated, the specimen was indexed back to the load position. It could then be removed and replaced by a new bare specimen. The entire process could then be automatically repeated by again depressing the "run" pushbutton.

As discussed above, spraying on each scan line was terminated when a "minimum acceptable coating thickness" was measured. To achieve a statistically acceptable confidence level that the actual applied coating thickness exceeded the minimum tolerance level, the "minimum acceptable thickness" was generally taken as the

minimum tolerance level plus 12.7 μm (0.5 mil). The remainder of the tolerance band (e.g., 63.5 μm (2.5 mils) for a +38.1 μm (+1.5 mils) tolerance band) was the resultant process high-side tolerance before the deposited coating was too thick. It was desirable to keep this process high-side tolerance as large as practical.

All system software and firmware was stored in the type 2708 (1k x 8 bits) EPROM's. Approximately 8k of EPROM was used. There was room for 16k on the memory board used in the APS process microprocessor. The information stored on EPROM could be categorized into three types. Four of the eight devices were used to store the software subroutines. These included all the program instruction statements. One device stored the control firmware. This included all the system constants, time delays, etc., utilized by the software with the exception of those unique to the type of specimen being sprayed. The remaining three devices contained the specimen firmware: one, the spray scan line coordinate lookup table for the base coat constituent; the second, the spray scan line coordinate lookup table for the barrier coat constituent; and the third, the gage point lookup table. Separating the software and firmware data in this manner greatly eased the task of updating and/or modifying the process parameters. This also allowed the software to be "universal." The parameters which were unique to the specimen type and geometry were all located in the firmware for that specimen.

Software Program Options

The previous section described the general executive program flow chart for the APS process software. There were, however, a number of options provided in the software. The options selected were normally specified in the process firmware or the specimen firmware. The firmware specification, however, could be overridden from either a remote terminal or from the microprocessor front panel controls. Unless overridden, however, the firmware specification prevailed as the default option.

In the flow chart of Figure 22, four different spray subroutines were indicated - an initial and a finish spray for both the base coat constituent and the barrier coat constituent. As was mentioned in the discussion, however, the same software subroutine was actually used in all instances. The subroutine was configured differently for the four cases by parameters specified in the control firmware. The configuration parameters specified four factors for the spray subroutine:

1) the powder hopper (or hoppers) to be actuated.

2) the spray scan line coordinate table to be used.

3) the calculation formula to be used in determining the number of deposition passes to be made by the spray gun on each scan line, and

4) A maximum repetition limit number which would limit the number of times a particular spray sequence configuration could be accessed in the absence of any other limiting control logic.

51

A spray pointer was utilized in the software to indicate the configuration parameters to be used for the spray subroutine.

The firmware provided for specification of up to seven sets of spray subroutine configuration parameters for use in one automatic sequence. Thus there was provision to use different calculation formulae on different areas of the specimen if desirable. Another example would be deposition of a graded layer, or mixture of the two constituent powders, as a transition layer between the bond and barrier coats. It was also possible for the firmware to specify less than four spray sequences during automatic operation. In particular, either one or both of the finish spray loops on Figure 22 could be deleted. This was practical, for example, when the tolerances on thickness uniformity of the bond coat layer were not extremely tight, or when this layer was thin enough that there was likely not a need for finish passes. The desired coating thicknesses for the bond coat layer and for the total coating deposition were specification parameters stored in firmware. The fraction of the total desired coating thickness to be applied during the initial spray subroutine was also a firmware specification parameter. This could be specified as any number of eighths of the total desired thickness. As discussed previously, the initial spray thickness was usually less than the desired value to assure that no lines were coated too heavy due to unanticipated process variations.

The firmware provided for specification of up to 128 scan lines or 128 gage points in each coordinate table. Any number of these gage points could be located on the same scan line. In the case of multiple gage points on the same scan line, the software would select the point with the minimum deposition thickness for use in calculating the number of finish passes required in the finish spray subroutine. The software also calculated the high, the low and the average coating thickness deposited on the blade for each layer along with the corresponding locations for the high and low spots. Although always available, this data was not used unless specifically called for. It could, for example, have been utilized in a calculation formula for defining parameters in a finish spray subroutine.

The firmware could modify the number of coating thickness printouts generated on the digital printer. Thus printouts could be generated only for the total applied coating thickness, for each of the coating constituent layers, or after each spray sequence including each finish spray sequence. This latter option was useful during initial setup for a specimen to monitor process step-by-step performance.

Up to eight breakpoints could also be specified in the automatic sequence. This allowed the automatic sequence to be interrupted at any place for intermediate evaluations. This was also primarily a diagnostic tool.

Two other options were previously discussed in the metrology subsystem section. These were the ability to specify the FIFO length and the number of optical detector readings averaged after each motor step in the optical detector measurement subroutines. These specifications allowed the system sensitivity to electrical noise or fixture vibration to be minimized. There was, however, a tradeoff to be considered with system response time. The gaging subroutine could be slowed unnecessarily if the values specified for these parameters were too large.

In the feasibility demonstration efforts, coating deposition specimens were primarily JT9D first stage turbine blades. This specimen was selected as representative of the most difficult specimens which would be encountered due to its small size and small radii of curvature. Only three configurations of the spray subroutine were used on the JT9D specimens. The finish spray loop was not used for the NiCrAlY bond coat. The coat was thin enough, 127 µm (4.6 mils) that it was applied in two passes of the spray gun. The ±38 µm (±1.5 mil) tolerance thus represented a relatively loose percentage tolerance even without finish passes. It was felt that proper specification of the scan line coordinates would achieve this percentage tolerance without the additional finish spray loop. If consideration were directed toward the possibility of changing the NiCrAlY spray parameters to deposit a thinner coating layer per pass, it could then prove desirable to incorporate the finish spray loop on the bond coat as it was for the barrier coat.

For the feasibility demonstration, the selection of the desired coating thicknesses was relatively arbitrary. The values which were used for most JT9D specimens were 117 µm (4.6 mils) for the NiCrAlY bond coat and 290 µm (11.4 mils) for the yttria-stabilized zirconia barrier coat for a total coating thickness of 406 µm (16 mils). This appeared to be a reasonable thickness without using excessive amounts of powders for the feasibility investigations. It may prove desirable to use somewhat thinner coatings for aircraft jet engine and thicker coatings for electric utility engine applications.

Since no finish spray subroutine was utilized on the bond coat, the initial spray subroutine was configured to deposit the nominal 117 µm (4.6 mils) on JT9D specimens. The calculation formula in the firmware was therefore:

$$\text{No. of Passes} = 1 + \frac{T_B - 3}{1.6} = 1 + \frac{4.6 - 3}{1.6} = 2 \qquad (1)$$

where T_B was the desired thickness of the bond coat in mils.

For the zirconia barrier coat the firmware for the JT9D specimens designated deposition of three-fourths of the desired barrier coat thickness on the initial spray subroutine. The calculation formula for this subroutine was therefore:

$$\text{No. of Passes} = \frac{(T_c - 1 - T_B) \times 0.75}{0.8} = \frac{(16 - 1 - 4.6) \times 0.75}{0.8} \approx 10 \qquad (2)$$

where T_c was the desired total coating thickness in mils. For the finish spray subroutine the calculation formula used for each line was:

$$\text{No. of Passes} = \frac{(T_c - 1 - T_A)}{0.8} = \frac{15 - T_A}{0.8} \qquad (3)$$

where T_A was the actual total coating thickness in mils previously deposited on that line as determined by the microprocessor during the last "gage part" subroutine.

In the various calculations used above, the calculation formula and the various specimen constants were taken from the firmware by the microprocessor. The nominal coating depositions per pass (i.e., 3 mils and 1.6 mils for the first and subsequent NiCrAlY passes, respectively, and 0.8 mils per zirconia pass) were constants in the control firmware. These values were determined in the latest spray deposition profile study. (See section 5.)

Many alternate possibilities could have been considered for the calculation formulae. One interesting possibility was for the microprocessor to compute the actual average deposition thickness per pass on previous scans on each line instead of using nominal values from the deposition profile study. This could conceivably reduce the process time required for the finish spray subroutine, but needed careful study to determine the probability of overspraying some lines if process variations occurred. The approach used, while sometimes requiring multiple finish pass cycles on areas such as the blade leading edge, minimized the danger of overspraying.

A total of 24 scan lines was used on the JT9D specimens. This was based on results of the deposition study summarized in section 5. This number could probably have been reduced somewhat, particularly for the NiCrAlY. The last JT9D specimens utilized only one gage point on each scan line for a total of 24 points. All thickness evaluations previously made revealed little problem with thickness uniformity along a scan line. There would have been no problem adding additional points on each line if needed. The penalty paid for more points is extra time spent in each "gage part" subroutine indexing to the additional measurement locations. This would be even more obvious on larger specimens. On the W501B specimens, for example, 70 scan lines were utilized.

The FIFO length used on the final JT9D specimens was the full 32 memory locations. This provided maximum immunity to noise spikes prematurely indicating a "valley detect" during the gaging subroutines. The process could have been speeded up somewhat by reducing the FIFO length. Only one optical detector "read" was made after each Y-axis motor step during the gaging subroutine. Eight "reads" per step were used on many of the earlier specimens. There was no noticeable increase in noise or gaging repeatability problems after the change. This indicated that the noise levels were not at a seriously high level in the APS process facility.

One software option not previously mentioned was also used on the APS process hardware used in the feasibility demonstration. The Model No. 1 mechanism developed considerable wear in many of the instrument-quality mechanical components. This resulted in considerable backlash in several axes. The software was therefore configured to remove this backlash during the gaging subroutines. This was done by "swinging" the suspect axes away from the gage point locations and back again before each measurement to "windup" the backlash in the same direction on all occasions. Again this extended the total process time. This option may not be required on new mechanical fixtures built to production hardware specifications. This option, however, did demonstrate the capability to hold the repeatability of the gaging subroutine at a standard deviation of approximately ± 7.5 μm (± 0.3 mils).

Further detail may be obtained on the APS process firmware and software by referring to the detailed software flow charts and software assembly listings in the Appendix.

4.2.5 Plasma Spray Subsystem

As discussed in Section 4.1, standard commercial plasma spray equipment was selected for utilization in the feasibility demonstration APS process systems. This equipment, supplied by Plasmadyne, Inc., had a number of features which made it amenable to easy interfacing to the APS process controller. These included the capability for precise pre-adjustment of the various gas and powder flow rates, dual powder input ports to the plasma spray gun and actuation of automatic sequencing of the various process steps by remote contact closures. Any other type of equipment which has comparable features could also have been selected.

During the course of work on this program, several observations were made of potential areas of improvement of the plasma spray subsystem hardware for use in automated applications. These are indicated in the process evaluation discussions in Section 5. The most significant of these areas pertained to the plasma gun and to the powder supply subsystem.

Redesign of the plasma spray gun to provide more consistent control of the deposition pattern would greatly simplify the APS process control task. The model used on this program ejected the two powders utilized in two different directions. This required the use of different scan line parameter tables for the two powders. There were also indications that these deposition patterns varied on some occasions, although sufficient data was not acquired to verify this possibility.

On the present plasma spray equipment shutoff valves are located in each powder supply line at the hopper end. On a number of occasions significant traces of NiCrAlY were observed mixed in with subsequent depositions of the zirconia. Presumably this resulted from NiCrAlY powder residual in the supply hose between the shutoff valve and the plasma gun, despite the automatic purge of this hose after gun shutoff. Insertion of shutoff valves at the gun end of the hoses could significantly reduce this occurrence. These would be actuated by the microprocessor after purge of the hoses was complete.

As mentioned above, variations in the plasma spray deposition patterns are believed to have occurred. One theory is that this resulted from variations in powder particle size with time. The powder utilized on this program ranged from -200 to +325 in mesh size. Since the finer particles were observed to settle to the bottom of the cans, the same thing probably happened in the powder hoppers. Thus the powder particle size probably varied with time. Even bigger variations could occur if the can was not mixed thoroughly before pouring some of its contents into the hopper. Some means of keeping the hopper contents thoroughly mixed on a continuous basis would be highly desirable. One alternative would be to specify a smaller range in powder particle size, but that would result in much higher material cost.

In the plasma spray hardware for a production APS system, provisions could be made to allow microprocessor adjustment of the various process parameters (e.g., voltage, current, gas and powder flow rates, etc.). The APS system controller would then preset all the hardware when the specific part to be coated was identified. In the setups used in the feasibility evaluations, these parameters were all manually preset and then automatically selected by the microprocessor when required.

4.3   APS Process System Operation

In order to utilize the APS process system to coat a specimen, two preliminary steps had to be accomplished:

1)   A holding fixture was fabricated to mount the specimen on the APS system specimen manipulator.

2)   The firmware coordinates and constants defining the specific process and specimen options desired was inserted into the microprocessor.

Establishment of the firmware parameters for a new specimen type was initially done using a "master reference blade." The master reference was a typical specimen on which the desired scan lines were drawn. These lines were drawn on the specimen using the scan line spacing derived in the deposition profile study. (See Section 5.) The desired gage points were also marked on the specimen, including at least one on each scan line. Figure 23 is a photograph showing the master reference blade used for the JT9D specimens. The firmware tables were generated by placing the master reference blade in the specimen holding fixture normally supporting the specimen being sprayed. Each scan line of the reference was positioned in front of the plasma spray gun in the orientation required for spray deposition. The coordinates for each axis were then obtained by reading the corresponding position counters. Either the remote video terminal or the microprocessor front panel controls were used for this procedure. The gage point coordinates were obtained in a similar manner by positioning the reference blade in front of the optical detector and superimposing the optical detector light spot on the points marked on the reference blade.

For subsequent specimens an off-line computer program was developed for use on an H-P 9820A programmable calculator. This program consisted of two subroutines. The first subroutine utilized digital coordinate data from the specimen detail drawings. An interpolation procedure was applied to that data to generate blade coordinates of equally-spaced points around the blade cross-section with the desired scan line spacing. The surface normal at each point was also computed. The second subroutine utilized the output data from the first subroutine for two or more cross-sections. The second subroutine output was the scan line and gage point coordinates required for the APS system axes in hexadecimal notation. This procedure was utilized to obtain the firmware coordinate data for the W501B specimens coated during the latter phase of this program. Digital data is now available for most turbine blades which might be coated with the APS process.
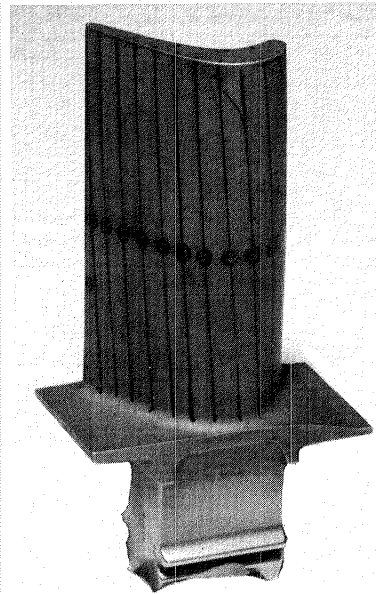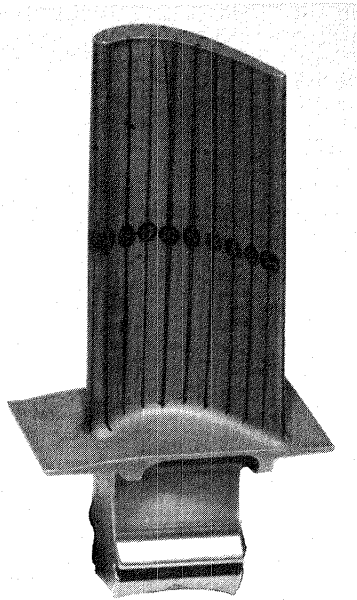
Figure 23.   Photograph of JT9D First Stage Turbine Blade Used as Master Reference for Establishment of APS Process Firmware.

The APS system was readied for use by programming the specimen firmware obtained above in EPROM. The various process control parameters were also placed in firmware if different from those already in the control parameter EPROM. The EPROM's for various specimens could be readily interchanged in the plug-in sockets in the microprocessor chassis. A production system could have the firmware for many different speicmens on one EPROM or on multiple EPROM's. Selection of the proper tables for the specimen being sprayed could then be by type number designation on a front panel switch register or similar convenient technique.

Before initiating the automatic sequence of the APS process feasibility implementation, the various spray parameters were manually preset on the plasma spray control console. These included parameters such as arc and auxiliary gas pressures, the feed rate settings on the two powder hoppers, the voltage levels for the two spray gun arc power conditions, etc. The spray control console was then switched to remote control status. From that point on the APS process microprocessor selected the proper parameters, actuated the equipment at the proper instants and otherwise controlled the operation. On a production system it would be a straightforward task to have the APS process microprocessor also preset the various spray console parameters as discussed in the previous section. This would be particularly advantageous if future process studies indicate the need or desirability for different settings for different applications. This would eliminate the possibility of a human error in process setup.

The specimen to be coated was prepared for spraying by grit blasting. A high purity alumina grit material was utilized. Relatively little attention was paid to the surface preparation process on early JT9D specimens. The concern on those specimens was obtaining deposition thickness uniformity. On the specimens for burner rig test and for coating quality evaluations, however, the surface preparation task was given careful attention. After grit blasting for surface preparation, the specimen was slipped into the specimen holding fixture on the APS specimen manipulator. A single set screw locked the specimen in the fixture. The APS process was then initiated by depressing the "Run" pushbutton.

The remainder of the APS process was completely automatic. This included determination of the actual bare specimen coordinates, deposition of controlled uniformity thicknesses of both the NiCrAlY bond coat and the yttria-stabilized zirconia barrier coat, printout of the actual deposition thicknesses deposited on each gage point as measured by the optical detector, and return of the specimen to the load position for replacement with the next specimen to be coated. Figure 24 is a photograph of the APS system during automatic operation spraying a JT9D specimen. The gun, the optical detector and the specimen are visible in this figure. Also visible are tubes directing the CO_2 cover gas at the specimen during spray application.
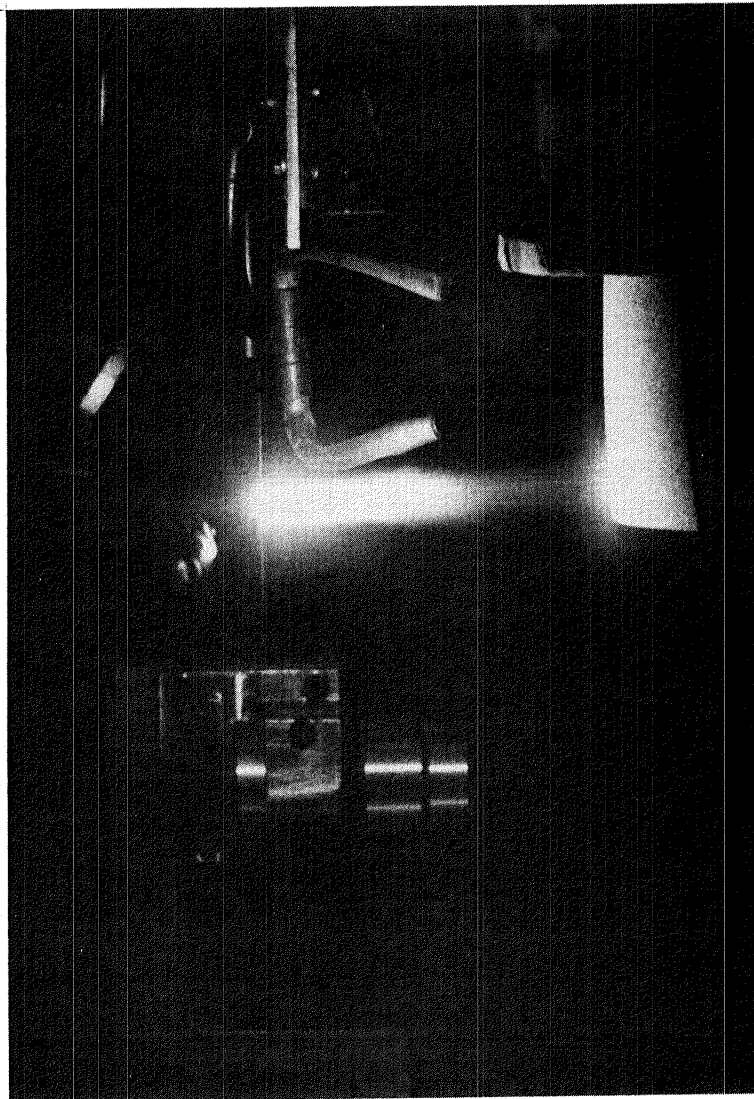
Figure 24.   Photograph Taken During Operation of the Automated Plasma
Spray (APS) System (A JT9D engine 1st stage blade (right)
is being sprayed by the plasma spray gun (left); the
noncontact optical metrology sensor is in the background
(lower center)).

5.0 PROCESS EVALUATIONS AND DISCUSSION OF RESULTS

This section describes evaluations both of the APS System and the process, i.e., the coatings that it produced. These two elements must be considered in conjunction, since evaluation of the coating thickness was one of the major methods used to evaluate APS System performance. During the course of the program, the chronological sequence of events involved spraying blades, evaluating both the APS measurement data and the coating by metallurgical means, modifying the spray parameters, the mechanical subsystem and/or the control subsystem and then spraying more blades and repeating the evaluations. In order to provide a summary view of the end results, however, each of these activities is described in a separate section without regard to chronological order. All preliminary system and process evaluations were carried out using the airfoil surfaces of JT9D 1st stage turbine blades.

During checkout and debug of the system, four blades were sprayed, Nos. 1 through 4. During initial system evaluation, seven more blades were sprayed, Nos. 5 through 11. An additional thirty blades were sprayed during the coarse of the various system modifications and demonstrations. These were Nos. 12 through 41.

5.1 Preliminary APS System Evaluations and Modifications

The APS System underwent a series of evaluations to analyze the initial design and the effects of modifications to the system to improve its performance. During these initial evaluations, the metrology subsystem was evaluated separately to determine its ability to repeatably locate the airfoil surface. Then an initial set of blades was plasma sprayed and evaluated to determine the effectiveness of the spray deposition subsystem to apply the coating with the desired uniformity and also to determine the ability of the metrology subsystem to accurately measure the coating that had been applied. These initial evaluations identified a number of improvements in the design that were required in order to achieve the desired coating uniformity. As a result, a number of modifications were made to the mechanical subsystem, the control subsystem and to the spray deposition process parameters. An additional set of blades was then sprayed and evaluated, both to determine the uniformity of the coating deposited and to determine the accuracy with which the coating thickness had been measured. While the modifications made resulted in a substantial improvement in system performance, the evaluations also identified the need to fabricate a new mechanism. Since the new mechanism would be required to handle the larger, heavier utility turbine blades to be coated in a subsequent task, the decision was made to fabricate the new mechanism and to discontinue work with the first model mechanism.

5.1.1 Metrology Subsystem Evaluations

Prior to overall system evaluation, the metrology subsystem was examined for its ability to make repeatable measurements. As described earlier, the metrology process

consisted of positioning the blade so that the optical probe was aimed normal to the surface on the blade at the point to be measured with the standoff within the focal length of the optical extender, and then moving the blade away from the probe in order to execute the measurement.

There were a number of variables within the system which could have an effect on the metrology process. These included the stepping rate of the motor, the number of individual voltage measurements per step, the voltage difference used to identify the focal point and the time delay between stepping the motor and strobing the A/D converter to make a voltage measurement. Since the specimen was mounted on a moving tower (specimen manipulator) and the tower's natural frequency of vibration could be comparable to the stepping rate, the tower vibrations also had an effect on measurement repeatability. The stepping rate during measurement was a function of the number of measurements per step so that the number of measurements influenced the effect of tower resonance. In order to optimize these various parameters to achieve the best possible repeatability, a visicorder was used to record the analog output of the optical probe and the strobe pulse to the A/D converter during measurement. Repeatability was measured for a number of combinations of parameters for which visicorder traces were made. The results were then compared to determine the factors that affected repeatability and their optimum values.

The printer on the APS control console was programmed to print out positive differences between two tables in microprocessor memory where the measurement values were stored prior to and after spraying. This approach worked well for printing out coating thicknesses, but was not suitable for recording repeatability data. The printer was not capable of printing out the negative numbers which could occur. In order to determine repeatability, it was necessary to read the measured values out of the microprocessor memory using a teletype or an alphanumeric CRT terminal. The values read were four digit hexadecimal numbers representing the measured valley locations in number of steps from the zero position of the Y-axis. This is the form in which the repeatability data is presented.

For repeatability testing the metrology subsystem was set up to measure four points on a JT9D blade, the last one twice. Repeatability runs consisted of five sets of measurements of each point at rates of 1, 2, 4, 8, 16, 32, 64 and 128 measurements per step (mt/st). It was found that 8 and 128 mt/st gave the best results, followed closely by 1 mt/st and then 16 mt/st. Visicorder runs were made during measurement of the fourth point at rates of 1, 8, 16 and 128 mt/st. An analysis of the visicorder data resulted in the following conclusions:

1)   The subsystem made correct measurements. In each case studied, the measurement stopped at the point where the value entering the FIFO was greater than the value in the tenth location. The point selected as the focal point was either the point of minimum voltage or one of two equal points of minimum voltage.

2) At 1 mt/st, the voltage curve was smooth with occasional ripples. There were no oscillations where the voltage slope actually changed from increasing to decreasing or vice versa. As a result, the measured values went down steadily to a minimum and then up again. The stepping rate was 333 Hz.

3) At 8 mt/st, the voltage curve had definite ripples on it, which, near the valley, resulted in plateaus or even slight reversals of slope. The frequency of these humps was 117 Hz. The stepping rate was 237 Hz. This meant that the two frequencies maintained an essentially constant phase relationship throughout the measurement, with two successive sets of measurements being taken 180° apart on each cycle of the voltage curve. The average voltage measured at each step went smoothly down to a minimum and then up again in spite of the ripples because of this constant phase relationship.

4) At 16 mt/st, the voltage curve had irregular ripples, or peaks for which no set frequency was assigned. The fluctuations were small, resulting in occasional plateaus near the curve's minimum but more commonly resulting in variations in the predominant slope. The stepping rate was 182 Hz. At this stepping rate, visicorder data was also taken after movement of the Y-axis stopped, and the tower was found to oscillate in two modes, one with a frequency of 20 Hz and the other with a frequency of 114 Hz.

5) At 128 mt/st the voltage curve oscillated continuously. It appeared that for each step the blade moved and then went through one complete cycle of overshoot before either damping out or receiving the next step pulse. The frequency of these oscillations was 42 Hz, the same as the stepping rate, so that for each step the 128 measurements were averaged over the same portion of the voltage oscillation. The average voltage moved smoothly down and then up.

If the stepping rate during measurement were independent of the number of measurements per step, the repeatability would have been expected to improve in direct proportion to the square root of the number of measurements averaged. This expected improvement due to averaging was not achieved because of the interaction of the varying stepping rate with the resonant frequency of the mechanism. The best results were not obtained when the stepping rate was out of phase with the natural frequency of the mechanism, but rather when the stepping rate was a harmonic of the natural frequency so that relatively large voltage oscillations occurred. The explanation was that the voltage measurements were always taken at the same relative position on the oscillation, so the voltage readings themselves formed a smooth curve. The evaluation of metrology subsystem repeatability at 8 mt/st is listed in Table III. The standard deviations at each point ranged from 0.9 to 1.5 steps with the average being 1.1 steps. This was ± 0.005 mm (± 0.0002 inches).

Table III

Metrology Subsystem Repeatability Data at 8 Measurements/Step

Run No.	Point No.				
	1	2	3	4a	4b
1	119F	ODC6	09A5	0A5B	0A5A
2	119F	ODC7	09A5	0A5B	0A5C
3	11A0	ODC4	09A6	0A5B	0A59
4	119E	ODC7	09A7	0A5D	0A5A
5	119D	ODC4	09A4	0A5C	0A5B
Ave.	119F	ODC6	09A5	0A5C	0A5A
St. Dev.	±1.1	±1.5	±1.1	±0.9	±1.1
Ave. St. Dev.	±1.1				

NOTE: The data values are expressed in hexadecimal number of steps from the zero position of the Y-axis.

5.1.2 Plasma Spray Subsystem Evaluations

After verification of the metrology subsystem operation, it was possible to perform the initial evaluation of the plasma spray subsystem. The initial spray pattern, which was based on the spray deposition data from Plasmadyne, consisted of seventeen vertical spray lines around the blade with one measurement point on each line as shown in Figure 25. The measurement points alternated from one scan line to the next between two cross-sections of the airfoil, one near the center and one near the tip. This was done to allow evaluations of the uniformity of the coating along the length of the airfoil.

The first two specimens in the initial evaluation, blades No. 5 and No. 6, were sprayed without using the finish spray routines, so that each spray line received four passes of NiCrAlY and ten passes of ZrO_2. These were sectioned to evaluate the performance of both the spray subsystem and the metrology subsystem. The No. 5 blade was cut at five cross-sections along the length of the airfoil and 100X micrographs were taken at five locations on each cross-section in order to take coating thickness measurements. The results are shown in Table IV. This table shows the NiCrAlY thickness, the zirconia thickness and the total thickness for each point on each blade cross-section. It also shows the average total thickness for each cross-section. The NiCrAlY varied from 0 to 254 μm (0.0 to 10.0 mils) and the zirconia from 178 to 340 μm (7.0 to 13.4 mils). The total thickness varied from 188 to 544 μm (7.4 to 21.4 mils). This indicated that spray lines on the low end of the range for NiCrAlY were also on the low end of the range for zirconia and those on the high end of the range for NiCrAlY were also on the high end of the range for zirconia. In spite of the wide point to point variations on each cross-section, the thickness range was almost identical for each cross-section   This was expected since the spray gun was driven at constant speed along each spray line the entire length of the airfoil.

The No. 6 blade was cross-sectioned near the tip at the section where the optical measurements were made. The coating thickness measurements for blade No. 6 showed the same general pattern as for blade No. 5. Thirteen 50X micrographs were taken around the airfoil, seven on spray line measurement points and six at locations between spray lines. Table V presents the coating thickness measurements made from the micrographs of blade No. 6 and compares them with the optical probe measurements for those locations where both measurements were made. A comparison of the optical probe data with the micrograph data showed agreement within ±36 μm (±1.4 mils) for the NiCrAlY except for micrograph No. 10 where the coating was separated from the blade. There was much poorer agreement for the zirconia. It was concluded that not only was the coating not uniform enough from one spray line to the next, but the measurement accuracy was not within the desired ±12.7 μm (±0.5 mils).

Five additional blades were sprayed with similar results. Observation of the system during spraying of these blades, in which a time delay was added between spraying and measuring, lead to the conclusion that there were two major problems. The first problem was that the plasma spray gun was not spraying along its centerline
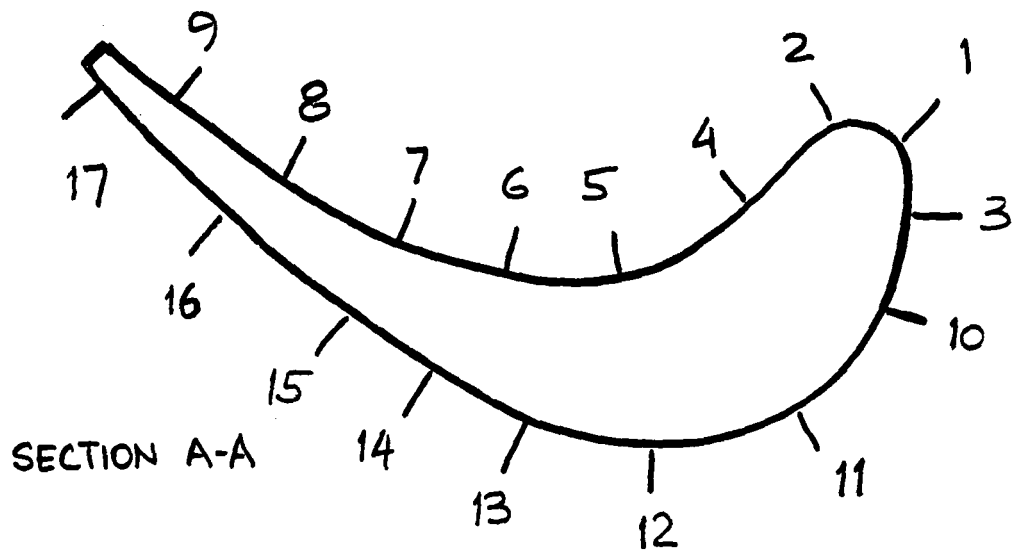
SECTION A-A

TOTAL NUMBER OF LOCATIONS: 17

SCALE : NONE

−3/16" (4.8 MM)

1−3/16" (3 CM)

A   A
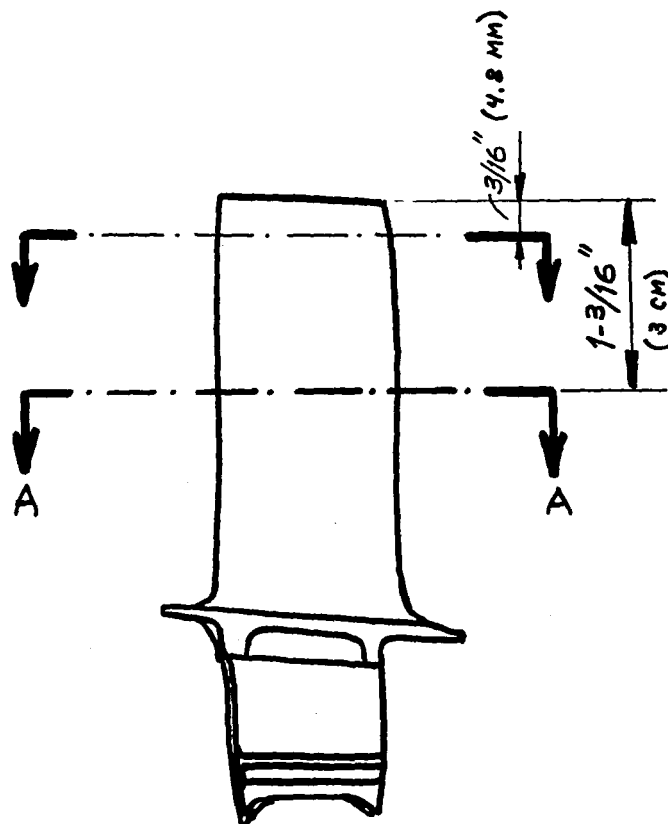
Figure 25.   Initial Measurement Locations on JT9D First Stage
              Turbine Blade Airfoil Section.

65

TABLE IV

Coating Thickness Evaluation on JT9D Blade Specimen No. 5

Measurement Locations		Coating Thickness (mils)			
Section(1)	Location(2)	NiCrAlY	ZrO_2	Total	Average
1	1	7.8	10.5	18.3	
	2	0.3	8.0	8.3	
	3	1.5	9.0	10.5	
	4	0.0	10.0	10.0	
	5	7.5	13.4	20.9	13.6
2	1	8.5	10.6	19.1	
	2	0.2	8.2	8.4	
	3	0.8	7.0	7.8	
	4	2.0	8.5	10.5	
	5	8.2	13.2	21.4	13.4
3	1	7.5	11.3	18.8	
	2	0.2	8.0	8.2	
	3	0.0	9.0	9.0	
	4	1.0	9.8	10.8	
	5	10.0	10.0	20.0	13.4
4	1	8.0	11.3	19.3	
	2	0.2	7.2	7.4	
	3	0.6	7.4	8.0	
	4	4.4	11.0	15.4	
	5	7.0	10.5	17.5	13.5
5	1	10.0	7.5	17.5	
	2	0.1	10.1	10.2	
	3	0.7	8.0	8.7	
	4	1.8	13.0	14.8	
	5	8.0	9.5	17.5	13.7

NOTES: (1) Blade sectioning was performed by NASA.

(2) Approximate measurement locations:

Location 1 - Convex side near trailing edge
Location 2 - Convex side near center
Location 3 - Convex side near leading edge
Location 4 - Concave side near leading edge
Location 5 - Concave side near trailing edge

66

TABLE V

Coating Thickness Evaluation on JT9D Blade Specimen No. 6

| Micrograph No. (1) | Coating Thickness, (mils) | | | | | |
| | NICrAlY | | | ZrO$_2$ | | |
	Micrograph	Optical Probe	Δ	Micrograph	Optical Probe	Δ
1 (convex TE)	7.2	6.8	-0.4	15.6	10.1	-5.5
2	7.6	-		21.2	-	
3	6.4	5.2	-1.2	22.8	16.4	-6.4
4	6.0	-		23.0	-	
5	2.0	0.6	-1.4	17.4	12.4	-5.0
6	1.2	-		17.4	-	
7 (convex LE)	0.4	0.0	-0.4	16.0	14.8	-1.2
8 (concave TE)	0.0	0.0	0	17.4	19.8	+2.4
9	2.6	-		18.0	-	
10 (2)	8.0	4.6	-3.4	24.0	25.4	+1.4
11	7.4	-		32.6	-	
12	8.0	8.6	+0.6	32.0	-	
13 (concave LE)	7.4	-		29.2	-	

NOTES: (1) Micrographs No. 1, 3, 5, 7, 8, 10 and 12 were at measurement points. Micrographs No. 2, 4 and 6 were to the left of the measurement points, and Micrographs No. 9, 11 and 13 were to the right of the measurement points.

(2) The NICrAlY was pulled away from the blade in the area of Micrograph No. 10. The coating thickness measured off the micrograph was of the coating only.

67

as assumed. Figure 26 depicts a top view of the plasma gun including the powder inlet tubes on opposing sides. The NiCrAlY powder, which entered from the left, was sprayed to the right and slightly up. The zirconia powder, which entered from the right was sprayed to the left and slightly down. This is not a problem for manual spraying, nor is it even observable, because the operator aims the gun by looking at the spray. In automatic spraying, this situation must be accounted for. Otherwise, when applying finish passes, the area needing the coating will not be sprayed. This was the prime cause of the leading and trailing edges not receiving uniform coating thickness.

The second problem was that the great amount of heat generated by the plasma gun was absorbed primarily by the specimen, specimen holder and C-axis shaft as the gun turned around at its upper extreme excursion point. Heat conduction up through the gimbals affected the A-axis and B-axis positions. This heat caused warpage of the blade and thermal shifting of the gimbals, resulting in blade position changes and measurement errors. The total effect was larger than the desired coating uniformity. In order to correct these problems, modifications were made which are described in the following sections.

5.1.3 Spray Deposition Process Modifications

To evaluate the extent to which the spray deposition patterns were offset from the gun centerline, the plasma spray subsystem was set up to spray only three lines on a blade: one on the flat portion of the convex side, one on the highly curved portion of the convex side, and one on the highly curved portion of the concave side. The lines were located far enough apart that they would not overlap. A bare blade (No. 21) was sprayed with four passes of NiCrAlY on each spray line. A previously sprayed blade (No. 7) was stripped of zirconia and sprayed with four passes of zirconia over the old NiCrAlY on each of the three spray lines. These blades were cut at two cross-sections, one near the tip and one near the center of the airfoil. Photomicrographs were taken at 50X over the entire width of the three spray lines. The coating thickness was measured every 254 μm (10 mils) along the width of each pass. This provided six sets of data points per coating material. The data sets were processed using a second order polynomial regression program to obtain a curve of coating thickness versus position which was used to determine the centerline of each set of data. The data for each material was then averaged by matching centerlines to determine the average thickness versus distance from the centerline. This data was then processed using an eighth order polynomial regression program to obtain a curve of thickness versus position. The curves for both coatings (Figures 27 and 28) had the appearance of normal distributions. The curves indicated that the NiCrAlY was sprayed $9.2°$ to the right and zirconia was sprayed $2.8°$ to the left. These curves were used to determine the maximum allowable scan line spacing to provide a uniform coating (3.5 mm (0.140 inches) for ZrO_2 and 9.1 mm (0.360 inches) for NiCrAlY). It was also determined that a scan line spacing for NiCrAlY of 3.5 mm (0.140 inches) would give a uniform coating. Therefore, to simplify the problem of setting up coordinate tables for spraying, a line spacing of 3.5 mm (0.140 inches) was selected for both materials. The standoff distance of the specimen from the spray gun was increased from 6.35 to 7.62 cm (2.5 to 3 inches) in order to reduce the heat input to the blade.
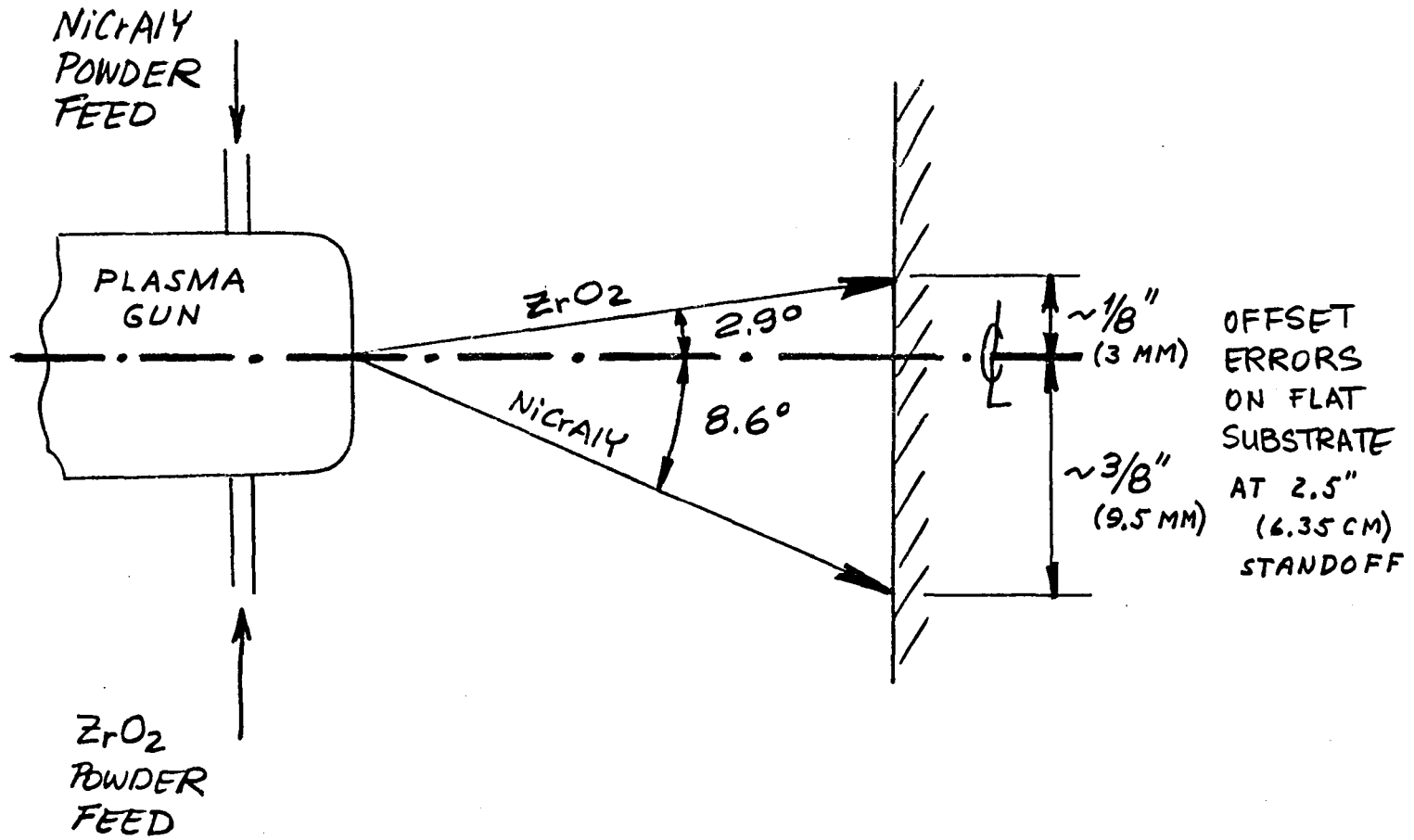
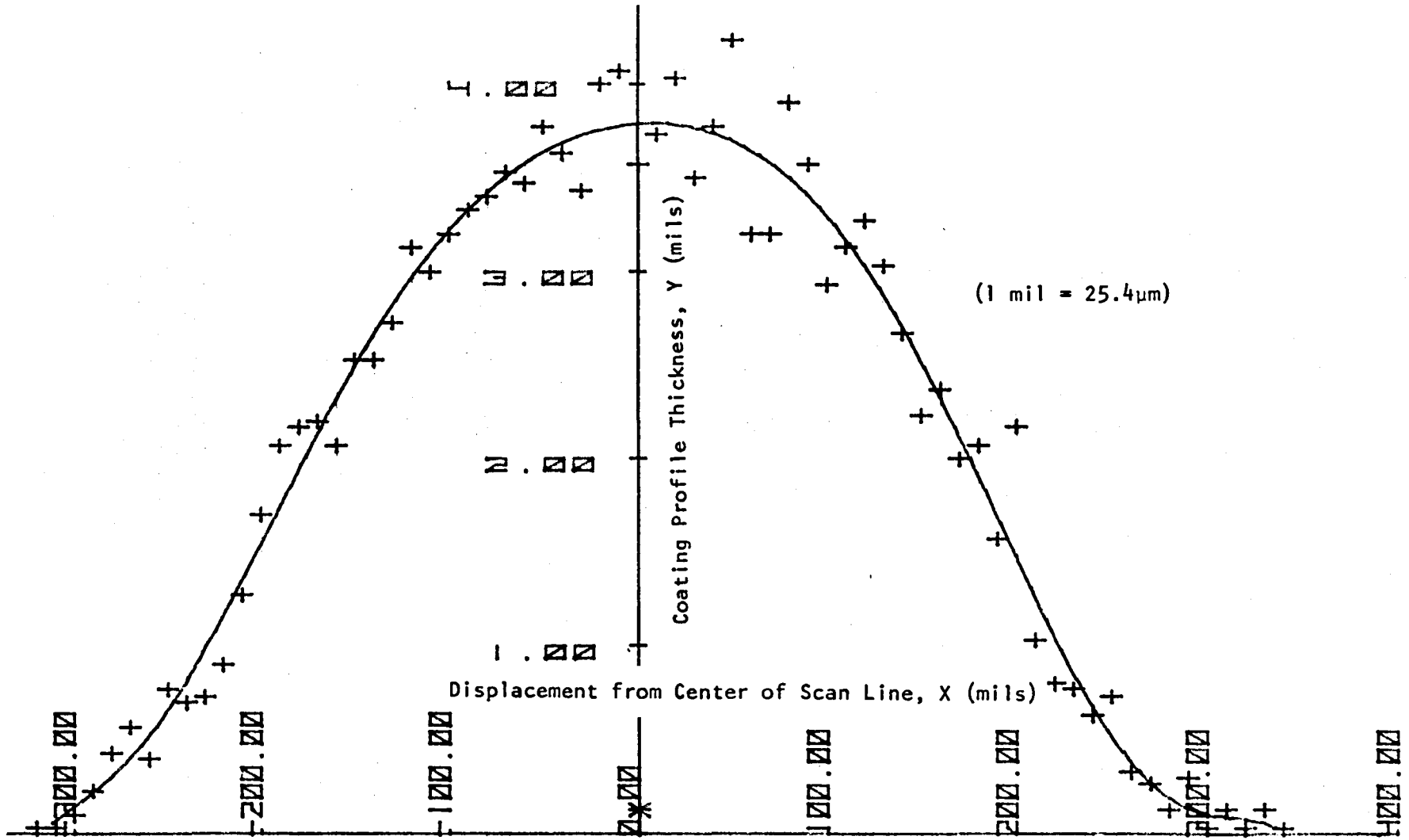Figure 26.   Spray Deposition Pattern of Plasma Gun in APS Process System.

Figure 27. Average Deposition Profile for NiCrAlY Spray (4 Passes).
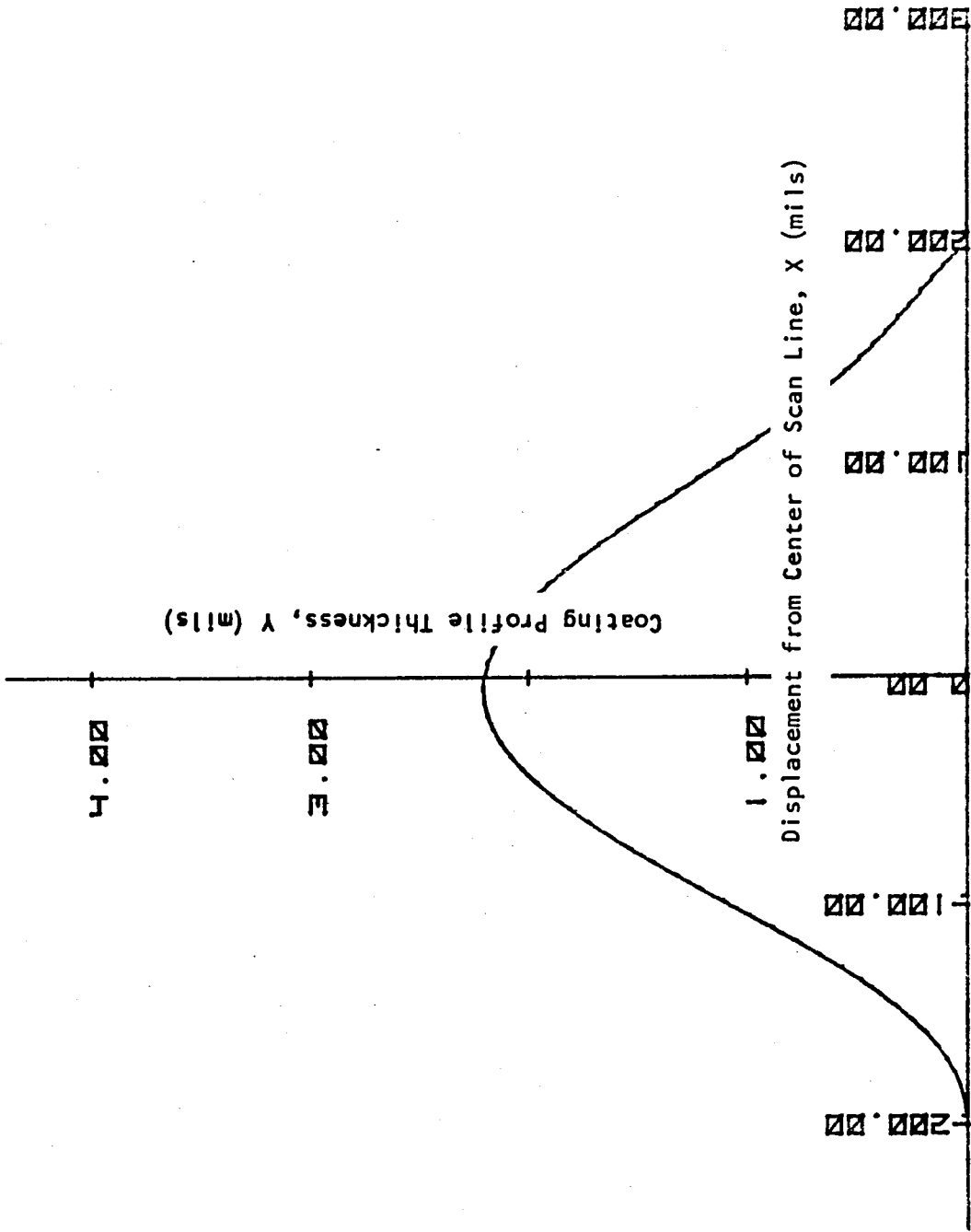
70

Figure 28. Average Deposition Profile for ZrO_2 Spray (4 Passes).

The change in scan line spacing required increasing the number of scan lines for JT9D specimens from 17 to 24 as shown in Figure 29. Two of these scan lines, the ones at the trailing edge on the convex and concave sides, were aimed to miss the blade with the center of the beam so as to overlap the adjacent line enough to bring the trailing edges up to uniform thickness. The measurement points for these lines were at the trailing edges of the blade and were the only ones not centered on the scan line. The line on the convex side of the leading edge was sprayed with the blade turned slightly off-normal in order to avoid depositing spray at an oblique angle on the trailing edge of the concave side. The order of scan lines was such that spraying started on the trailing edge of the convex side (scan line 0), moved around to the leading edge of the convex side (scan line 12), jumped to the trailing edge of the concave side (scan line 13) and moved around to the leading edge (scan line 23). This order was selected to minimize the amount of spray that could strike unsprayed surfaces at an oblique angle and to minimize the effects of backlash by reducing the number of reversals each axis made during spraying.

5.1.4 Mechanical Subsystem Modifications

Mechanical subsystem modifications were also made in the Model No. 1 mechanism to eliminate, or compensate for, the blade and fixture thermal warpages which introduced measurement inaccuracy. In addition to increasing the standoff distance used for spraying, modifications included:

1) A graphite barrier plate installed between the plasma spray gun and the specimen holding fixture. When the gun traveled above the root platform of the blade, slowed down, stopped and reversed direction, the plasma beam struck the barrier plate rather than the cover of the specimen holding fixture. The barrier plate was angled so that the plasma spray beam was deflected to the side, away from the specimen and the gun.

2) Specimen holding fixture and cover modifications to reduce their size to make room for the addition of the graphite barrier plate.

3) A line installed on the APS mechanism to provide CO_2 cover gas to the specimen being sprayed.

4) An air line installed on the specimen manipulator to provide cooling air for the gimbal area.

5) C-axis shaft and specimen holding fixture machining to accomodate cooling air through the inside of the specimen.

5.1.5 Control Subsystem Modifications

Since the APS process system was initially debugged and put into operation, no significant modifications have been required in the control subsystem hardware. The
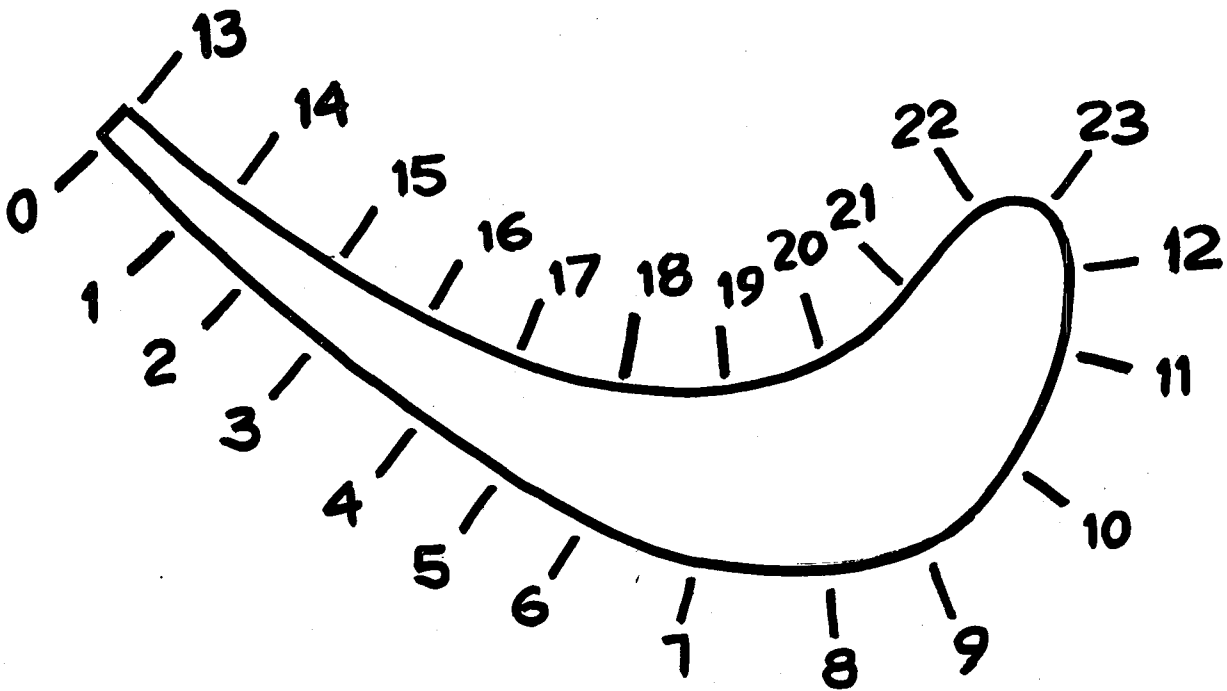
TOP VIEW

SCALE: NONE

Figure 29. First Modified Measurement Locations on JT9D
First Stage Blade Airfoil Section.

only major hardware changes incorporated were those necessitated by fabrication of the Model No. 2 mechanism. New motor drivers were required for the C-axis (specimen rotation) and ZZ-axis (plasma spray gun manipulator) on this mechanism. However, a number of modifications were made in the software and firmware based on the preliminary system and process evaluations:

1) The software was modified to allow only even numbers of plasma gun passes to reduce the heat input to the specimen holding fixture. Thus the plasma gun was always spraying below the specimen while it was being repositioned from one scan line to the next.

2) Two software tables of spray coordinates, one for each material, were specified in place of the one table provided previously. This was done to accommodate the difference in spray directions between the NiCrAlY and zirconia.

3) The number of scan lines and gage points in firmware was increased from 17 to 24 for the JT9D specimens to provide for the decrease in scan line spacing.

4) A short swing of both the A and B-axes before each gage point measurement was incorporated into the metrology subsystem software to minimize the effect of growing backlash caused by wear in the gimbals on the Model No. 1 mechanism.

Several additional software modifications were also made to increase system flexibility to provide for process changes or special tests. These modifications included:

1) Provisions for programming the length of the FIFO used in the metrology subroutine for any value up to 32 steps.

2) Provisions for inserting offsets into the spray coordinate tables for any coordinate axis. This feature allowed the gun/specimen standoff distance to be changed and the spray coordinate data offset to compensate for the angle of the plasma spray beam.

3) Special subroutines for use during manual operations such as establishing the spray and metrology coordinate tables.

5.1.6 Discussion of Preliminary Evaluation Results

The modifications described in the previous paragraphs were made over a period of time. The modifications to the specimen holding fixture and to the C-axis shaft to allow internal cooling of the specimen were major modifications and resulted in a significant shift in blade position in the specimen manipulator. This change required new tables of coordinates for both measurement and spray. A total of thirty JT9D

specimens, Nos 12 through 41, were coated during this period, some to aid in reestablishing the coordinate tables, some to determine the effects of the modifications and some during the course of various process demonstrations. The following paragraphs describe details of evaluations from which significant conclusions were drawn.

After all the above modifications were made except addition of internal cooling of the specimen and the antibacklash software during measurement, specimens No. 26 and 27 were coated. For specimen No. 26, a cooldown period of 10 to 15 minutes was inserted after spraying and before measurements were taken. For specimen No. 27, the entire operation was carried out continuously. The results of the optical probe measurements on these two specimens are compared in Table VI for the NiCrAlY coating, the initial layer of zirconia and the total coating thickness after the finish passes of zirconia. The table shows that for specimen No. 26, the NiCrAlY coating was 96.5 ±35.6 μm (3.8 ±1.4 mils) except for point 12, which was on the convex side of the leading edge, and point 13, which was on the concave side of the trailing edge. Slight adjustments of the spray coordinates for these two lines would have brought the NiCrAlY coating within the desired ±38.1 μm (±1.5 mils) tolerance band. The NiCrAlY measurements for specimen No. 27 showed the same uniformity, except that point 23, which was right on the leading edge, was also low. For the initial pass of zirconia, the pattern for specimen No. 26 was about the same as for NiCrAlY. The zirconia layer was 236.2 ±33 μm (9.3 ±1.3 mils), except for line 0, which was on the convex side of the trailing edge and lines 11, 12, and 23. In this case the spray that missed line 12 hit line 11, causing it to be oversprayed. Specimen No. 27 showed a similar pattern but an average of 94.0 μm (3.7 mils) less coating. The total coating thickness for specimen No. 26 came out 393.7 ±38.1 μm (15.5 ±1.5 mils) except for lines 11, 12 and 22. Additional finish passes would have brought lines 12 and 22 up to the desired coating, but would have caused line 11 to be badly oversprayed. It is reasonable to assume, however, that by adjusting line 12 and allowing an adequate number of finish passes, the entire specimen could have been coated within the desired range. The results for specimen No. 27 showed similar results for lines 11 and 12, but a heavier coating and a larger range of values on the other lines, 431.8 μm ±76.2 μm (17.0 ±3.0 mils).

It was concluded from these results that three corrections were needed in order to achieve a coating uniformity of ±38.1 μm (±1.5 mils):

1) A few scan lines needed adjustment to even out the deposition;

2) The heat generated during plasma spraying needed to be removed more efficiently in order to eliminate measurement errors caused by the effects of thermal expansion; and

3) Compensation was required for the growing backlash in the gimbals in the specimen manipulator on the Model No. 1 mechanism.

TABLE VI

Evaluation of APS Process System Using JT9D Specimens No. 26 & 27

Scan Line	NiCrAlY Blade No. 26	NiCrAlY Blade No. 27	Δ	1st ZrO$_2$ (10 pass) Blade No. 26	1st ZrO$_2$ (10 pass) Blade No. 27	Δ	Total Blade No. 26	Total Blade No. 27	Δ
0	3.0	2.8	0.2	7.4*	2.8*	4.6	14.0	14.8	-0.8
1	3.4	3.6	-0.2	8.4	4.0	4.4	16.2	17.8	-0.6
2	3.8	5.0	-1.2	10.6	5.6	5.0	17.0	18.4	-1.4
3	4.2	4.2	0.0	8.8	7.0	1.8	15.8	16.8	-1.0
4	4.6	4.6	0.0	8.4	6.8	1.6	15.8	16.0	-0.2
5	4.4	4.2	-0.2	8.4	6.6	1.8	16.0	16.4	-0.4
6	4.0	3.8	-0.2	8.2	7.0	1.2	15.2	16.4	-1.2
7	5.2	3.2	-2.0	8.0	7.0	1.0	15.8	16.2	-0.4
8	4.6	3.6	-1.0	8.8	6.6	2.2	16.0	16.2	-0.2
9	3.6	3.2	-0.4	9.0	5.8	3.2	14.8	15.6	-0.8
10	4.2	3.8	-0.4	10.0	6.0	4.0	16.0	17.2	-1.2
11	3.8	3.0	-0.8	11.6*	7.6*	4.0	18.6*	19.6*	-1.0
12	0.6*	1.2*	+0.6	6.0*	2.2*	3.8	11.8*	13.2*	-1.4
13	1.8*	2.2*	+0.4	9.4	5.4	4.0	14.0	14.6	-0.6
14	2.4	2.4	0.0	10.0	6.0	4.0	15.0	16.0	-1.0
15	3.2	3.2	0.0	9.4	6.2	3.2	14.8	16.2	-1.4
16	3.4	3.0	-0.4	10.0	5.8	4.2	14.8	15.6	-0.8
17	3.8	3.6	-0.2	10.2	5.4	4.8	15.2	16.6	-1.4
18	3.6	3.8	+0.2	9.6	5.6	3.0	14.8	17.0	-3.2
19	4.8	4.6	-0.2	10.0	5.4	4.6	15.0	18.0	-3.0
20	5.2	5.2	0.0	10.4	6.4	4.0	14.4	19.0	-4.6
21	4.4	4.8	-0.4	10.6	7.2	3.4	15.2	20.0	-4.8
22	-	2.4	-	-	4.0	-	13.6*	16.4	-2.8
23	2.8	1.8*	-1.0	5.6*	3.0*	2.6	14.0	14.0	0
Average	3.8	3.8		9.3	5.6		15.5	17.0	
Range	+1.4	+1.4		+1.3	+1.6		± 1.5	± 3.0	

* Not Included in Average or Range

(1) Measurement data is expressed in units of mils as printed by APS System.
    (1 mil = 25.4μm)

The errors in measurement caused by thermal effects are readily apparent by comparing the metrology result printouts for specimens No. 26 and 27 listed in Table VI. The measurements after spraying two passes per line of NiCrAlY showed very little difference between the two specimens. The measurement printouts after spraying ten passes per line of zirconia showed large differences on almost every line. The total coating thickness printouts after three sets of finish passes, with a measurement sequence after each set and only a few selected lines sprayed in the last set, showed large differences on only a few lines on the high curvature part of the concave side of the blade.

These results were consistent with the theory that the measurement values were in error by an amount that was proportional to the amount of heat buildup that the part was subjected to during the spray operation and the amount of time allowed for cooling before measurement. For specimen No. 26, a sufficient cooldown period (10 to 15 minutes) was allowed, so that true measurements were obtained and the coating uniformity was limited only by a few minor errors in the spray coordinate tables. For specimen No. 27, however, the measurements made after the first application of zirconia were low on some lines due to thermal warpage, causing too many finish passes to be applied on these lines during the first respray. During subsequent measurements, following finish passes in which only a few lines were sprayed, the specimen had time to cool down, so that the measurements revealed the overspray. This can be seen by comparing the measurements taken after each zirconia pass which are presented in Table VII along with the number of finish passes accumulated on each line. Lines 19, 20 and 21 all were judged to have had adequate coating after the first zirconia respray application and no additional finish passes were added. By the final measurement, the printouts for all three lines had increased by about 88.9 μm (3.5 mils) and indicated the overspray. It can also be seen from the data in Table VII that the effect of warpage was more predominant near the edges of the specimen. Lines 3 through 5 and 14 through 17, which were near the center of the airfoil and also had no finish passes after the first finish spray, showed considerably less change after cooldown, an average of 17.8 μm (0.7 mils). This indicated that the warpage included a significant twisting of the airfoil.

In order to correct this problem, additional cooling was provided in the form of air flow through the inside of the specimen. At the same time the antibacklash swing sequences before each gage point measurement were incorporated into the A- and B-axes to compensate for the effects of gimbal wear. At this time also, design considerations for a new mechanism were initiated. This mechanism would be required for the larger, heavier utility turbine blade specimens to be coated subsequently. It was also apparent that the early availability of this mechanism could circumvent the growing problems associated with the Model No. 1 mechanism on the smaller aircraft turbine blade specimens.

TABLE VII

Effect of Blade/Fixture Thermal Warpage on Coating Thickness

	Coating Thickness on JT9D Blade No. 27 (mils)[1]						
Scan Line	Total Coating After 1st ZrO_2	Total No. of Finish Passes	Total Coating After 1st Finish	Total No. of Finish Passes	Total Coating After 2nd Finish	Total No. of Finish Passes	Total Coating After 3rd Finish
0	5.6	12	11.4	18	13.6	20	14.8
1	7.6	10	14.6	12	16.8	12	17.8
2	10.6	6	17.0	6	18.8	6	18.4
3	11.2	6	16.0	6	16.4	6	16.8
4	11.4	6	15.6	6	15.6	6	16.0
5	10.8	6	15.4	6	15.6	6	16.4
6	10.8	6	14.6	8	15.6	8	16.4
7	10.2	6	14.6	8	15.8	8	16.2
8	10.2	6	14.4	8	16.0	8	16.2
9	9.0	8	13.4	10	14.6	12	15.6
10	9.8	8	14.8	10	16.6	10	17.2
11	10.6	6	17.4	6	18.6	6	19.6
12	4.4	14	9.2	22	11.4	28	13.2
13	7.6	10	14.6	12	15.4	12	14.6
14	8.4	10	15.6	10	16.6	10	16.0
15	9.4	8	16.2	8	16.6	8	16.2
16	8.8	8	15.0	8	15.8	8	15.6
17	9.0	8	15.0	8	16.2	8	16.6
18	9.4	8	14.4	10	15.8	10	17.0
19	10.0	8	15.4	8	16.6	8	18.0
20	11.6	6	15.6	6	16.6	6	19.0
21	12.0	4	16.4	4	17.4	4	20.0
22	6.4	12	12.8	16	15.4	16	16.4
23	4.8	14	11.2	20	14.4	22	14.0

NOTES: (1) Measurement data is expressed in units of mils as printed by APS System. (1 mil = 25.4 μm)

5.2 APS Process Evaluations

5.2.1 General Discussion

The automated plasma spray (APS) process developed in this program was designed to provide uniform and reproducible coatings on airfoils. Specifically, a two-layered thermal barrier coating of NiCrAlY and yttria stabilized zirconia was used to demonstrate the process. All preliminary evaluation efforts utilized a single airfoil geometry: the JT9D first stage turbine blade. This specimen was selected as representative of the most difficult specimens to coat uniformly. Process evaluation criteria included: 1) coating thickness uniformity and reproducibility, 2) coating structure, and 3) coating integrity.

The prime objective in the APS process/system development was coating thickness uniformity and reproducibility. Since the APS system contained an optical dimensional metrology subsystem, the system evaluation relied heavily on this device. This approach was not only feasible but was cost-effective once initial calibrations proved the approach accurate. Subsequent specimen sectioning was also done and dimensional measurements were obtained from photomicrographs to verify coating thickness performance.

Coating structure was to be maintained at the level of prior art demonstration (Ref. 1). Coating optimization, as such, was not an objective of the program. Evaluations of coating structure were performed relying on established procedures of part sectioning and metallography. Preliminary evaluations of coating integrity in a torch test and burner rig tests were performed. The results of the various evaluations are discussed in the following paragraphs.

5.2.2 Coating Deposition Thickness Control Evaluations

Evaluations of coating deposition thickness uniformity were performed by sectioning sprayed specimens and making measurements on photomicrographs taken of the sections. Micrographs taken at 50X provided an area for coating thickness measurements comparable to the area measured by the optical probe. Coating thickness evaluations covered both manually sprayed and APS system coated JT9D first stage blade specimens.

5.2.2.1   Manually Sprayed Aircraft Turbine Blades

Evaluations were performed on two JT9D specimens (Nos. X and Y) hand sprayed by two different operators with the blades clamped in a vise. These specimens were representative of manual plasma spray (MPS) production operations using no mechanization. These evaluations were performed to provide baseline data for comparison with the data obtained on the APS process.

Figure 30 illustrates the specimen sectioning scheme. Cuts were made perpendicular to the length of the airfoil at about 32 mm (1-1/4 inch) and 50 mm (2 inches) from the tip. The tip end portion of the airfoil was then sectioned along its length at about 7.6 mm (0.3 inch) from the leading edge. Surfaces "A" and "B" were polished and photographed. Figures 31 through 34 show surfaces "A" and "B" for specimens No. X and Y. These figures show an overall view of the coating distribution and uniformity. Figure 33 shows that the coating pulled away from the specimen surface on the concave side. Measurements of the coating thickness were made on surface "A" of each specimen at the same points at which optical probe measurements were made on the automatically sprayed specimens (Figure 29). Surface "B" of each specimen was measured every 6.4 mm (0.25 inches) along its length on each side. The results of these measurements are presented in Table VIII. For both operators the uniformity along the length of a line averaged about $\pm$38.1 μm (1.5 mils) for NiCrAlY and 45.7 μm (1.8 mils) for total. The average variation between points on the cross-section, however, was much greater: $\pm$112 μm (4.4 mils) for NiCrAlY and $\pm$417 μm (16.4 mils) total. The average NiCrAlY thickness was 180 μm (7.1 mils) and the average total thickness was 886 μm (35.9 mils). While the data was limited, it suggested that the spread in coating thickness was a relatively fixed percentage of the thickness rather than a fixed number, so that for a total coating thickness of 406 μm (16.0 mils) the uniformity would be expected to be about $\pm$190 μm (7.5 mils).

Although the average coating thicknesses and the spread in thicknesses were not drastically different between the two specimens, there were significant differences between the two as seen by comparing Figures 31 through 34. Specimen No. Y had a fairly uniform coating except for a few locations which were considerably thinner or thicker. The concave side had only a slightly thicker coating than the convex. Specimen No. X had a much thicker coating on the concave side and was very nonuniform on the convex side. These differences illustrated that, for manually sprayed specimens, the problem was not just nonuniformity of the coating on a particular specimen. An even greater problem was lack of reproducibility from one specimen to another because of the many factors affecting human operator performance.

5.2.2.2   APS Process Coated Aircraft Turbine Blades

Of the many JT9D blade specimens (over 50) that were coated using the APS process system, about twenty were coated completely and had printouts of the coating thicknesses. Table IX lists the spread of the best specimens done during the time when there was still a thermal warpage problem. The best uniformity achieved on these specimens was $\pm$43 μm (1.7 mils) for NiCrAlY and $\pm$79 μm (3.1 mils) for total thickness. The average for the ten specimens was $\pm$68.1 μm (2.68 mils) for NiCrAlY and $\pm$98.3 μm (3.85 mils) for total thickness. (The comparable average results for manually sprayed blades were $\pm$112 μm (4.4 mils) for NiCrAlY and $\pm$190 μm (7.5 mils) for total thickness.) Thus, even at that stage of process development, the specimens coated by the APS process exhibited approximately half the variation in overall deposition thickness uniformity achieved with the MPS process. The reproducibility in the coating deposition profiles from specimen to specimen with the APS process was vastly improved.
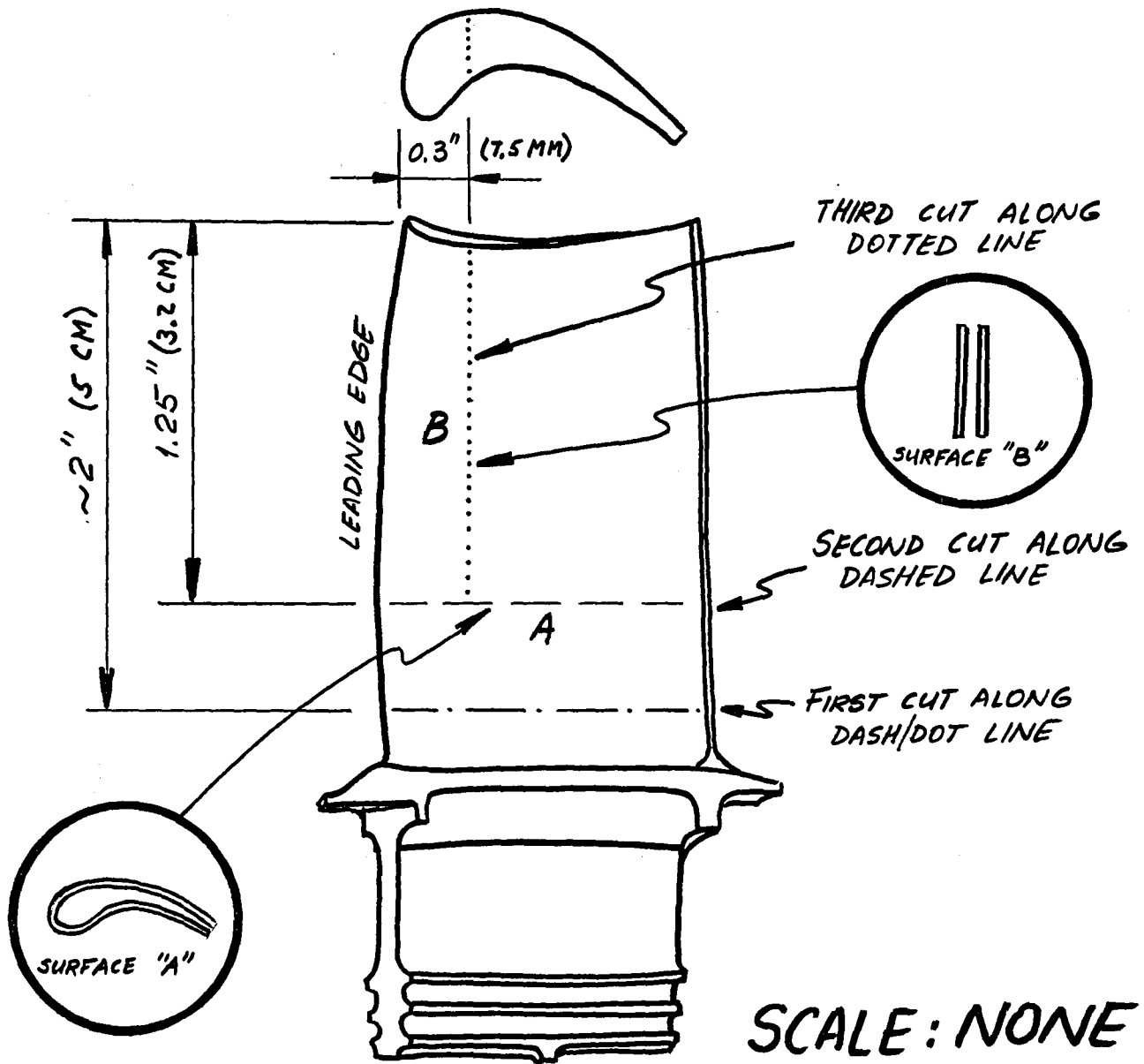
80

Figure 30.   Locations of Sections Examined for
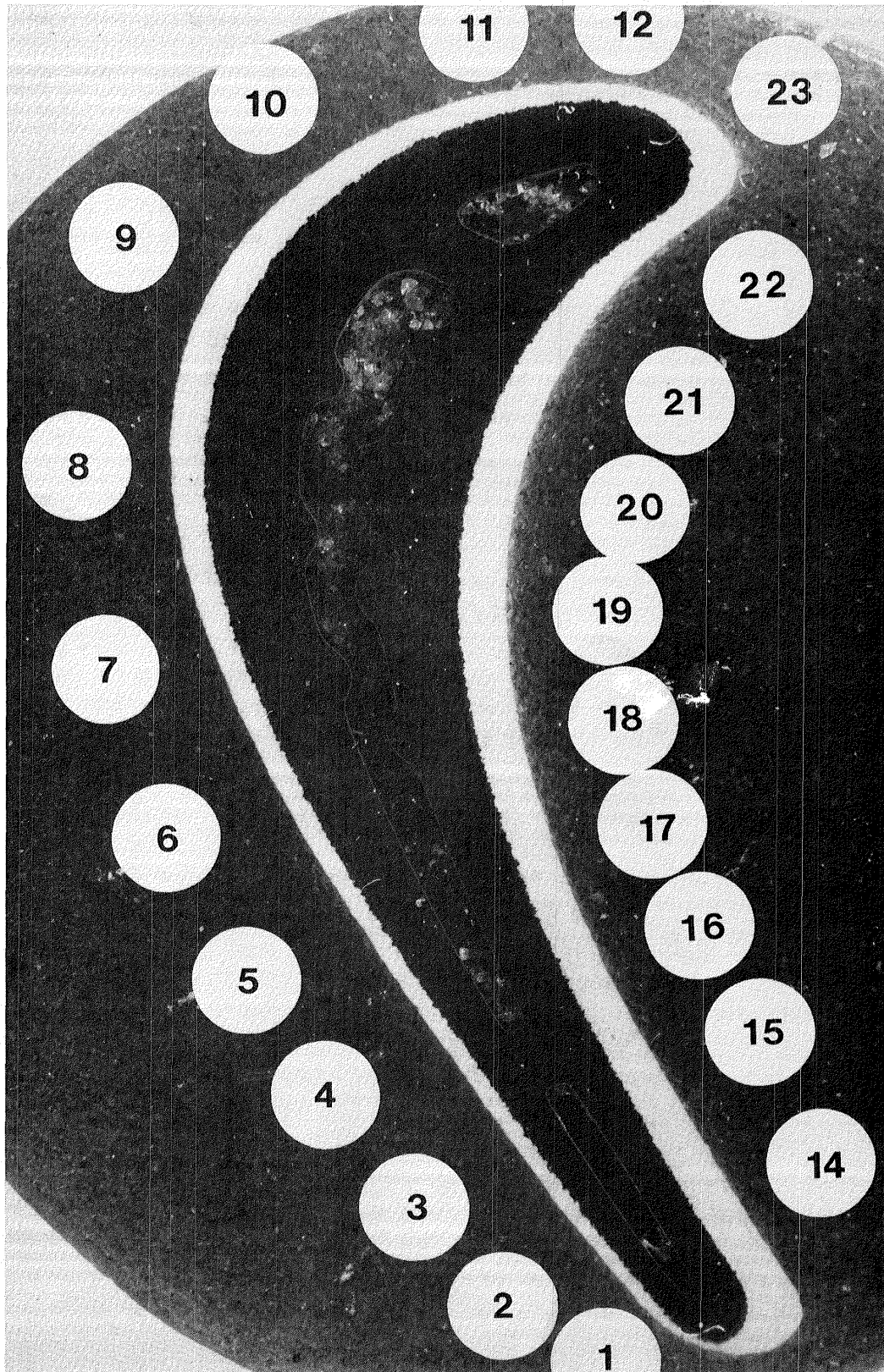Manually Sprayed JT9D Blade Specimens.

Figure 31.   Photomacrograph Cross-section of Manually Sprayed
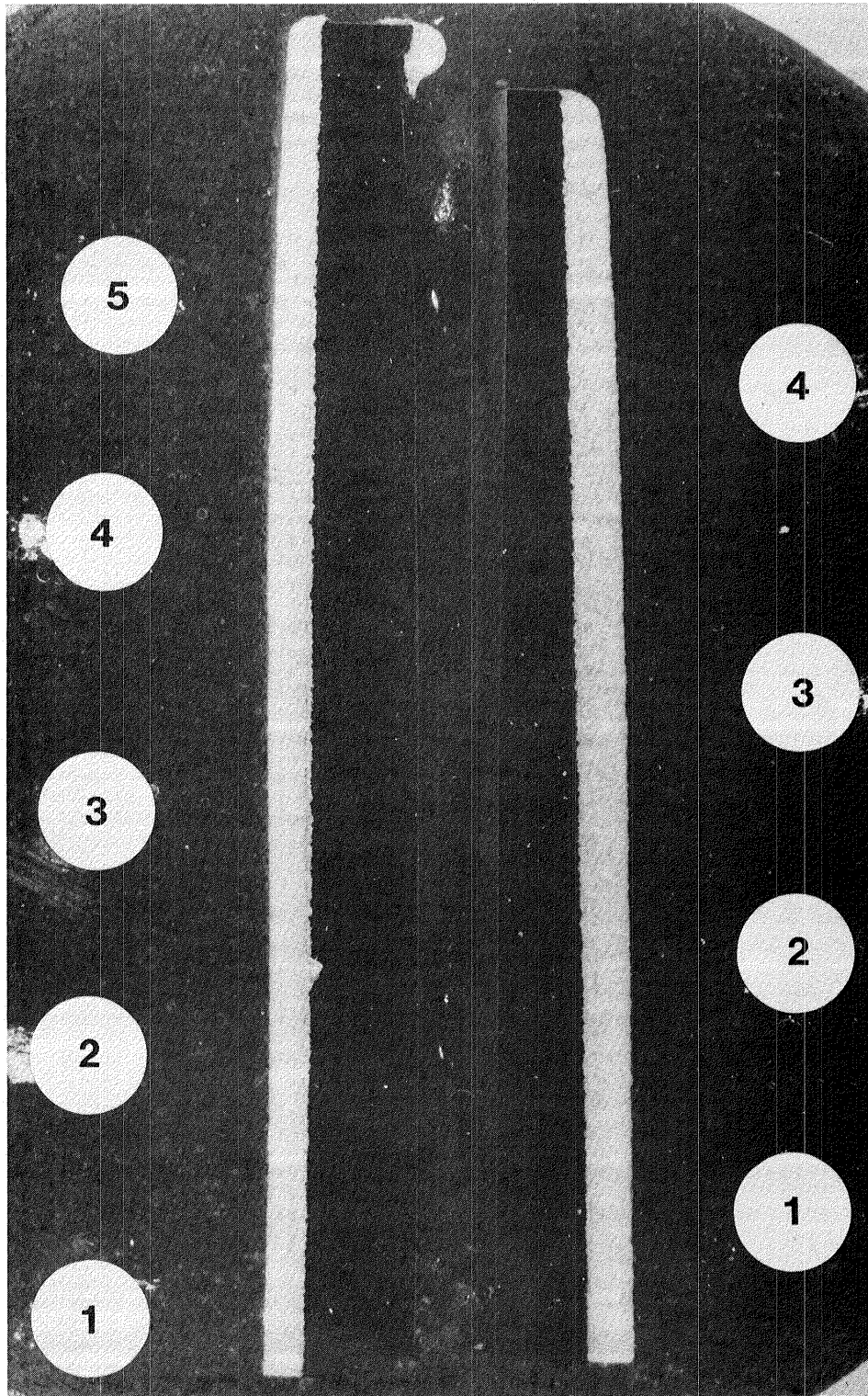JT9D Blade Specimen No. "X" at Surface Location "A".

Figure 32. Photomacrograph Cross-section of Manually Sprayed
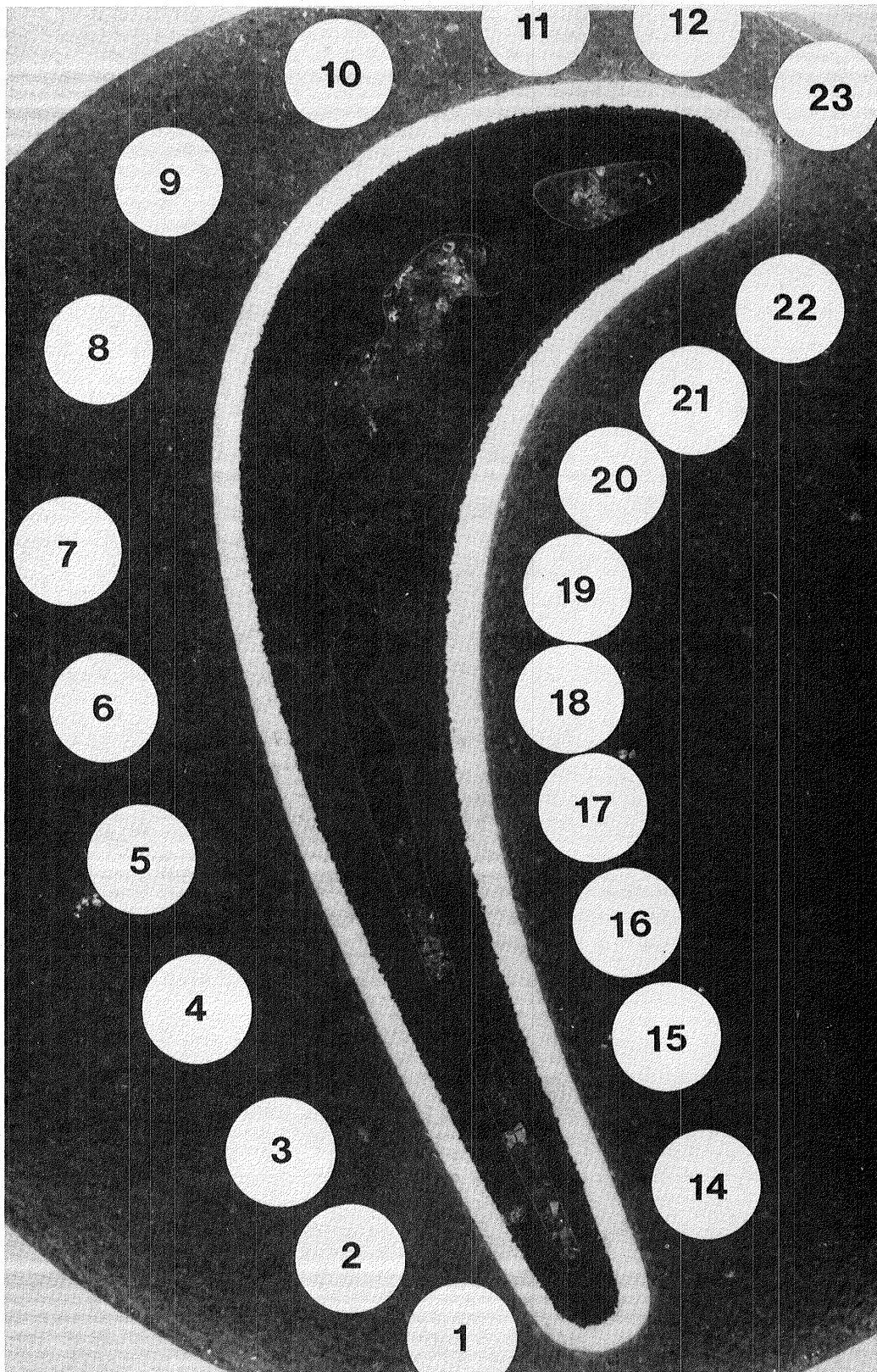JT9D Blade Specimen No. "X" at Surface Location "B".

Figure 33. Photomacrograph Cross-section of Manually Sprayed
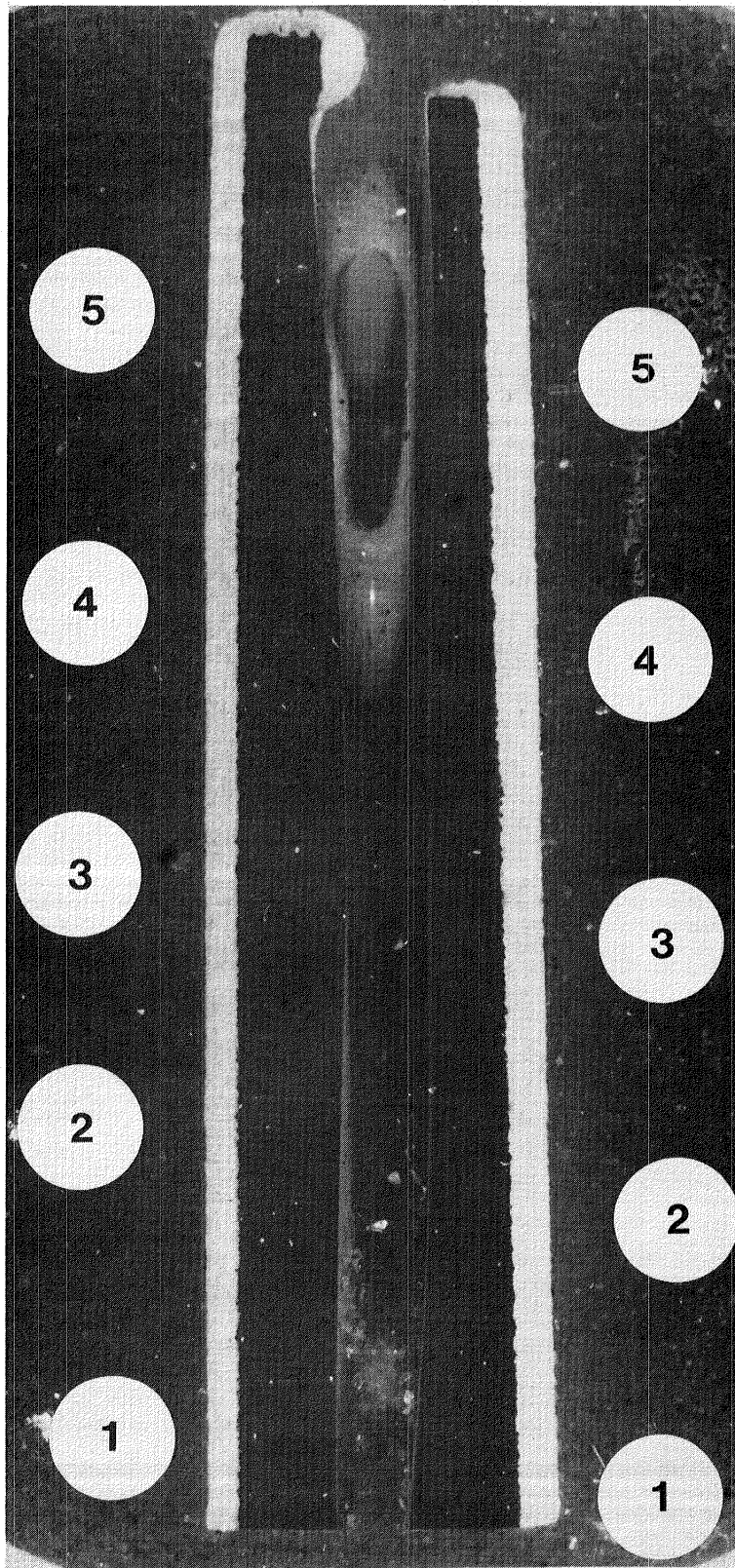JT9D Blade Specimen No. "Y" at Surface Location "A".

Figure 34. Photomacrograph Cross-section of Manually Sprayed
JT9D Blade Specimen No. "Y" at Surface Location "B".

TABLE VIII

Coating Thickness Measurements on Manually Sprayed JT9D Blade Specimens

Side	Location No.	Surface A — Specimen No. X NiCrAlY	Surface A — X Total	Surface A — Y NiCrAlY	Surface A — Y Total	Location No.	Surface B — Specimen No. X NiCrAlY	Surface B — X Total	Surface B — Y NiCrAlY	Surface B — Y Total
Suction (Convex)	1	3.9	15.0	2.4	26.0	1	3.9	43.3	3.9	33.1
	2	5.5	18.1	4.7	30.7	2	5.5	47.3	3.9	31.5
	3	5.5	22.1	4.7	31.5	3	5.5	44.9	4.7	31.5
	4	6.3	22.1	3.9	31.5	4	6.3	44.1	5.5	34.7
	5	6.3	23.6	3.9	32.3	5	8.7	45.7	4.7	30.7
	6	7.1	28.4	5.5	32.3					
	7	8.7	33.5	6.3	33.9					
	8	9.5	43.3	4.7	31.5					
	9	9.5	47.3	5.5	32.3					
	10	9.5	39.4	5.5	33.9					
	11	7.1	27.6	7.1	31.5					
	12	7.9	23.6	7.9	30.7					
	median spread	6.70 +2.80	31.15 +16.15	5.15 +2.75	29.95 + 3.95		6.30 +2.40	45.3 + 2.0	4.70 +0.80	32.70 + 2.00
	average std dev.	7.23 +1.83	28.67 +10.17	5.18 +1.49	31.50 + 2.02		5.98 +1.75	45.06 + 1.54	4.54 +0.67	32.30 + 1.60
Pressure (Concave)	14	3.9	47.3	7.1	37.0	1	3.9	49.6	7.9	47.3
	15	4.7	47.3	9.5	39.4	2	5.5	51.2	8.7	46.5
	16	4.7	47.3	9.5	43.3	3	5.5	50.4	9.5	44.9
	17	5.5	48.1	11.8	44.9	4	5.5	48.1	9.5	44.1
	18	6.3	49.6	13.4	47.3	5	–	–	11.8	45.7
	19	7.9	53.6	13.4	48.9					
	20	5.5	52.0	11.8	43.3					
	21	5.5	46.5	9.5	33.1					
	22	3.9	29.9	3.9	22.1					
	23	3.2	41.8	5.5	31.5					
	median spread	5.55 +2.35	41.75 +11.85	8.65 +4.75	35.5 +13.4		4.70 +0.80	49.65 + 1.55	9.85 +1.95	45.70 + 1.60
	average std dev.	5.11 +1.36	46.34 + 6.60	9.54 +3.23	39.08 + 8.30		5.10 +0.80	49.83 + 1.32	9.48 +1.46	45.70 + 1.26
Total	median spread	6.25 +3.25	34.30 +19.30	7.90 +5.50	35.50 +13.40		6.30 +2.40	47.25 + 3.95	7.85 +3.95	39.00 + 8.30
	average std dev.	6.27 +1.93	36.70 +12.41	7.16 +3.25	34.95 + 6.82		5.59 +1.41	47.18 + 2.85	7.01 +2.81	39.00 + 7.19

Notes: 1) Values listed for the "Total" column are the sum of the NiCrAlY and ZrO_2 coatings.

2) Values are expressed in mils (1 mil = 25.4 μm).

TABLE IX

Coating Thickness Uniformity Achieved by APS Process on JT9D Turbine Blade Specimens Prior to System Modifications for Specimen Internal Cooling

Specimen No.	Coating Thickness (Mils)	
	NiCrAlY (Average/Spread)	Total (Average/Spread)
22	4.7 ± 3.5	11.2 ± 3.2
23	4.9 ± 3.7	16.5 ± 3.7
26	2.9 ± 2.3	15.2 ± 3.4
27	3.2 ± 2.0	16.6 ± 3.4
29	2.4 ± 2.4	16.3 ± 3.1
30	4.2 ± 2.6	18.8 ± 3.8
31	7.3 ± 3.5	14.8 ± 4.2
34	3.5 ± 1.7	20.8 ± 5.0
35	3.9 ± 3.3	19.1 ± 4.9
37	4.2 ± 1.8	17.8 ± 3.8
Average	4.12± 2.68	16.71± 3.88

Specimens No. 26 and 27 were sectioned and photographed to verify the actual coating uniformity. Section A (cross-section) on each specimen was made in about the same location as on the manually sprayed blades. Section B was only cut on specimen No. 26 and was located at approximately the center of the airfoil rather than near the leading edge. Section A on specimen No. 26 included only the part of the specimen from Section B to the leading edge. Figures 35, 36 and 37 show photomacrographs of Section A and B of specimen No. 26 and Section A of specimen No. 27, respectively. These figures provide an overall view of the coating distribution and uniformity. 50X photomicrographs were made around Section A of each specimen approximately at the points where optical probe measurements were made during spraying, and along Section B of specimen No. 26 at 6.4 mm (0.25 inch) intervals on both sides. The coating thicknesses at each location, both for NiCrAlY and for total coating thickness, were measured on each photomicrograph. The results of these measurements are listed in Table X.

Figures 38 and 39 show two of the most difficult areas to spray on specimen No. 27. Figure 38 shows the area with the highest radius of curvature, the leading edge (Point 23). Figure 39 shows one side of the trailing edge adjacent to the cooling passage opening (Point 1). The coating tapered down to the edge of the cooling passage without blocking the opening. This excellent result was accomplished without masking. The data in Table X show that the uniformity along the length of a scan line (Section B) was ± 10 μm (0.4 mils) for NiCrAlY and ± 20 μm (0.8 mils) for total, which was about a factor of three better than on the manually sprayed specimens. The uniformity between scan lines (Section A) was ± 57 μm (2.2 mils) for NiCrAlY and ± 66 μm (2.6 mils) for total thickness. Both of these values were considerably better than could be done by manual spraying. Also, the average coating thicknesses for each portion of a specimen, and for each entire specimen, were within the desired ranges of 79 to 155 μm (3.1 to 6.1 mils) for NiCrAlY and 368 to 445 μm (14.5 to 17.5 mils) for total coating thickness. These results demonstrated that, even with the problem of thermal warpage when these specimens were sprayed, the APS system was considerably better than manual spraying in deposition uniformity and reproducibility both between specimens and around each specimen.

Figure 40 is a graph comparing coating thicknesses taken from the optical probe data in Table VI with the photomicrograph data in Table X for specimen No. 27. The agreement was quite good. A carefully controlled experiment, in which special precautions were taken to identify the exact locations of the optical probe and metallurgical measurement points, would be required to determine whether or not the differences shown in Figure 40 were statistically significant.

Another comparison that can be made is the coating uniformity as indicated by the two types of measurements. If the results for specimens Nos. 26 and 27 are compared over the regions where data is available by both methods, the average spread for the two types of coatings on the two specimens was ± 64 μm (2.5 mils) based on photomicrograph measurements and ± 71 μm (2.8 mils) based on the optical probe measurements. These results verified that the metrology subsystem could make in-process, on-the-machine specimen profile measurements providing a reliable indication of the coating uniformity. Figure 40 thus displays a unique feature of the developed APS system.
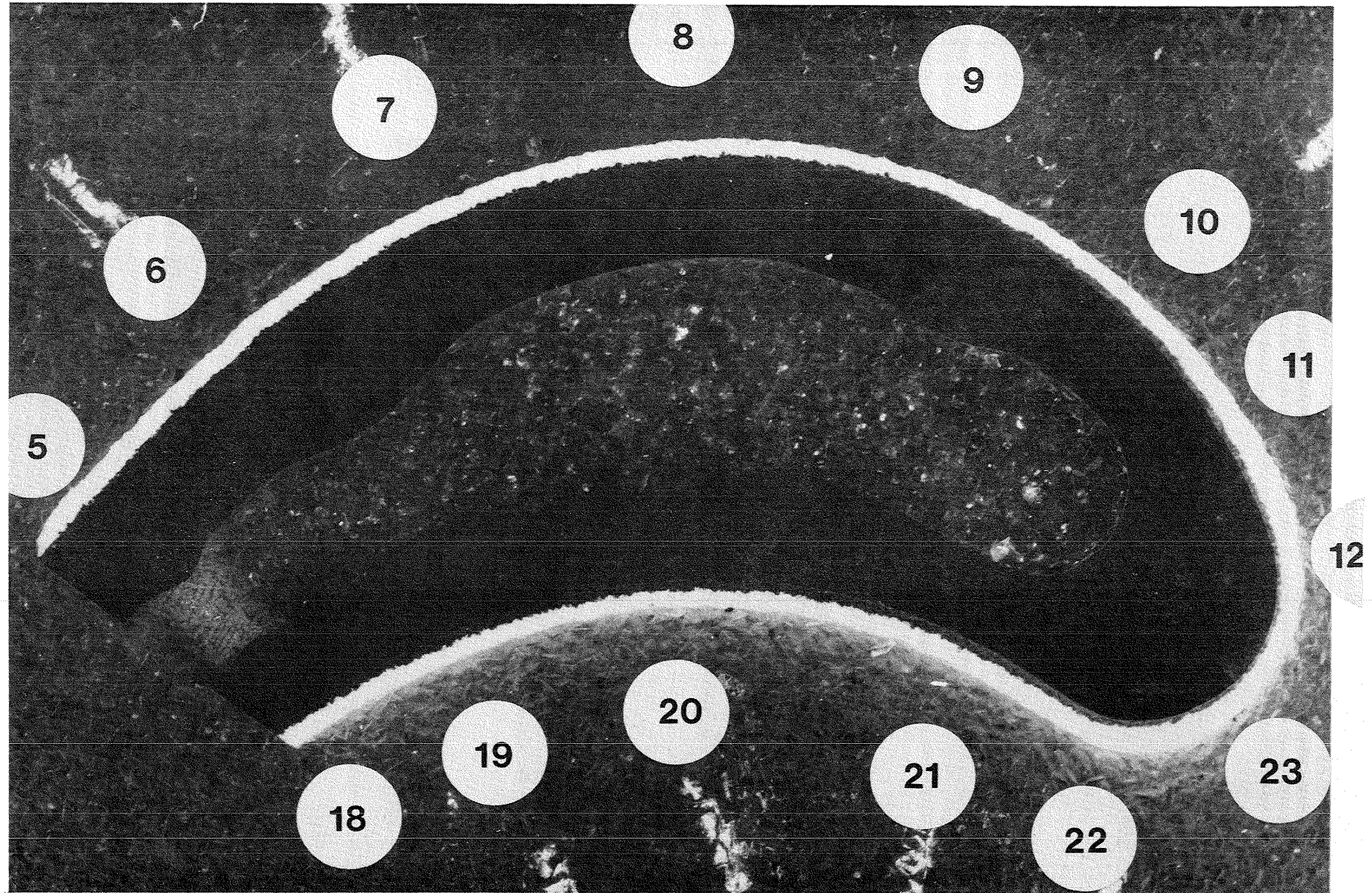
Figure 35. Cross-section of JT9D Blade Specimen No. 26 from Center to Leading Edge after Coating with APS System and Torch Test (Approximate locations where micrographs were taken are indicated by numbers).
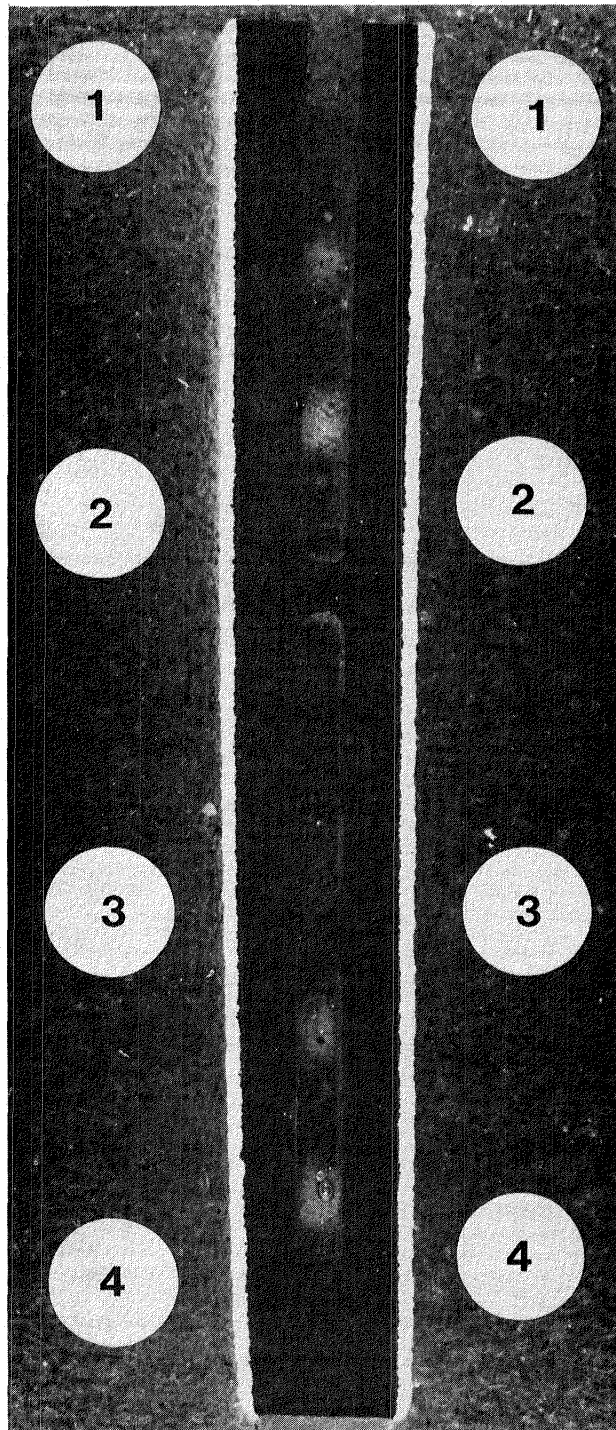
Figure 36.   Length Section of JT9D Blade Specimen No. 26 from Tip to Section "A" after Coating with APS System and Torch Test (Approximate locations where micrographs were taken are indicated by numbers).
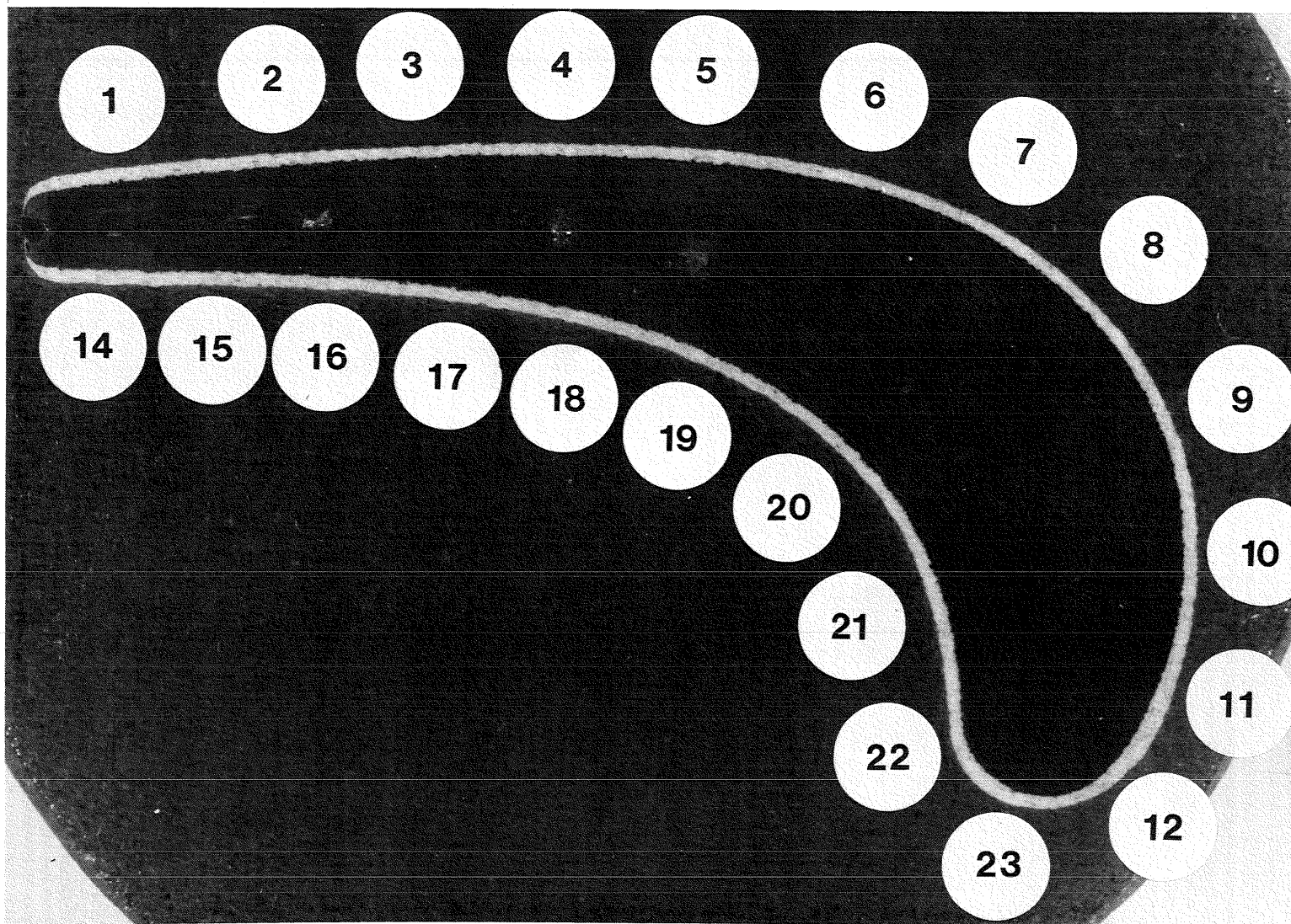
Figure 37.   Cross-section of JT9D Blade Specimen No. 27 after Coating
by APS System (Approximate locations where micrographs were
taken are indicated by numbers).

TABLE X

Coating Thickness Measurements on JT9D Turbine Blade Specimens
Coated by the APS Process Before Addition of Specimen Internal Cooling

Side	Location No.	Surface A (Cross-Section) Specimen No. 27 NiCrAlY	Total	Specimen No. 26 NiCrAlY	Total	Location No.	Surface B (Length) Specimen No. 26 NiCrAlY	Total
Convex	1	3.7	17.1			1	5.1	17.3
	2	5.0	17.6			2	5.5	18.1
	3	4.9	16.2			3	5.3	17.3
	4	4.1	15.6			4	5.3	16.4
	5	4.2	16.5	3.9	15.4			
	6	3.9	16.5	4.2	15.8			
	7	4.7	16.0	5.0	16.0			
	8	3.9	16.2	5.1	15.4			
	9	3.9	16.0	4.7	14.2			
	10	4.2	16.5	4.3	13.8			
	11	3.9	19.5	3.5	17.7			
	12	1.3	15.2	1.6	11.8			
	median	3.15	17.35	3.35	14.75		5.30	17.25
	spread	+1.85	± 2.15	+1.75	± 2.95		+0.20	+0.85
	average	3.98	16.58	4.03	15.01		5.30	17.28
	std. dev.	+0.94	± 1.11	+1.12	± 1.76		+0.16	± 0.70
Concave	14	4.2	18.4			1	4.3	16.2
	15	4.2	17.9			2	4.7	15.8
	16	4.5	16.3			3	4.7	15.8
	17	4.2	16.5			4	5.5	17.3
	18	4.2	17.3	5.1	15.4			
	19	5.4	17.1	5.8	15.8			
	20	5.8	17.9	6.0	16.4			
	21	5.4	18.7	6.0	17.6			
	22	3.2	17.9	4.3	16.2			
	23	1.6	15.0	2.7	15.0			
	median	3.70	16.85	4.35	16.30		4.90	16.55
	spread	+2.10	± 1.85	+1.65	± 1.30		+0.60	± 0.75
	average	4.27	17.30	4.98	16.07		4.80	16.28
	std. dev.	+1.21	± 1.12	+1.30	± 0.91		+0.50	± 0.71
Total	median	3.55	17.25	3.80	14.75		4.90	16.95
	spread	+2.25	± 2.25	+2.20	± 2.95		+0.60	± 1.15
	average	4.11	16.90	4.44	15.46		5.05	16.78
	std. dev.	+1.06	± 1.15	+1.25	± 1.51		+0.44	± 0.84

Notes: 1) Values listed for "Total" columns are the sum of the NiCrAlY and ZrO_2 coatings.

2) Values are expressed in mils (1 mil = 25.4 μm).
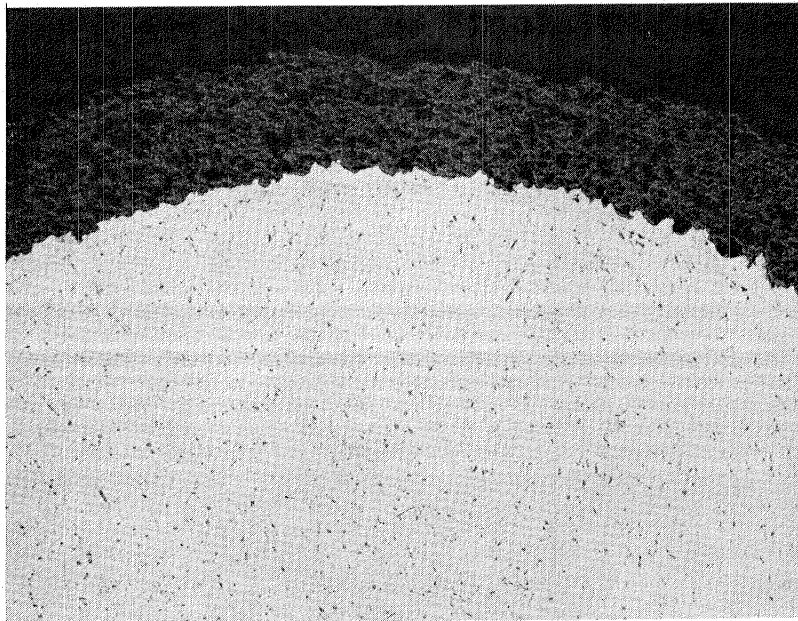
Figure 38. Photomicrograph of APS-Coated JT9D Blade Specimen No. 27 at Point No. 23 (Leading Edge)(50X).
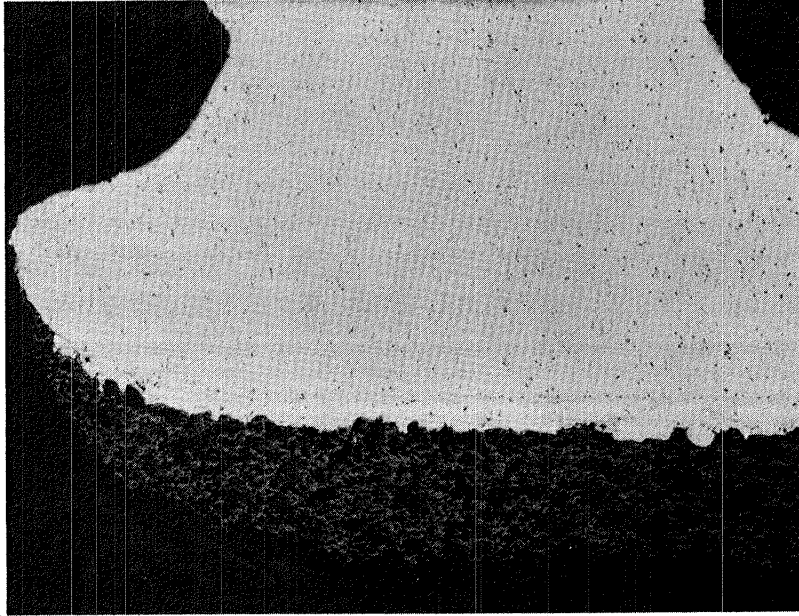
Figure 39.   Photomicrograph of APS-Coated JT9D Blade Specimen No. 27
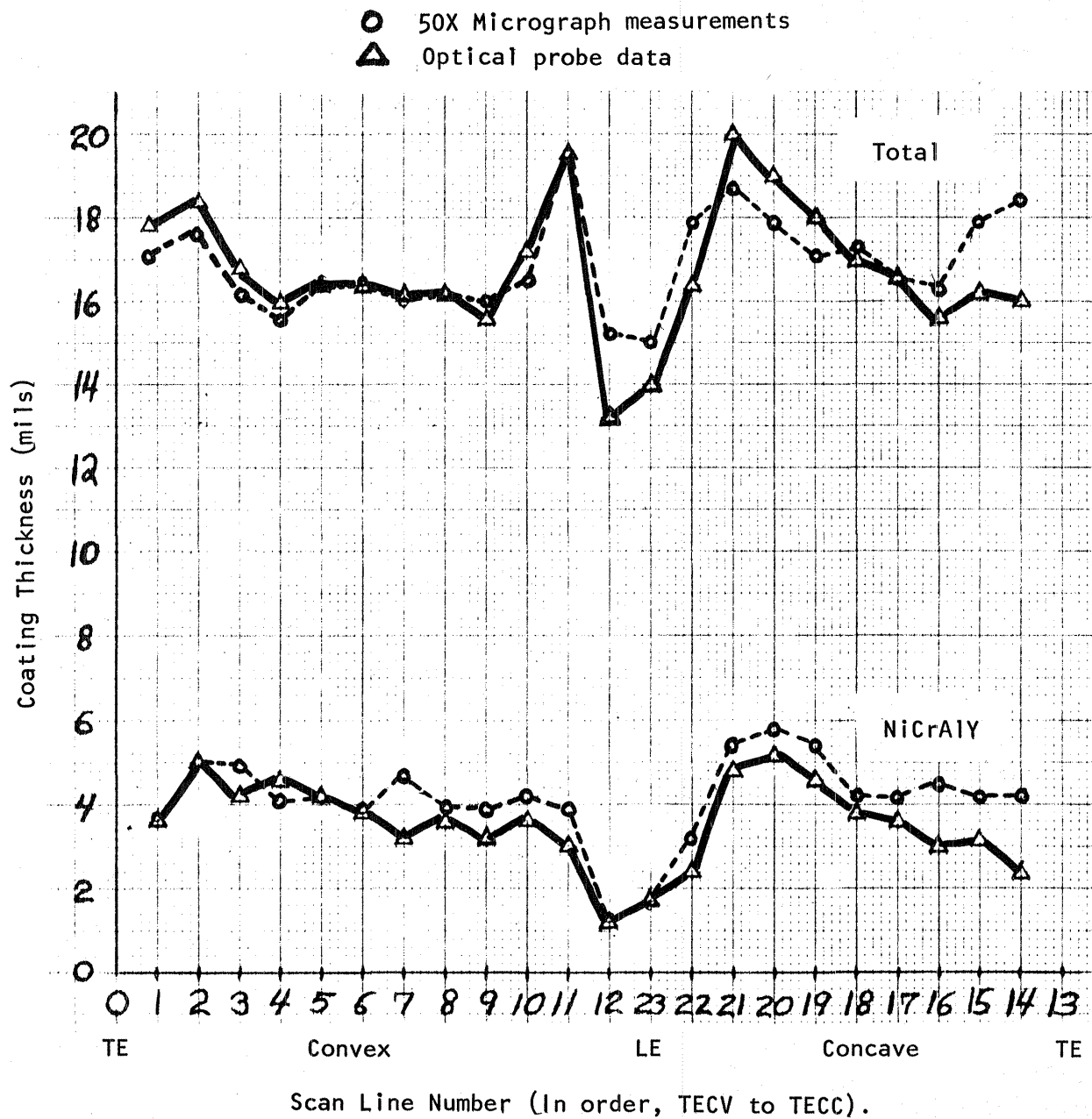   at Point No. 1 (Trailing Edge) (50X).

Figure 40. Comparison of Photomicrograph and Optical Probe Coating Thickness Measurements on JT9D Blade Specimen No. 27.

5.2.3 Macro Coating Characteristics

In addition to evaluating the APS process coatings and manually sprayed coatings for thickness uniformity, the coatings were visually examined at 50X for evidence of cracking, oxides, interface quality, etc. Figures 41 through 48 illustrate the features observed in the coatings on specimens X and Y which were manually sprayed. On these two specimens the coating was applied over an aluminide coating on the specimen surface. The photomicrographs show the variation in the substrate/bond coat interface quality and the range of porosity and cracking found in the zirconia coating. Figures 49 through 52 show the substrate/bond coat interface quality and the porosity found in the coatings deposited by the APS process system. It should be noted there was no cracking in the APS process coatings, while there was in the manually applied coatings. The photomicrographs illustrated that neither coating process was optimized, although, as a whole, the APS process coatings appeared to be better quality.

5.2.4 Torch Test Evaluation of Aircraft Turbine Blade

One of the JT9D blade specimens coated by the APS process (No. 26) was submitted to a torch test at NASA to determine coating integrity. After 23 one-hour thermal exposures, the test was stopped because of surface spallation. The localized thermal barrier spallation on the leading edge (see arrow) is shown in Figure 53. Under macroscopic examination, three small localized spallation areas on the leading edge were observed. Figure 54 shows the spallation areas at 40X and 100X. In the spalled area just to the right of the arrow in Figure 53 (the area closest to the root platform), the total coating thickness was reduced approximately 20% by the spallation.

Microscopic examination of the spalled region showed a thin bond coat, varying from one to three mils in thickness. This corresponded with the printouts obtained from the APS process system optical detector for the NiCrAlY coating on the leading edge (Figure 55, at lines 12 and 23). No cracks, either parallel to or at an angle to the bond coat/zirconia interface were present in the area of spallation. The localized spallation was probably due to exfoliation of loosely bonded outer layers of the ceramic.

5.2.5 Burner Rig Tests on Cylindrical Specimens

This section summarizes results of work which was not part of the APS Feasibility Study contract. However, it was a direct application and evaluation of the APS process. Coating of burner rig test specimens was performed under separate NASA/LeRC Purchase Order No. C-34826-D. Subsequent burner rig testing was done by NASA, while metallurgical evaluations were done by the TRW Materials Technology Laboratory Coatings Section.

The burner rig specimens were 12.7 mm (0.5 inch) diameter by 102 mm (4.0 inch) long cylinders. The cylinders were covered with a thermal barrier coating consisting of 127 ±38 μm (5 ±1.5 mils) of NiCrAlY and either 254 ±38 μm (10 ±1.5 mils) or 381 ±38 μm (15 ±1.5 mils) of zirconium oxide. Since these were the first official specimens
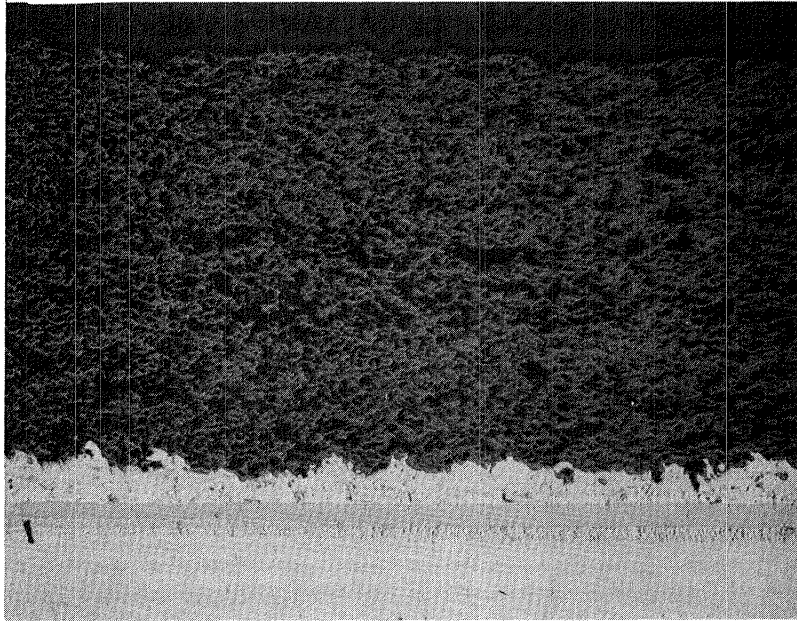
Figure 41. Photomicrograph of Manually Coated JT9D Blade Specimen No. "X" (Surface "A") at Location 14 (50X).
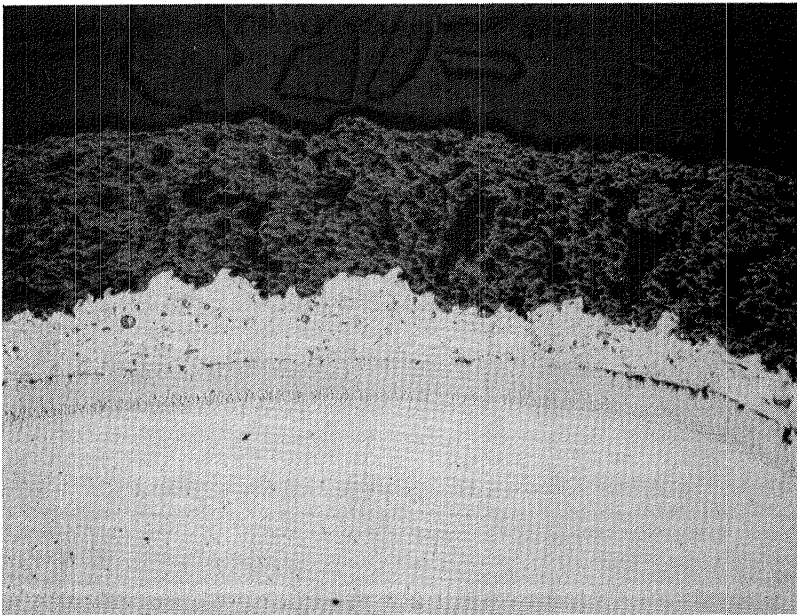

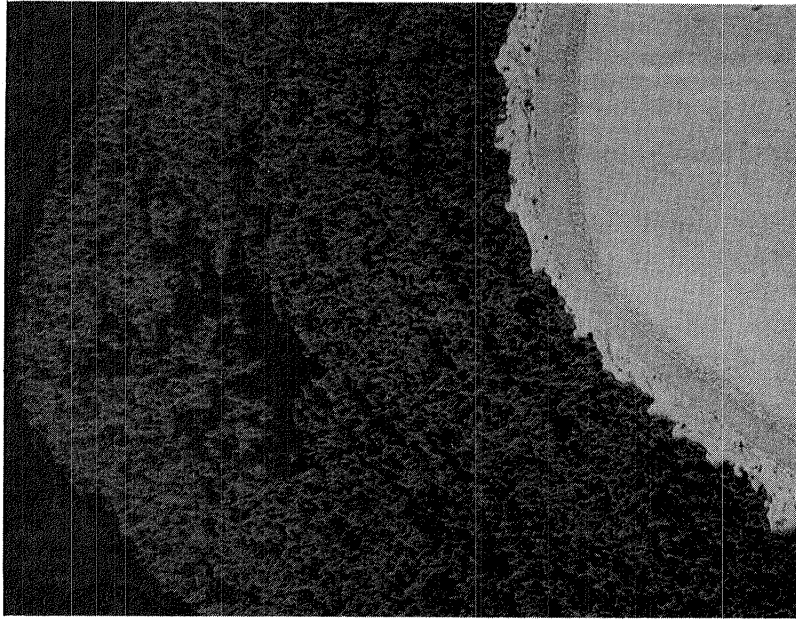Figure 42. Photomicrograph of Manually Coated JT9D Blade Specimen No. "X" (Surface "A") at Location 12 (50X).

Figure 43.   Photomicrograph of Manually Coated JT9D Blade Specimen
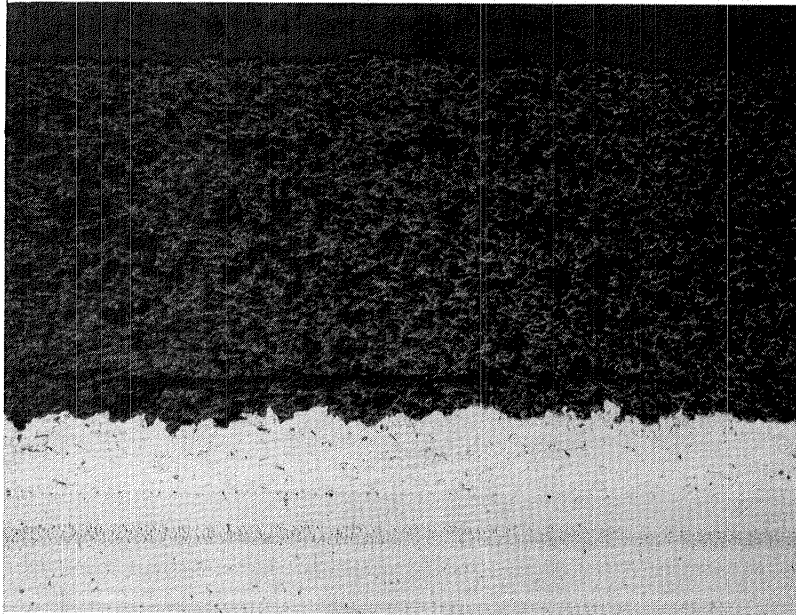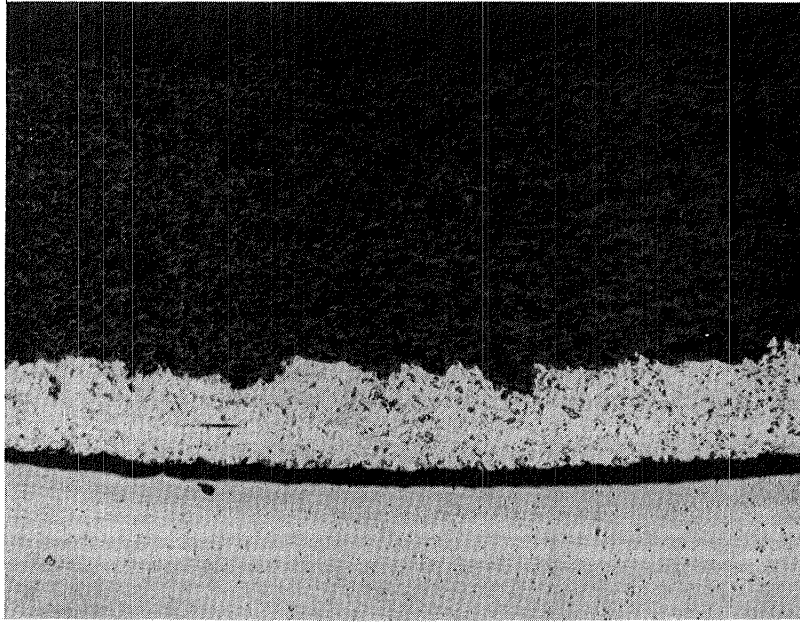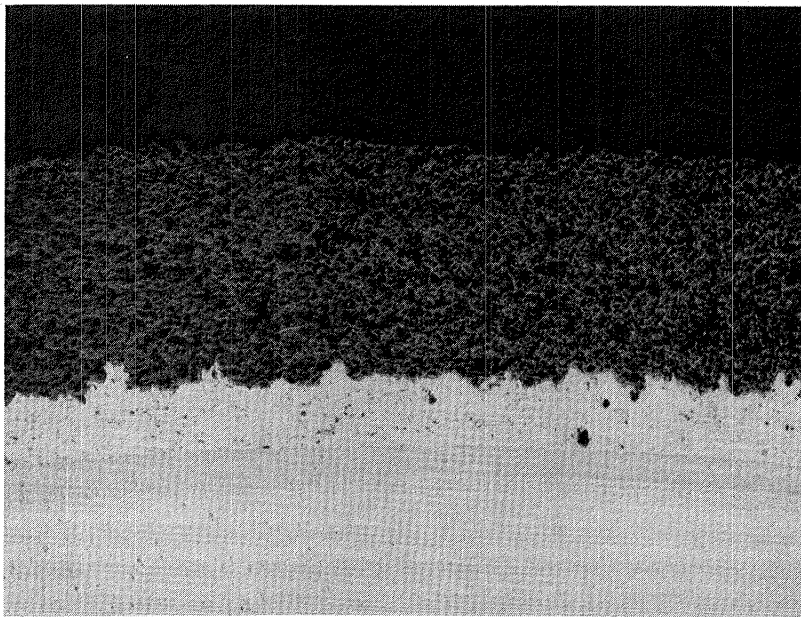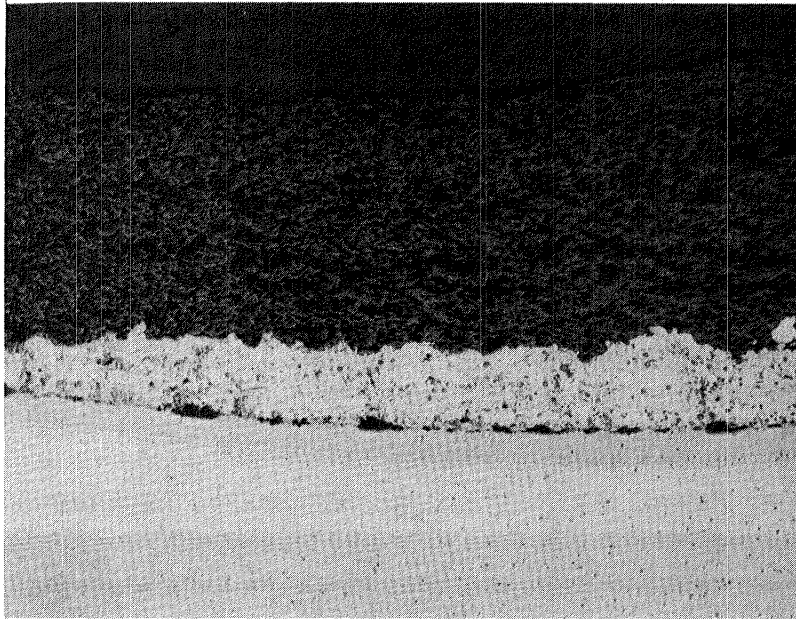No. "X" (Surface "A") at Location 13 (50X).

Figure 44.   Photomicrograph of Manually Coated JT9D Blade Specimen
No. "X" (Surface "B") at Location 5 (50X).

Figure 45.   Photomicrograph of Manually Coated JT9D Blade Specimen
No. "Y" (Surface "A") at Location 20 (50X).

Figure 46.   Photomicrograph of Manually Coated JT9D Blade Specimen
No. "Y" (Surface "A") at Location 11 (50X).

Figure 47. Photomicrograph of Manually Coated JT9D Blade Specimen
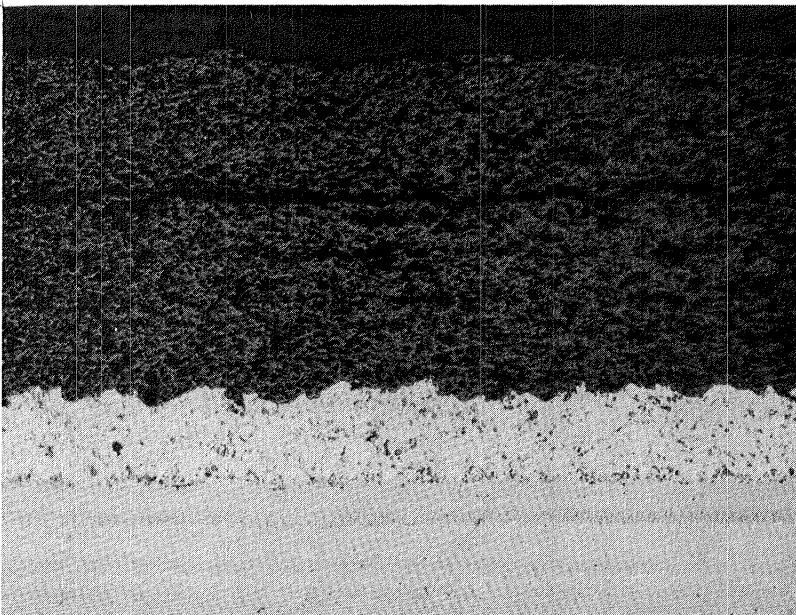No. "Y" (Surface "A") at Location 21 (50X).

Figure 48. Photomicrograph of Manually Coated JT9D Blade Specimen
No. "Y" (Surface "A") at Location 8 (50X).
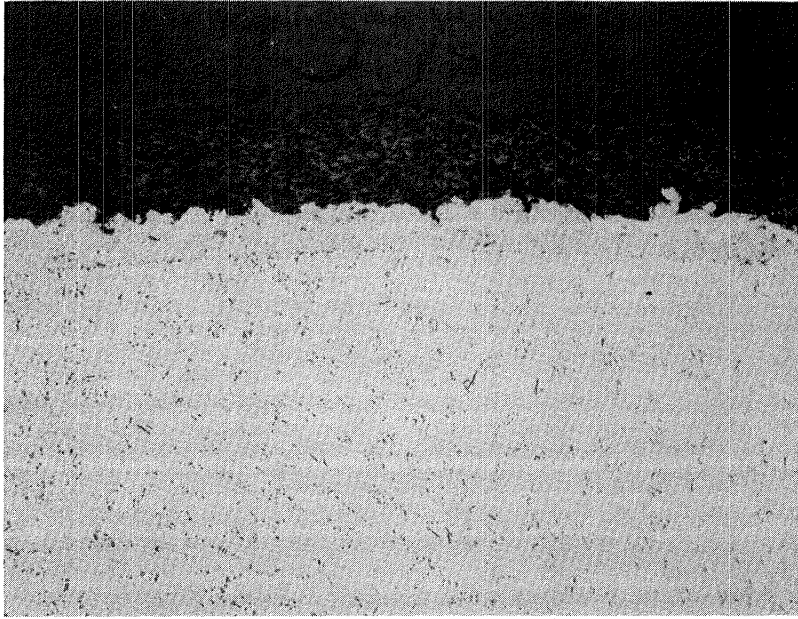
Figure 49.   Photomicrograph of APS Process Coated JT9D Blade Specimen
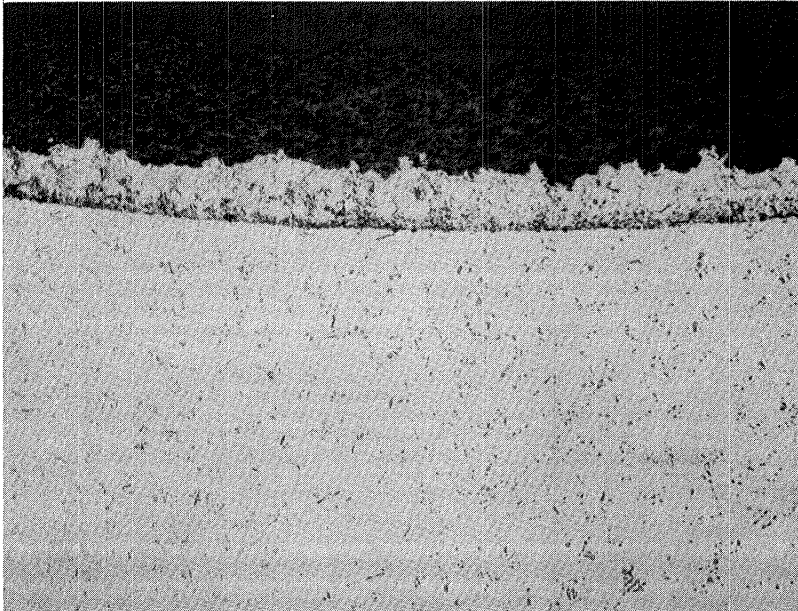No. 26 (Surface "A") at Location 9 (50X).

Figure 50.   Photomicrograph of APS Process Coated JT9D Blade Specimen
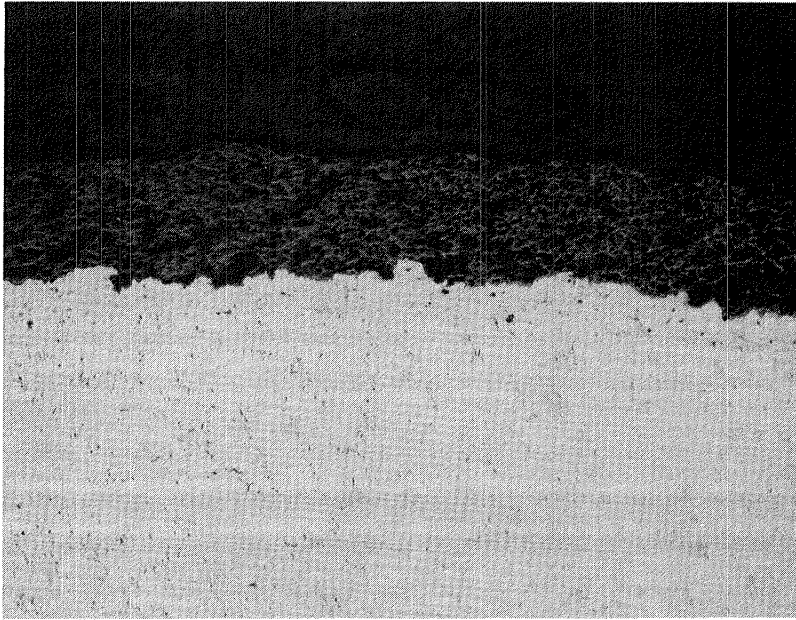No. 26 (Surface "A") at Location 21 (50X).

Figure 51.   Photomicrograph of APS Process Coated JT9D Blade Specimen
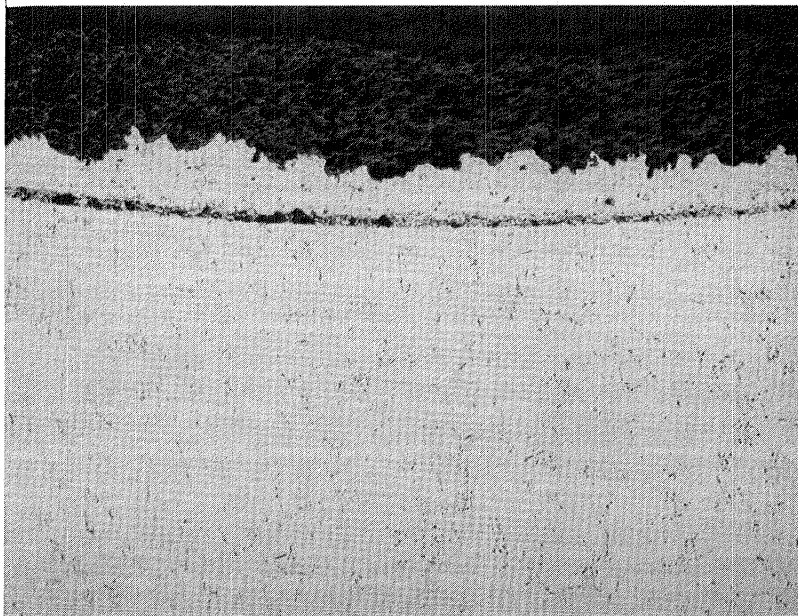No. 27 (Surface "A") at Location 10 (50X).

Figure 52.   Photomicrograph of APS Process Coated JT9D Blade Specimen
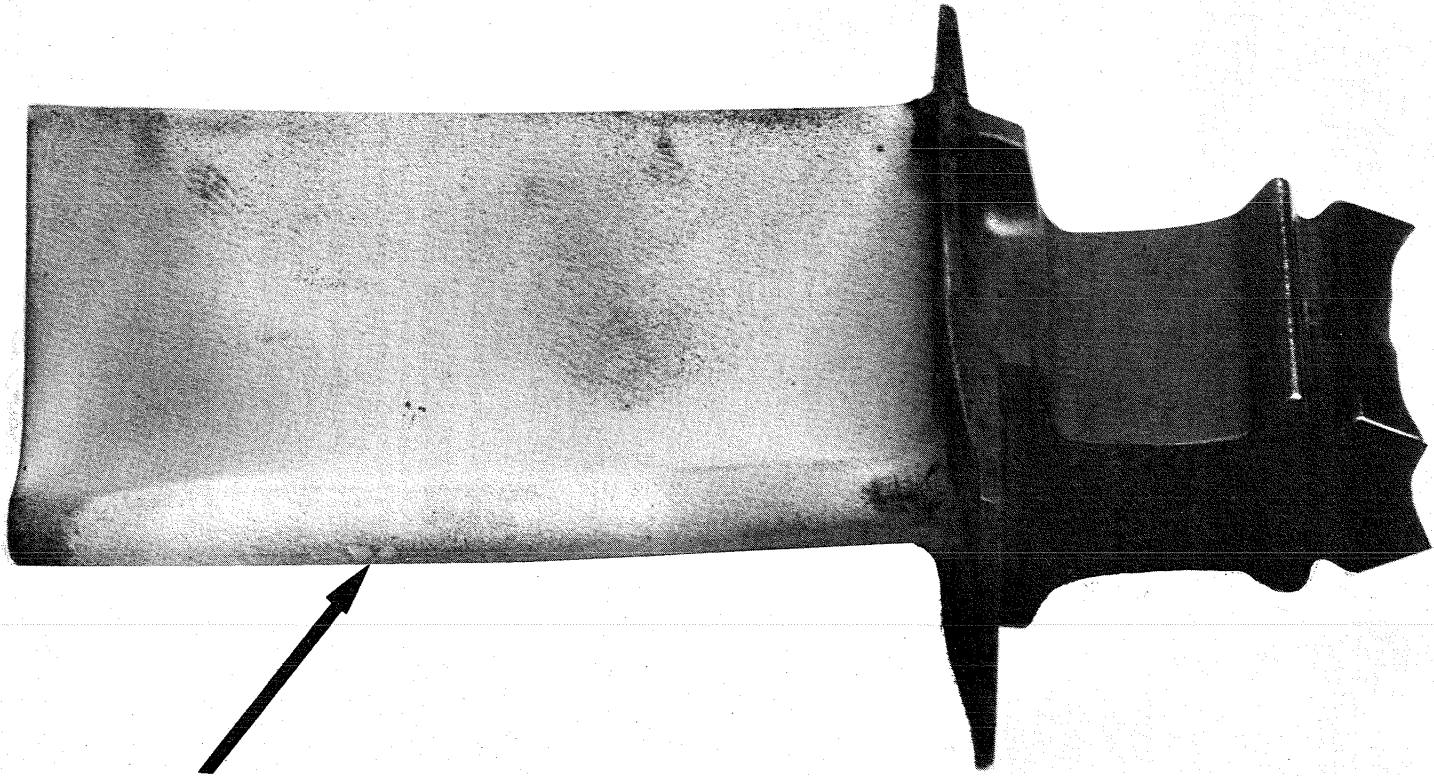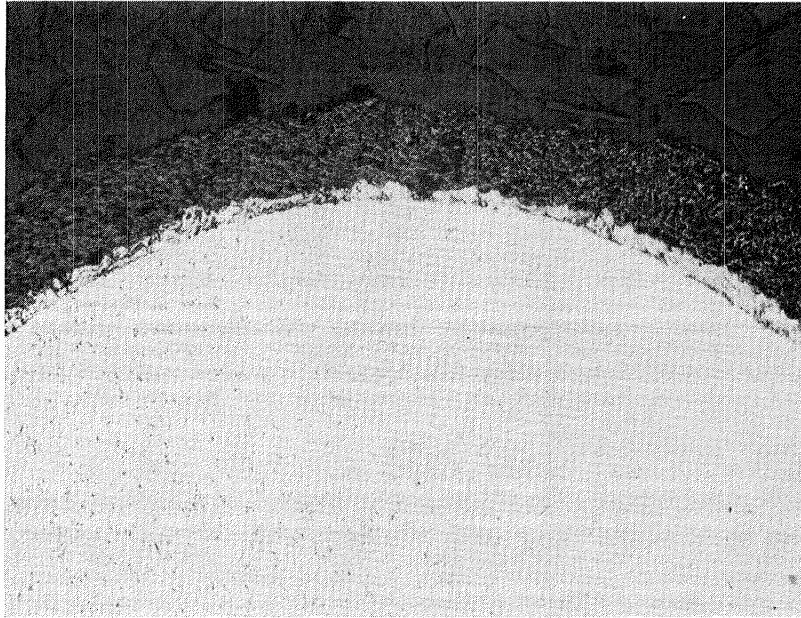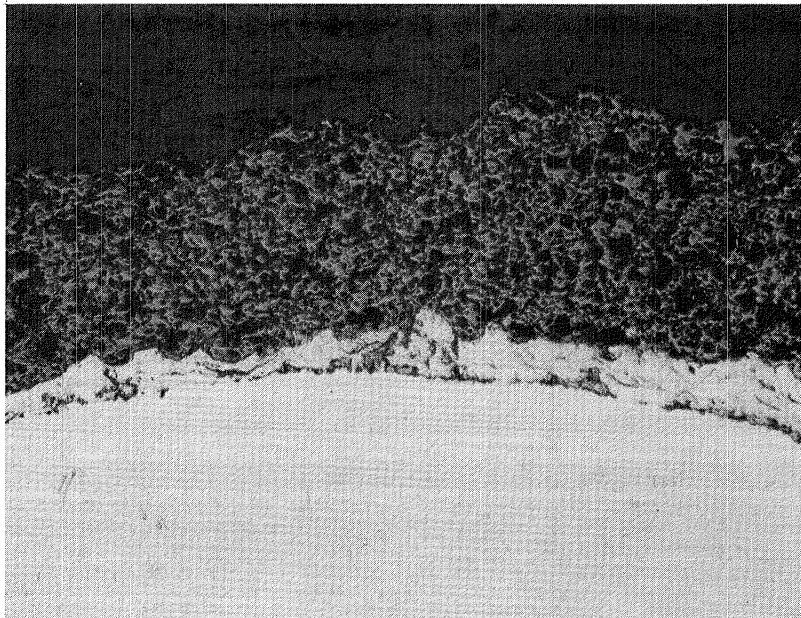No. 27 (Surface "A") at Location 20 (50X).

Figure 53.   APS Process Coated, NASA Torch Tested, Specimen No. 26 after 23 Hour
Exposure.   (Note location of arrow showing some localized thermal
barrier coat spalling.)

(40X)

(100X)

Figure 54.   Photomicrographs of APS Process Coated Specimen No. 26 after
              23 Hour Torch Test Exposure Showing Localized Thermal Barrier
              Coat Spalling.

NiCrAlY Only		Total Coating		
0 0	0 3.0	0 0	1 4.0	─ T.E.
0 1	0 3.4	0 1	1 6.2	
0 2	0 3.8	0 2	1 7.0	
0 3	0 4.2	0 3	1 5.8	
0 4	0 4.6	0 4	1 5.8	
0 5	0 4.4	0 5	1 6.0	
0 6	0 4.0	0 6	1 5.2	Airfoil
0 7	0 5.2	0 7	1 5.8	Convex Surface
0 8	0 4.6	0 8	1 6.0	
0 9	0 3.6	0 9	1 4.8	
1 0	0 4.2	1 0	1 6.0	
1 1	0 3.8	1 1	1 8.6	
1 2	0 0.6	1 2	1 1.8	─ L.E.
1 3	0 1.8	1 3	1 4.0	─ T.E.
1 4	0 2.4	1 4	1 5.0	
1 5	0 3.2	1 5	1 4.8	
1 6	0 3.4	1 6	1 4.8	
1 7	0 3.8	1 7	1 5.2	
1 8	0 3.6	1 8	1 4.8	Airfoil
1 9	0 4.8	1 9	1 5.0	Concave Surface
2 0	0 5.2	2 0	1 4.4	
2 1	0 4.4	2 1	1 5.2	
2 3	0 2.8	2 2	1 3.6	
		2 3	1 4.0	─ L.E.

Note: Location No. 22 data for NiCrAlY thickness is missing on printout due to printer malfunction.

Figure 55.   Data Printouts from APS Process System Showing Actual Deposition Thicknesses (in mils) of NiCrAlY and Zirconium Oxide Coatings on JT9D Specimen No. 26 as Determined by Optical Sensor at Each Gage Point.

coated by the APS process using the new (Model No. 2) mechanism, the thickness and uniformity of the coatings deposited were verified using a scanning laser gage. Coating deposition was done using a scan line spacing of 3.5 mm (0.140 inch) for both powders. This resulted in 12 scan lines and 12 measurement (gage) points around the cylinders.

Initially 18 specimens were coated, three each for six different sets of process parameters listed in Table XI. These six sets of parameters included variations in standoff distance, powder feed rate for the NiCrAlY, arc gas flow rate and arc current. These sets of parameters were specified by NASA. Based on results of initial burner rig tests on these specimens, three additional specimens were coated for each of Conditions II and VI, bringing the total to 24 specimens coated. Figure 56 shows two of these specimens.

The burner rig test consisted of cycles of five minutes heating followed by three minutes of forced air cooling. The initial set of eighteen specimens was tested up to approximately 1000 cycles. The specimens with only 254 μm (10 mils) of zirconium oxide coating failed early. The specimens with 381 μm (15 mils) of zirconium oxide lasted much longer in all cases. Based on these results, the process parameters tabulated under Conditions II and VI, with 381 μm (15 mils) of zirconium oxide, were selected for further evaluation testing. Two of these specimens, coated using the parameters shown in Condition II, lasted approximately 2000 cycles before failure (Specimen II-9, 1850 cycles and Specimen II-10, 2050 cycles). The failure surfaces of these two specimens are shown in Figure 57.

5.2.6 Coating Deposition on Utility Turbine Blades

A batch of ten W501B utility turbine blades was coated with thermal barrier coatings to demonstrate applicability of the APS process to other than the JT9D aircraft turbine blade specimens. The utility blade specimens were coated using the process parameters established in cylindrical specimen testing as producing the longest burner rig life. These parameters were designated as Condition II in Table XI.

The coordinate data for deposition scan lines and measurement or gage points on the utility blade specimens was determined from blade coordinate data on the part drawing. Offline computer programs for the HP9820 calculator were used to calculate equally spaced points around each of three airfoil cross-sections; then to convert the coordinates of these points from the blade coordinate system to the APS mechanism coordinate system. The outputs of these programs were coordinate tables for deposition scan lines for both the NiCrAlY and zirconia and a table of coordinates for the gage points, one on each scan line. All tables were in hexadecimal notation, ready for loading into APS firmware EPROMs. The deposition scan line coordinates were calculated for specified standoff distances between the plasma gun and the specimen, using the previously determined angular offsets between the plasma beam and the gun centerline. The scan lines were projected slightly above and below the specimen to allow gun turn-around off the specimen surface. Scan line spacing used for the utility blade specimens was 3.5 mm (0.140 inch) for both the NiCrAlY and zirconia. This

TABLE XI

APS Process Parameters Used for Burner Rig Test Specimens

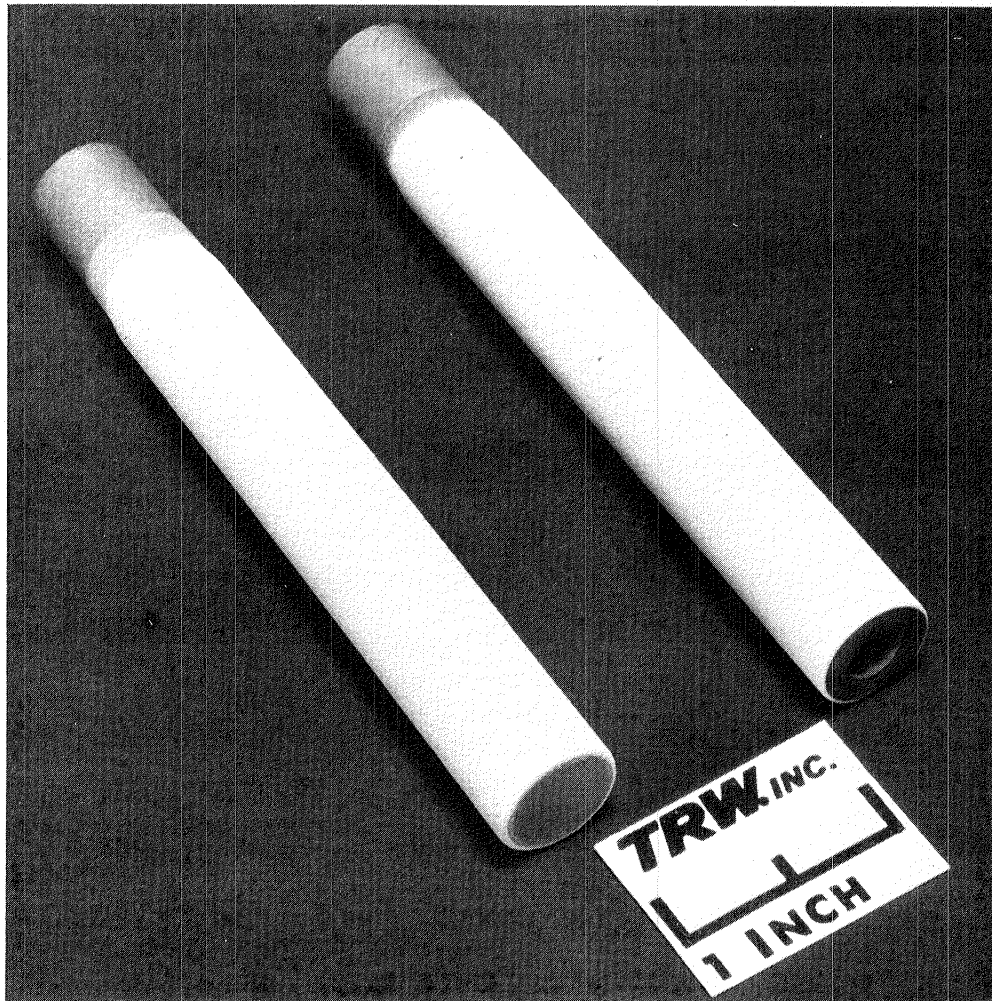| Condition Number	Coating Material	Standoff (inches)	Arc Current (amperes)	Arc Gas Flow (SCFH)	Powder Flow (g/min)
I	NiCrAlY ZrO_2	3.5 3.5	700 800	98 98	42 38
II	NiCrAlY ZrO_2	4.5 3.5	700 800	98 98	42 38
III	NiCrAlY ZrO_2	3.5 3.5	500 550	65 65	25 38
IV	NiCrAlY ZrO_2	4.5 3.5	500 550	65 65	25 38
V	NiCrAlY ZrO_2	3.5 3.5	400 550	65 65	25 38
VI	NiCrAlY ZrO_2	3.5 3.5	500 550	65 65	42 38

Figure 56.   Specimens Coated by APS Process for Burner Rig Testing.
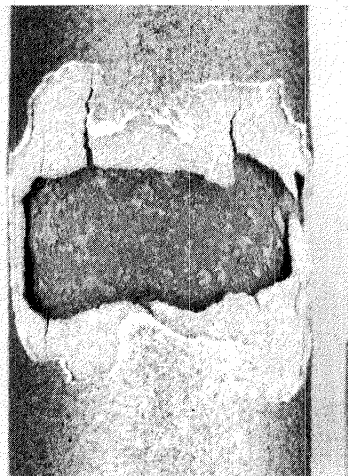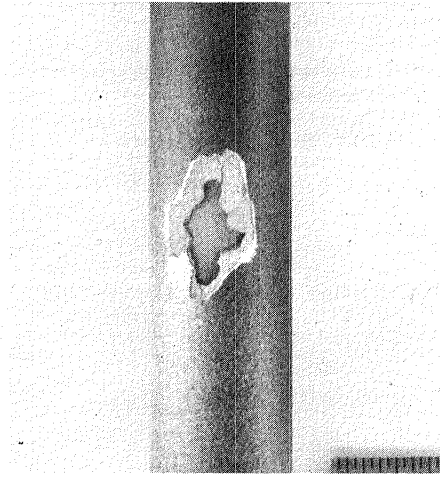
Figure 57.   Two Layer Thermal Barrier Coated Samples After 1850 Cycles (Left)
and 2050 Cycles (Right) Under Burner Rig Test Conditions.

resulted in seventy deposition scan lines for each powder and seventy gage points around the airfoil. Spray deposition started at the breakpoint between the leading edge and the convex side of the airfoil, proceeded around the convex side, the trailing edge, the concave side and finished with the leading edge.

Five of the utility blade specimens were coated during preliminary APS process system checkouts with the new mechanism. The other five specimens (Figure 58) were delivered to NASA. Figures 59 and 60 show closeup views of both sides of one of these specimens.

Only one significant problem was encountered with the utility blade specimens. Due to the large projections of the blade platform at some points and the short standoff distance required (3.5 inches), it was not possible to leave the barrier shield in place while spraying the zirconia portion of the coating on the airfoil surfaces. The shield assembly had to be withdrawn during this portion of the deposition cycle, allowing the plasma beam to impact on the specimen holding fixture during gun turn-around. Figure 61 is a closeup photograph of the gun and specimen with the barrier shield assembly in place. The deposition patterns of the zirconia on the fixture are also evident in this photograph. Concepts have been evolved for a new barrier shield assembly formed on the specimen holding fixture to allow for shorter gun/specimen standoff distances. This shield would be cooled to prevent transfer of excessive heat into the specimen holding fixture. No damage was done to the specimen holding fixture while allowing the gun to turn around on it while spraying the final specimens on this contract. However, the fixture became extremely hot during this phase of the deposition cycle, requiring fifteen minutes or more to cool to the point where it could be handled with bare hands after completion of a specimen. Since this degree of heating causes errors in the deposition thickness gaging, it was necessary to halt the process cycle before deposition of the finish passes of zirconia on these specimens. The thickness of the zirconia portion of the thermal barrier coating on these specimens was therefore slightly less than nominal, particularly around the leading and trailing edges. To have continued without the accurate gage point measurements on these specimens, however, would have resulted in excessive depositions on some scan lines. The new fixture/barrier shield assembly will be required to eliminate this problem on these specimens.

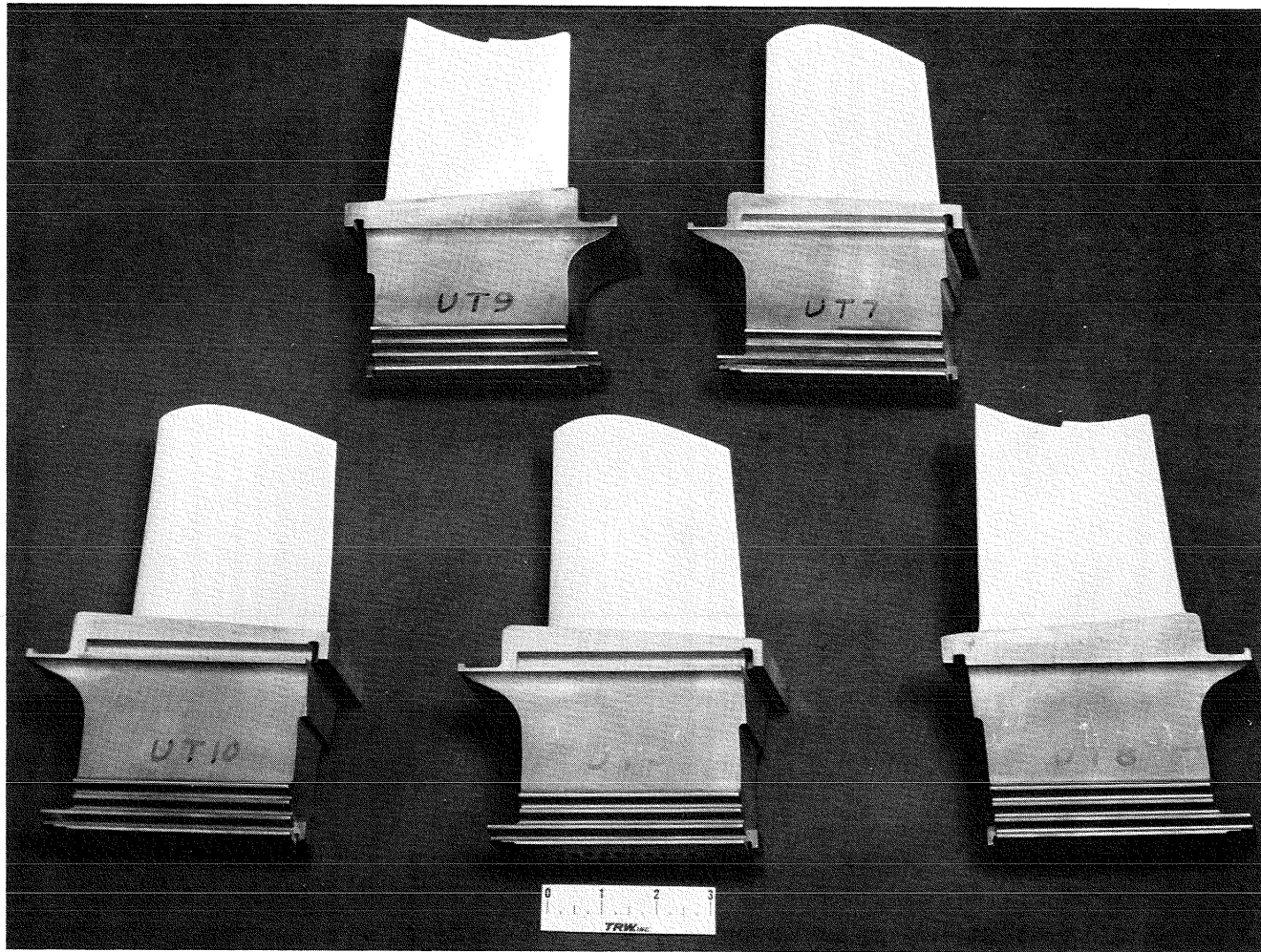Figure 58. W501B Utility Turbine Blade Specimens Coated with Thermal Barrier Coatings by APS Process.

Figure 59.   Photograph of W501B Utility Turbine Blade Specimen
No. UT6 (Convex Side) After Coating with Thermal
Barrier Coating by APS Process.
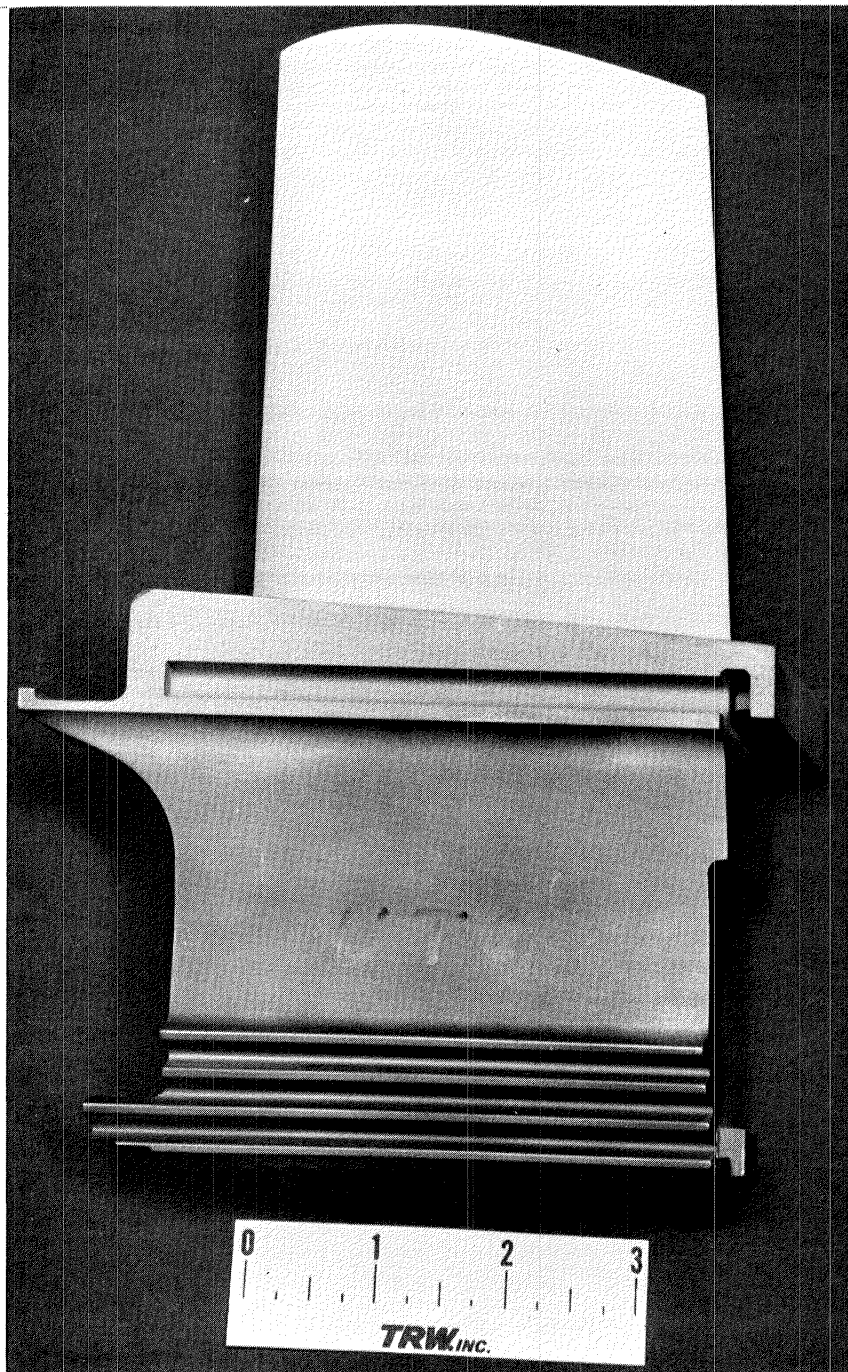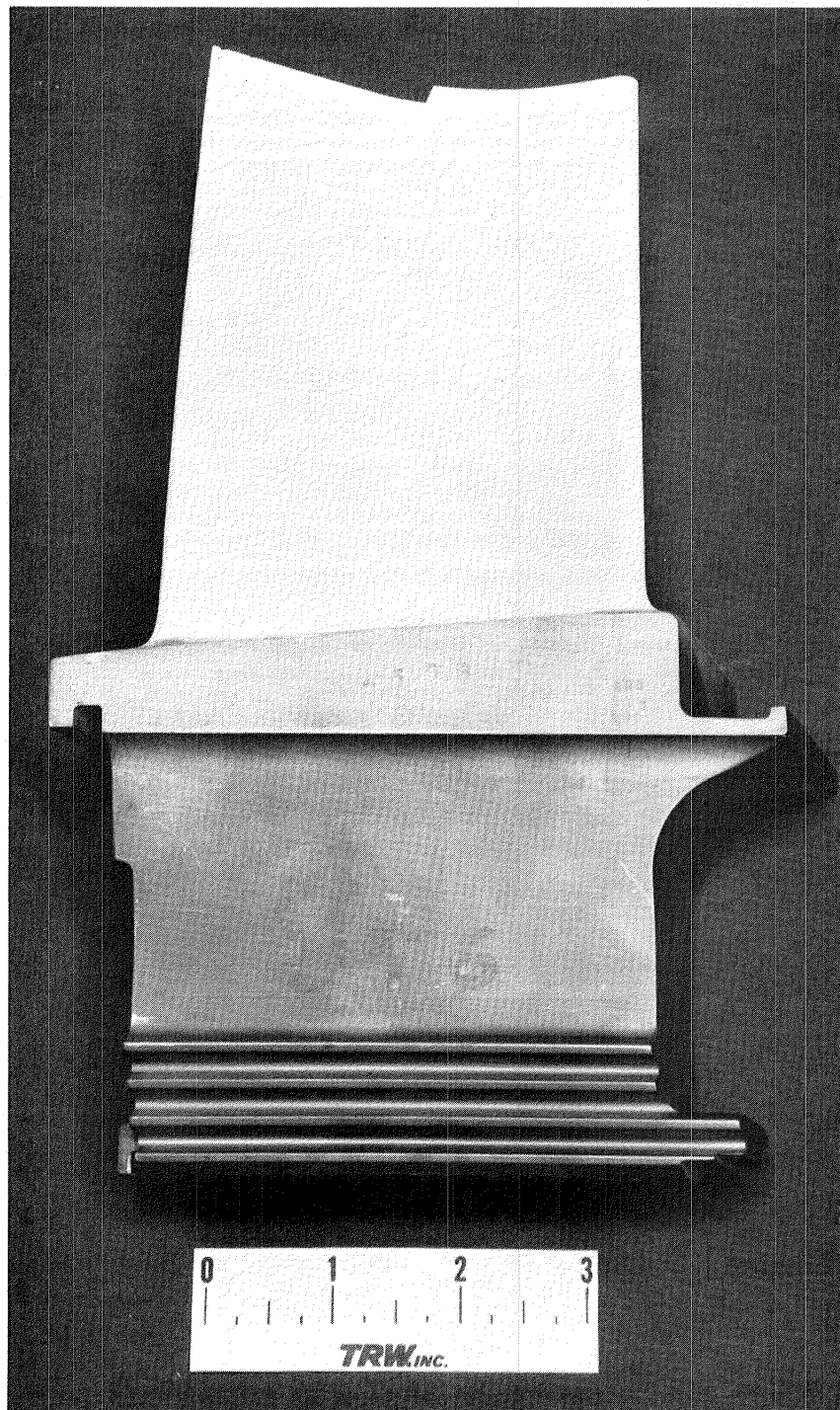
Figure 60.   Photograph of W501B Utility Turbine Blade Specimen
              No. UT6 (Concave Side) After Coating with Thermal
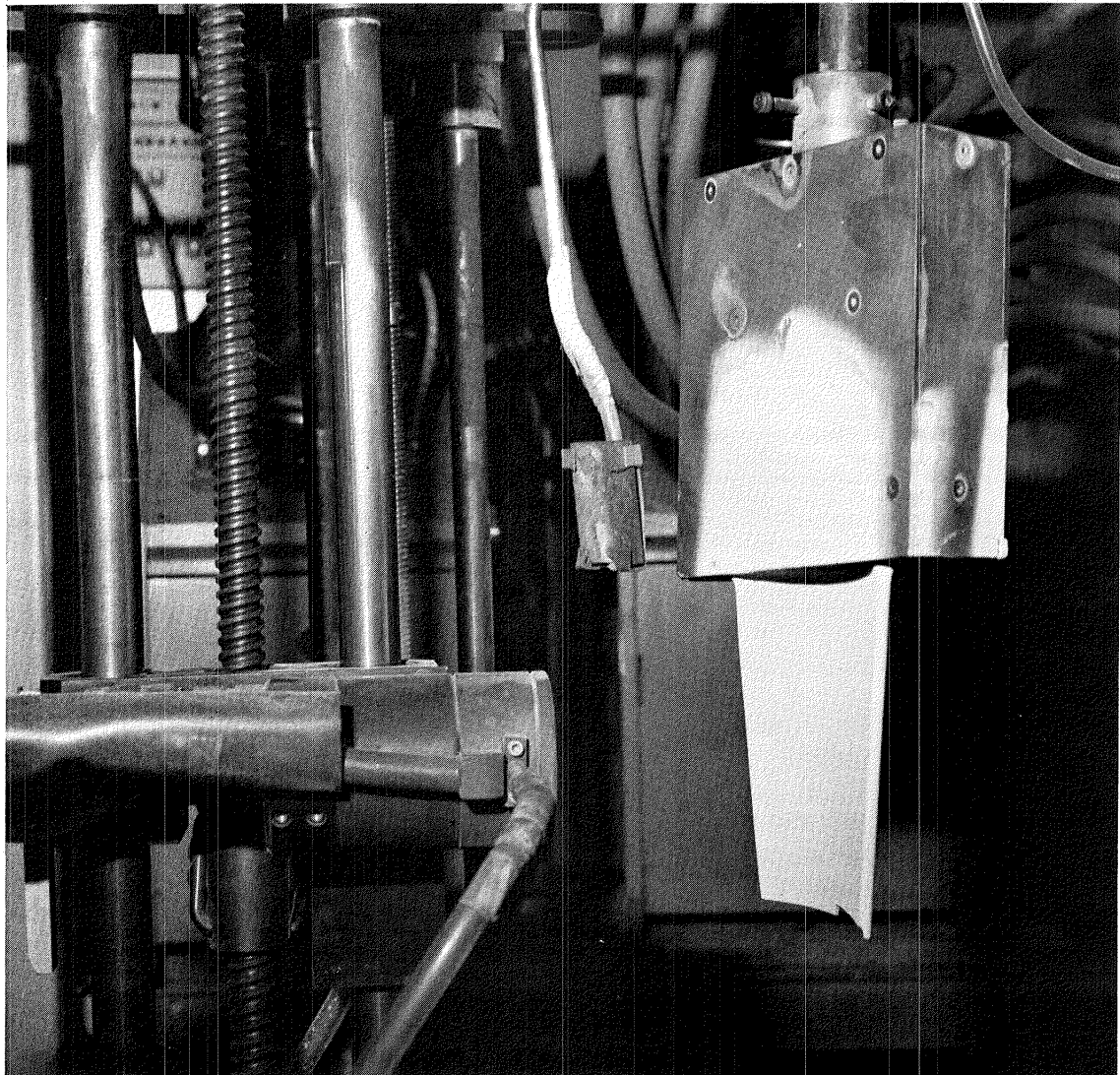   Barrier Coating by APS Process.

Figure 61.

Closeup Photograph of Plasma Gun, Barrier Shield Assembly and Specimen Holding Fixture.
(Zirconia deposition patterns on fixture caused by withdrawal of barrier shield assembly
may be observed.)

6.0 CONCLUSIONS AND RECOMMENDATIONS

A feasibility study of an automated plasma spray (APS) process to uniformly and reproducibly apply a NASA-developed two-layer (NiCrAlY and yttria-stabilized zirconia) thermal barrier coating to aircraft and utility gas turbine engine airfoils was conducted. Specially developed process hardware and software were utilized in this study along with standard commercial plasma spray equipment.

Based on the data acquired during this study, the following conclusions were reached:

1) Feasibility has been demonstrated for an automated process for deposition of plasma-sprayed two-layer thermal barrier coatings on aircraft and utility gas turbine blade airfoils. This process incorporates noncoherent optical sensing of actual in-process coating buildup on the specimen and provides adaptive closed loop control of the deposited coating thickness profiles. The process can be programmed to provide a specified, controlled nonuniform deposition coating thickness over the airfoil surface as well as a uniform thickness. The APS process system is readily adaptable to coating other complex geometry shapes.

2) Extrapolation of preliminary data obtained on the APS process on JT9D first stage aircraft turbine blades indicated that the desired ± 38 μm (1.5 mils) coating thickness uniformity over the entire airfoil surface is achievable. This uniformity was subsequently demonstrated on cylindrical specimens. Extrapolation of process performance to other types of specimens was demonstrated by the coating of W501B utility gas turbine blade airfoils with the APS process.

3) The variations in deposition coating thickness are essentially independent of total coating thickness using the APS process. With manual plasma spraying, on the other hand, variations tend to be a fixed percentage of total coating thickness. Thus the advantages of the APS process are particularly significant for thicker coatings such as thermal barriers. The APS process advantages could also be exploited with thinner coatings by application of thinner deposits with each spray gun pass.

4) The APS process has demonstrated the capability of coating JT9D blade airfoil surfaces with a two-layer thermal barrier coat without masking the blade root/platform section and without masking or plugging the trailing edge cooling gas exit ports.

5) The noncoherent optical metrology subsystem developed for the APS process has demostrated gaging performance capabilities to ± 2 μm (0.08 mil). Despite deficiencies in the system mechanical hardware, this subsystem demonstrated a standard deviation of ± 7.5 μm (0.3 mil) on turbine blade airfoils in the APS process system. This accuracy was limited only by the resolution and repeatability of the mechanical axes in this system.

6) Application of the APS process to a wide range of airfoil products may be readily achieved utilizing off-line computer programs to generate APS process deposition parameters from the part specification drawings.

Based on the foregoing conclusions and the process performance observations discussed in the body of this report, the following recommendations are offered for further activities in development of the APS process for utilization:

1) A new type specimen holding fixture incorporating an integral, cooled, barrier shield assembly should be evaluated. Fixtures of this type will allow full realization of the APS process performance capabilities on a wide range of specimen types.

2) Extensive statistical evaluations of the APS process performance should be made. These should involve coating formulations developed subsequent to those utilized on this contract. The reproducibility achievable with the APS process can be utilized in optimization of the spray deposition process parameters for these coatings. Evaluation criteria would include the performance integrity of the coatings as well as the reproducibility and uniformity (or degree of control of a specified nonuniformity) of the deposition thickness profiles. APS process evaluations should also include the use of inert gas and low pressure envelopes around the specimen as well as normal ambient atmosphere as utilized on this contract.

3) Plasma spray gun designs better suited to high accuracy automated coating deposition thickness buildup should be investigated and/or developed. The certainty to which the beam deposition profiles are known will prove to be the ultimate limit on the controllability of the coating deposition thicknesses. The plasma gun utilized on the current contract ejected beam profiles in different directions for the different coating constituents. There were also indications of some variations in the beam profiles with time.

4) Detailed design of a preproduction prototype APS process system should be made. This design would be predicated on extensive observations made to date as well as results of the subsequent activities recommended above. Many details are already obvious, e.g., provision of dust seals and shields, more rugged and durable mechanical construction, upgrading of the electronic hardware, etc. Other possibilities for consideration would include provision of automatic preset and adjustment of the various plasma spray parameters by the APS process controller microcomputer based on the specific specimen to be coated.

116

7.0 APPENDICES

7.1 List of Abbreviations and Symbols

Symbol	Quantity	Unit
A	Specimen angular rotational axis of motion (around linear motion of X axis)	-
A/D	Analog to digital converter	-
APS	Automated Plasma Spray	-
B	Specimen angular rotational axis of motion (around linear motion of Y axis)	-
C	Specimen angular rotational axis of motion (around its own longitudinal axis)	-
CPU	Central processing unit	-
CRT	Cathode raytube	-
EMI	Electromagnetic interference	volt/meter
EPROM	Erasable programmable read only memory	-
FIFO	First-in-first-out (usually refers to computer memory stack or register)	-
g	Mass	gram
g/min	Flow rate	gram/minute
g/s	Flow rate	gram/second
Hz	Frequency	hertz
I/O	Input/output	-
l	Volume	liter
L.E.	Leading edge (of turbine blade)	-
LED	Light emitting diode	-
l/min	Flow rate	liter/minute

7.1 List of Abbreviations and Symbols (cont'd)

Symbol	Quantity	Unit
l/s	Flow rate	liter/second
LeRC	Lewis Research Center (NASA)	-
min	Time	minute
MPS	Manual plasma spray	-
mt/st	Measurement per step	-
PC	Printed circuit	-
PIA	Peripheral interface adaptor	-
RAM	Random access memory	-
ROM	Read only memory	-
s	Time	second
TB	Thermal barrier	-
T.E.	Trailing edge (of turbine blade)	-
TTL	Transistor-transistor-logic	-
W	Power	watt
X	Specimen linear axis of motion (perpendicular to plasma spray direction)	-
Y	Specimen linear axis of motion (parallel to plasma spray direction)	-
Z	Optical detector linear axis of motion	-
ZZ	Plasma gun linear axis of motion	-
μP	Microprocessor	-

7.2 Prefixes

Decimal multiples and submultiples of the engineering units are formed by means of prefixes. A partial list of the NBS recommended units of prefixes are listed below:

Symbol	Prefix	Factor by Which the Unit is Multiplied
G	giga	10^9
M	mega	10^6
k	kilo	10^3
d	deci	10^{-1}
c	centi	10^{-2}
m	milli	10^{-3}
μ	micro	10^{-6}
n	nano	10^{-9}
p	pico	10^{-12}

7.3 APS Mechanism Model No. 1 Drawings

7.4 APS System Circuit Diagrams

7.5 APS Process Software Flow Charts and Assembly Listings

7.6 APS Mechanism Model No. 2 Drawings

The materials of Sections 7.3, 7.4, 7.5 and 7.6 listed above were published and submitted separately. For further information contact J. P. Merutka, MS 49-1, NASA/LeRC, 21000 Brookpark Road, Cleveland, Ohio 44135.

8.0 REFERENCES

1. Stecura, Stephan: Two-Layer Thermal Barrier Coating for Turbine Airfoils - Furnace and Burner Rig Test Results. NASA TM X-3425, 1976.

2. Gerdeman, D.A. and Hecht, N.L.: Arc Plasma Technology, Materials Science, Springer - Verlang, 1972.

3. Stecura, Stephan: Effect of Compositional Changes on the Performances of a Thermal Barrier Coating System, NASA Technical Memorandum 78976, 1979.

4. McDonald, G. and Hendricks, Robert C.: Effect of Thermal Cycling on $ZrO_2-Y_2O_3$ Thermal Barrier Coatings. NASA TM 81480, 1980.

End of Document